Biomimetic strain-stiffening hydrogels

BIOMIMETIC STRAIN-STIFFENING HYDROGELS

PROEFSCHRIFT

ter verkrijging van de graad van doctor aan de Technische Universiteit Eindhoven, op gezag van de rector magnificus prof.dr.ir. F.P.T. Baaijens, voor een commissie aangewezen door het College voor Promoties, in het openbaar te verdedigen op woensdag 28 maart 2018 om 11:00 uur

door

Marcos Fernández-Castaño Romera

geboren te Madrid, Spanje

Dit proefschrift is goedgekeurd door de promotoren en de samenstelling van de promotiecommissie is als volgt:

voorzitter:	prof.dr.ir. R.A.J. Janssen
1e promotor:	prof.dr. R.P. Sijbesma
copromotor:	prof.dr. C. Storm
leden:	prof.dr. A.E. Rowan (The University of Queensland)
	prof.dr. G. Koenderink (VU)
	prof.dr. E.W. Meijer
	prof.dr.ir. J.C.M. van Hest
adviseur:	dr. A.W. Bosman (SupraPolix B.V.)

Het onderzoek of ontwerp dat in dit proefschrift wordt beschreven is uitgevoerd in overeenstemming met de TU/e Gedragscode Wetenschapsbeoefening.

"We have a 'strategic' plan. It's called doing things."

−Herb Kelleher−

Co-founder & former CEO of Southwest Airlines.

To my parents Eduardo & Mari Cruz.

Cover design: Jeffrey Grashof & Rachael Arnott

Printed by: Gildeprint, Enschede

A catalogue record is available from the University of Technology Library

ISBN: 978-94-6233-902-6

This work has been financially supported by the European Union's Seventh Framework Program for research, technological development and demonstration under the grant agreement nº. 607602- SASSYPOL project, and the Dutch Ministry of Education, Culture, and Science (Gravity program 024.001.035).

Table of contents

Chapter 1:

Introduction

Abstract: *Fibrous protein networks are ubiquitously present in biology both in the intra- and extracellular milieu. They are the principal promoters of mechanical strength, support and integrity and are crucially implicated in various biological processes of paramount importance, such as cell motility, differentiation or communication at long distances. For some time now, such networks, taken as a whole, are known to exhibit unusual mechanical properties, unmatched by traditional synthetic hydrogels, that stem directly from their architecture at the single filament level, i.e. they consist of hierarchically self-assembled bundles or fibrils integrating by up to hundreds of individual filaments. Bundling is an essential process in structural biopolymers as it imparts high persistence lengths which in turn translates into enhanced flexural rigidity and stretching resistance. At the network level, this leads to materials able to become orders of magnitude stiffer when exposed to mechanical stimulus exerted from both external and internal cues. Here, we review the origins of mechano-responsiveness in biopolymer networks and discuss recent advancements in the field of supramolecular organic chemistry towards the rational design of materials that mimic living systems with particular emphasis on their nanoscale organisation, dynamics and mechanical properties.*

1.1. Strain-stiffening in fibrous protein networks

Cells and connective tissues are subjected continuously and must respond to a variety of mechanical stimuli, such as shear flow caused by passing blood in the endothelium[1], compressive forces on bone cells[2] and tensile stresses experienced by the epithelium[3]. To this end, biology makes use of assembled fibrous protein networks that are the key promoters of mechanical strength, support and integrity while, at the same time, exhibit a highly dynamic behaviour that enables cells to sustain substantial changes in shape as they move, grow or divide[4,5]. How nature achieves such remarkable balance between mechanical stability and dynamic shape control is a question yet to be fully elucidated.

Inside cells, three distinct types of fibrillar structures can be found: actin, tubulin and different types of intermediate filaments, all of them acting synergistically in combination with a myriad of crosslinking and motor proteins. The interplay of these elements enables cells to perform a wide variety of tasks ranging from cell motility or division to mechano-responsiveness[6–9]. In contrast to the cytoskeleton (CSK), the extracellular matrix (ECM) is comparatively more static and is rife with fibrin and collagen fibers. Fibrin is actively involved in the formation of blood clots and plays a major role in wound healing.[10] On the other hand, collagen is the most abundant extracellular protein encompassing a family of 28 subtypes, of which type I is the most abundant acting as the main load-bearing component in tissues such as fascia, tendons and bones where it imparts strength, elasticity and structural stability[11].

When examined up-close, CSK and ECM networks share two critical architectural features: (1) they are composed of rigid-to-semi-flexible polymer bundles –able to integrate by up to hundreds of individual filaments–[12]; (2) they possess large mesh sizes that facilitate transport of matter across the intra- and extracellular milieu. The combination of these two design principles has essential implications concerning mechanics: networks of CSK and ECM proteins exhibit a remarkable propensity to stiffen in response to mechanical stimuli. Such process is referred to as strain-stiffening and is crucially implicated in maintaining tissue and cell integrity under forces generated by both, external or internal sources. Recently, strain-stiffening has also been identified to play an important role in enabling transduction of mechanical cues at distances of the order of hundreds of microns[13,14]. The physical origins of

nonlinearity in these systems are tightly coupled to the structural and morphological characteristics of the constituent biopolymers.

In this chapter, we unveil the underlying physical principles that govern strain-stiffening in biopolymer networks and illustrate how these principles can be extrapolated to engineer synthetic materials that are mechanically and structurally akin to natural systems. In line with these efforts, we discuss recent developments in the field of synthetic organic chemistry to rationally design self-assembling small molecules and polymers able to aggregate in water into supramolecular polymers and hydrogels that recapitulate some of the most fundamental structural, morphological, dynamic and mechanical features of filamentous proteins and their networks.

1.2. Understanding the physical origins of strain-stiffening in fibrous protein networks

In recent years, a plethora of techniques has provided the means to probe the mechanical response at a single-cell or tissue level, usually by inducing local or widespread deformations[15,16]. These type of measurements have yielded valuable information into overall tissue and cell mechanics. However, the structural heterogeneity and complexity inherent to biological systems, in combination with numerous elements acting synergistically, often hampers an unambiguous interpretation of the results.

To address this issue, rheology and theory on reconstituted gels from isolated extracellular or cytoskeletal proteins have become popular complementary approaches. Such *in vitro* studies capture some of the features measured *in vivo* such as strain-stiffening and negative normal stress[18,19] (*i.e.* the network contracts in the normal direction when sheared) and have led to very detailed predictive models that seek to bridge the gap between single-filament and macroscopic rheological measurements. In this context, early theoretical work suggests that strain-stiffening is inherent to any connected meshwork of semi-flexible polymers[17]. As mentioned above, biopolymers owe their stiffness to the formation of hierarchically self-assembled bundles or fibrils held together via various non-covalent and covalent interactions[12,20–22].

1.2.1. The role of backbone stiffness

The rigidity of a polymer backbone determines how an individual polymer chain responds to an external loading. Typically, a flexible polymer chain can sustain very large deformations without opposing significant resistance before reaching full elongation. Conversely, semi-flexible and rigid polymers, due to generic geometric reasons, can access their non-linear extensional regimes prompted by small strains. The onset of nonlinearity in these polymers is determined by their persistence length L_p. L_p is defined as the typical length at which thermal fluctuations k_BT are sufficient to reverse the direction of the filament. In a semi-flexible polymer, L_p is comparable to its contour length L_c (*i.e.* the length at full extension) where $L_p/L_c \sim 1$. Besides semi-flexible polymers, two additional regimes can be distinguished based on backbone stiffness (Fig. 1.1)[23]: (1) Rigid rods ($L_p/L_c >> 1$), corresponding to a nearly fully stretched conformation of the backbone. Nonlinear elasticity in these systems arises from pulling of molecular bonds along the filament axis. (2) Flexible chain ($L_p/L_c << 1$), wherein thermal energy bends the filament into a random coil and mechanics are dominated by entropic elasticity whereby the polymer chain loses conformational entropy as it approaches full elongation. Most synthetic polymers fall within this category as they lack the molecular complexity to undergo hierarchical self-assembly to form stiffer bundles.

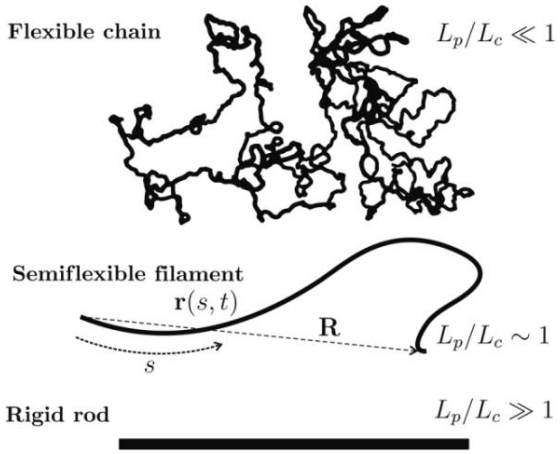

Fig. 1.1 | Classification of polymers based on backbone stiffness: Flexible chains adopt a random coil conformation, semi-flexible filaments are nearly straight with thermal undulations, and rigid rods are not influenced by thermal energy. Figure reprinted with permission from ref. [23]. Copyright © 2014, Royal Society of Chemistry.

As a consequence, the elasticity of most synthetic polymer gels, such as polyacrylamide- or polyethylene glycol-based hydrogels shares similarities with that of rubber-like materials. As such, the mechanical response can be rationalised through classic rubber elasticity theory[24]. In contrast to synthetic gels, in biopolymer networks (*e.g.* fibrin or collagen), rubber elasticity theory does not adequately account for strain-stiffening or negative normal stress. Ultimately, the elastic behaviour in these materials is governed by resistance to bending and stretching of the semi-flexible filaments. Filament stretching leads to an affine-type of deformation (*i.e.* the local strains are uniformly distributed within the material and follow the imposed macroscopic strain), whereas filament bending exhibits signatures of non-affinity (Fig. 1.2)[25].

Two types of theoretical models have been developed on the basis of affinity and non-affinity, both of which, successfully predict strain-stiffening and negative normal stress: (1) Affine or entropic models in which biopolymers are described as entropic springs whereby strain-stiffening arises from the non-linear force-extension curve of individual filaments resisting elongation[17,26]. (2) Non-affine or enthalpic models where non-linearity stems from non-affine network rearrangements that lead to a transition from a low-strain linear regime dominated by soft bending modes, to a nonlinear regime where stiffening arises from enthalpic filament stretch at larger strains[27–29].

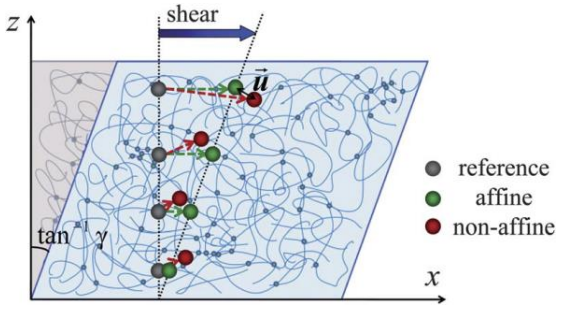

Fig. 1.2 | Illustration of affine and non-affine deformations in a hydrogel subjected to shear strain with embedded tracer particles. In affine deformations, the particles displace in line with the imposed (or real) deformation. The non-affine deviation $\vec{\mu}$ is quantified by the difference between real and affine displacement. Figure reprinted with permission from ref. [25]. Copyright © 2012, Royal Society of Chemistry.

1.2.2. Measuring strain-stiffening

The nonlinear elasticity of hydrogels can be characterized using oscillatory shear rheology. In a conventional strain-controlled rheometer apparatus, the gel is placed (or formed *in situ*) between two plates. While the lower plate remains stationary, the upper plate imposes a sinusoidal strain on the gel of the form $\gamma = \gamma_0 \sin(wt)$ and the shear stress σ needed to induce such deformation is measured. The output stress is also recorded in the form of a sinusoidal function with an associated phase shift (φ) such that $\sigma = \sigma_0 \sin(wt+\varphi)$. The elasticity of the gel, given by its storage modulus G', is obtained from the part of stress that oscillates in phase with the imposed strain, where $G' = \sigma_0 \gamma_0^{-1} \cos(wt)$. Concurrently, the out-of-phase stress yields the viscous contribution given by its loss modulus G", whereby $G" = \sigma_0 \gamma_0^{-1} \sin(wt)$.

For biopolymer networks, since the stress does not increase linearly with the applied strain, the stress response cannot be described accurately by a simple sinusoidal function (*i.e.* higher order harmonics come into play). An alternative method to probe the nonlinear regime is to impose a constant pre-stress σ to the material. Parallel superposition of a low-amplitude oscillatory stress allows to calculate the so-called differential modulus $K' = \delta\sigma/\delta\gamma$ (*i.e.* the derivative of the stress-strain curve) which gives a more accurate description of the modulus in its stressed state[30–32].

As predicted by rubber elasticity theory, the stiffness of most synthetic gels composed of individual flexible polymers is characterized by a linear regime where K' is constant over broad ranges of applied stress (or strain), followed by a non-linear extensional regime dominated by entropic elasticity[24]. In practice, however, probing the non-linear regime of these materials becomes challenging due to detachment of the gel from the rheometer plates at the strains needed to stretch out the polymer coils[33]. By contrast, the onset of non-linearity of most biopolymer gels, represented by the so-called critical stress σ_c, is reached at much smaller stresses –typically in the range of 1-10 Pa[17]– consistent with the traction forces that cells impart to their surrounding matrix[34]. Herein, two distinct regimes arise on stressing the material: A linear, low-stress regime where K' is defined by the plateau storage modulus ($K' = G'_0$) and a stress-stiffening regime beyond σ_c where the magnitude of K' increases as a power law $K' = \sigma^m$. The index m, known as the stiffening exponent, yields a direct measure of the degree of mechanical responsiveness, reaching an upper limit $m = 3/2$ at large stresses ascribed to the stretching out of thermal undulations that corresponds

to the terminal scaling predicted by the theory of semi-flexible networks[31,35]. The combination of these parameters provides a direct measure of the gel's sensitivity and mechanical responsiveness towards applied stress (Fig. 1.3).

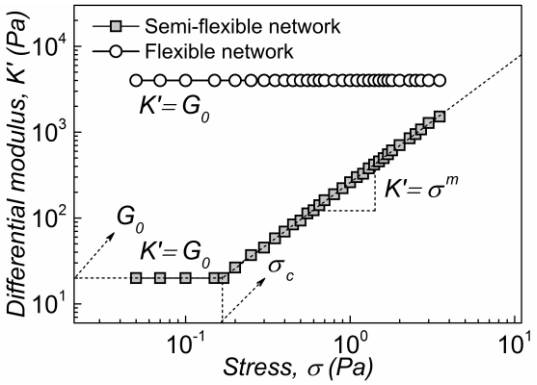

Fig. 1.3 | Differential modulus K' plotted against stress σ for an hydrogel composed of flexible polymer chains (circles) vs a gel based on semi-flexible polymers (squares) illustrating the difference in mechanical behaviour between common synthetic- and biopolymer hydrogels in response to applied stress.

1.3. Networks of cytoskeletal fibrous proteins

The cytoskeleton integrates three distinct types of filamentous proteins: actin (AFs), microtubules (MTs) and intermediate filaments (IFs). Together, they form highly interactive and dynamic structures able to assemble/disassemble on the minute timescale[36,37]. Reconstituted gels of isolated cytoskeletal proteins have been extensively researched. The most recurrent example found in the literature are actin gels.

F-actin filaments are ubiquitously present beneath the plasma membrane and form through supramolecular polymerization of globular G-actin, leading to long fibrils with a diameter of 8 nm, contour lengths that extend across several microns and L_p ~17 μm[38,39]. AFs are reversibly crosslinked in the presence of filamin –a large and flexible cytoskeletal protein– forming quasi-orthogonal networks at remarkably low concentrations. Filamin crosslinks are short-lived with dissociation rate constants in the order of K_{off} ~0.6 s^{-1} that allow actin gels to exhibit fluid-like behaviour at low filamin concentrations[32,40,41]. Within this regime, the mechanical response of actin networks is governed by non-affine soft bending modes characterized by the absence of strain-stiffening[42,43]. However, above a critical crosslinker concentration, filamin induces bundling of AFs, thereby, enhancing their bending stiffness and yield stress[44,45]. As a result, the entropic axial stretch of the bundles at high stress becomes

the dominant source of nonlinearity, and the network becomes mechanically responsive entering the terminal scaling of semi-flexible networks at high stresses with an associated stiffening index of m = 3/2 [31].

IFs encompass a large family of cytoskeletal proteins that form through bundling of helical fibrous proteins[46]. Similarly to actin filaments, IFs undergo continuous assembly/disassembly yet the underlying molecular mechanisms governing these processes remain largely unknown[47]. At a single filament level, IFs are the softest with L_p values that range from a few hundreds of nanometers to 1 μm –comparable to their contour lengths– and a diameter of about 10 nm[16,46,48]. This has significant implications concerning their mechanical properties as they can withstand elongations by up to 3 times their original length[49]. Consequently, IF networks tend to be softer at low strains yet they exhibit pronounced stiffening responses at much larger deformations[50] showing, moreover, a power-law exponent m = 3/2 ascribed to entropic filament stretching[35,51]. Thus, IFs are believed to dominate the mechanical response of cells at large deformations, consistent with recent coarse-grained simulations[52].

MTs comprise the stiffest of all fibrous proteins found in the intracellular milieu remaining relatively straight at lengthscales that span vast regions of the cell[53]. Their L_p is not constant but increases with the length of the tubule displaying, for instance, a L_p = 110 μm for filaments of L_c = 2.6 μm to a striking L_p = 5 mm as the filament progresses to L_c = 47.5 μm all while retaining a constant cross-sectional diameter of 25 nm[54]. In analogy to AFs or IFs, MTs go through rapid stages of disassembly and growth via polymerization of α- and β-tubulin dimers with turnover rates on the order of minutes[55] yet, unlike in AFs or IFs, strain-stiffening is absent in microtubule networks owing to the high stiffness of the constituent filaments[56]. It was found, however that MTs work synergistically with other cytoskeletal subsystems leading to mechanical properties that cannot be realised merely by a linear combination of the parts. For example, MTs embedded within an elastic continuum of AFs and IFs can counteract compressive forces 100-fold larger than the typical buckling force of an isolated microtubule[57]. Further, the inclusion of MTs in a loosely crosslinked actin matrix can suppress non-affine soft-bending modes, thereby, activating strain-stiffening in an otherwise mechanically non-responsive material[58]. MTs have also been identified to play a pivotal role in guiding the growth of filopodia in a specific direction during cell migration[6,59].

1.4. Networks of extracellular fibrous proteins

The extracellular space that stretches beyond and mechanically supports cells is also rife with filamentous proteins arranged into network architectures. The most common fiber-forming proteins found in the ECM are collagen, fibrin and elastin. Together, they give rise to composite materials with highly adaptive elastic properties. The extracellular environment is less dynamic than the cytoskeleton. Here, the formation of covalent crosslinks between and within fibers plays an important mechanical role.

Collagen type I is by far the most abundant and the most heavily researched amongst all extracellular proteins; accordingly, plain collagen refers to collagen I in this chapter. Single collagen molecules consist of right-handed helical peptide strands that self-assemble via multiple hydrogen bonds into long, right-handed triple helices – or tropocollagen[60]. Tropocollagen molecules aggregate into fibrils composed of arrays of staggered molecules aligned parallel to the fibril axis (Fig. 1.4), primarily through non-covalent interactions yet, covalent crosslinking via enzymatic lysine post-modifications[22,61], plays an important mechanical role. Formation of covalent crosslinks renders stiffer and more brittle fibers. Meanwhile, at low crosslinking collagens become more dissipative and able to sustain larger strains[62]. The underlying physical origins of collagen elasticity remain unresolved. In this context, although affine models of entropic elasticity cannot be discarded, many reports suggest that the mechanics of collagen gels are better described by athermal models of non-affine stretching[63–65], consistent with recent observations of reversible strain-induced alignment of collagen fibers in reconstituted gels[66]. Along these lines, collagen-based gels stress-stiffen featuring unusual, yet universal power-law rheology with a distinctive stiffening exponent of $m = 1$ that is below the upper limit $m = 3/2$ described thus far for AF and IF gels. These results support the notion that, entropic fiber stretching is not sufficient to account for the elasticity of collagen networks[29].

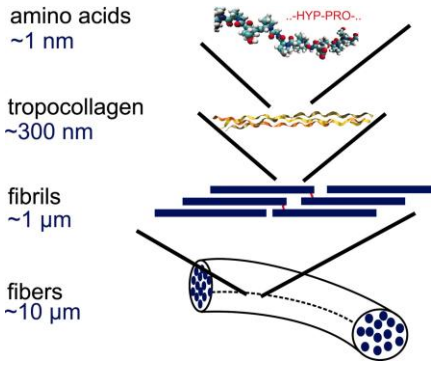

Fig. 1.4 | Process of collagen-fibril hierarchical formation, ranging from single-molecules at the nanoscale scale up to the formation of micrometer-long fibers or fascicles. The figure also illustrates the formation of covalent crosslinks between tropocollagen molecules that strongly influence the mechanical properties of collagen fibers. Figure reprinted with permission from ref. [60]. Copyright © 2006 by The National Academy of Sciences of the USA.

Another major component found in the extracellular environment is fibrin. Fibrin forms through polymerization of fibrinogen and self-assembles into branched fibrous networks that serve as the primary structural scaffold in blood clots[67]. Similarly to collagen, covalent crosslinking within fibrin fibers –mediated by Factor XIII– stiffens the fibers and protects clots against degradation[21,68–70]. Concurrently, the size of fibrin fibers varies depending on formation conditions leading to diameters that range between 10 and 200 nm with essential implications concerning mechanics[18,71]: At a diameter of 10 nm, fibers behave as semi-flexible polymers with a L_p on the order of 500 nm[17]. At larger diameters of ca. 200 nm, aggregation of fibrin protofibrils produces a quadratic increase in L_p, and the fibers behave essentially as stiff beams where non-linearity reflects enthalpic stretching of the fibers[72,73]. Interestingly, at intermediate diameters of about 80 nm, the elasticity of fibrin gels mirrors the complex hierarchical structure found within fibrin fibers where, in spite of their high L_p, intense hydration of the fibers induces a loose packing of fibrin protofibrils[71,74,75]. Consequently, fibrin gels go through different elastic regimes as the fibers begin to stretch in the direction of the applied shear deformation (Fig. 1.5): At low stresses (regime 1 and 2) non-linearity onsets due to stretching out of thermal fluctuations of fiber segments between crosslinks. At higher stresses (regimes 3 and 4), flexible inner regions of the fibers are pulled out followed by regime 5 –that precedes network failure–, in which, the upper limit of $m = 3/2$ is ultimately attained suggestive of a forced-molecular unfolding of fibrin monomers as the primary mechanism governing

nonlinearity[76,77]. Altogether, fibrin gels exhibit unique and rich mechanics that reflect the extraordinary resilience measured for individual fibrin fibers[76,78]. These responsiveness set in at stresses comparable to those exerted by cells to their matrix and protect clots from shear fluid forces caused by passing blood.

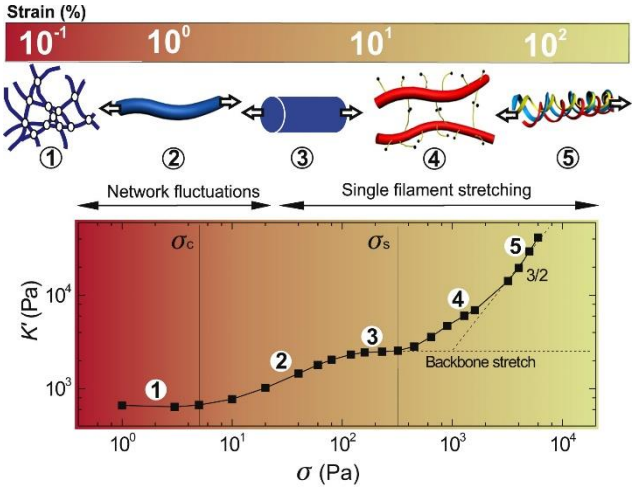

Fig. 1.5 | Hierarchical mechanics of fibrin gels. Increasing strain/stress levels induce structural changes on fibrin fibers that result in distinct elastic regimes indicated by the colour coding of the background that illustrates a transition from entropic elasticity at the network level (red) to entropic elasticity at the fiber level (yellow). Regimes 1 and 2 entail pulling out of thermal undulations from fiber segments between crosslinks, whereas regimes 3 and 4 indicate stretching of flexible regions within the fibers. Stiffening in regime 5 is associated to the unfolding of fibrin monomers showing a $K' \propto \sigma^{3/2}$ dependency that reaches the terminal scaling of semi-flexible networks. Figure reprinted with permission from ref. [77]. Copyright © 2010, Elsevier.

1.5. Mechanical properties of synthetic hydrogels in tissue engineering

Tissue engineering and regenerative medicine are areas that seek to develop therapies that replace or regenerate cells, tissues and organs aiming at restoring impaired functions caused by genetic disease, trauma or ageing. In both disciplines, there is a growing need to develop rationally designed materials with on-demand, purposely targeted properties that are compatible with and mimic complex functions of the ECM.

Along these lines, two main approaches have been conceived to meet requirements such as biocompatibility, biomimicry, bioactivity or injectability[79], each of which,

holds advantages and limitations: (1) Hydrogels based on naturally-occurring building blocks –including reconstituted protein gels–. These type of bio-based materials often display excellent performance, yet they are challenging to functionalise and standardise. (2) Hydrogels based on synthetic polymers. They offer much broader scope for manipulation but are difficult to endow with complex mechanical properties and the correct bioactivity. From now on, we will focus on this type of materials.

Synthetic hydrogels are formed by crosslinking hydrophilic macromolecules into 3D networks that can immobilise large quantities of water (ca. 90 up to >99 wt%) and have physical characteristics that are reminiscent of cellular matrices[80]. The use of synthetic gels for biomedical purposes started approximately 60 years ago with the development of contact lenses based on crosslinked poly(hydroxymethyl methacrylate) (PHEMA)[81]. Thenceforth, the field has experienced a period of fruition, where synthetic hydrogels have played an increasingly important role as platforms for drug delivery[82–84], regenerative medicine[85–88] and tissue engineering[88,89].

Much attention has been paid to engineer hydrogels that recapitulate some of the mechanical and morphological features of protein networks and, more specifically, of the ECM[90,91]. The interest in creating artificial ECM mimics has both, fundamental and application-oriented relevance. From a theoretical perspective, it will help to elucidate the underlying physical principles that govern the unique and rich mechanics of biopolymer networks. From an applied perspective, it may open up new markets towards transnatural, bioinspired materials that harness both, the high performance of biogels and the remarkable versatility inherent to synthetic polymers.

In this context, earlier work showed that the stiffness of the matrix crucially determines the differentiation of stem cells cultivated on synthetic substrates[92,93]. Complementarily, it was also revealed that cells spread and grow faster on stiffer artificial matrices than they do on softer ones[94,95]. While the stiffness of a hydrogel –defined by its G'– can be easily modulated by either changing polymer or crosslinker concentration as was shown for polyacrylamide networks[96], emulating the elasticity and, in particular, the mechanical responsiveness of biogels has proven to be a challenging task. The reasons are briefly outlined in section 1.2 and allude to the general difficulty in obtaining synthetic polymers able to aggregate into robust, stiff bundles.

Recent developments in the creation of synthetic strain-stiffening materials have been introduced by Sheiko and co-workers[97]. Here, comb- and brush-like elastomers based on poly(dimethylsiloxane) (PDMS) and poly(n-butyl acrylate) (PBA) were engineered to replicate the strain-stiffening mechanisms of a variety of soft tissues, including lung or arterial tissue. These novel elastomers showcase how a precise control over architectural parameters can be actively exploited to modulate the mechanical features of the elastomers. Nonetheless, the absence of water (or any solvent whatsoever) within these materials limits their resemblance with biological networks.

Alternatively, some physically associating polymer networks containing solvent have been shown to exhibit pronounced stiffening response to deformation prior softening[98–101]. Nevertheless, the delayed onset of strain-stiffening in these system lies well beyond the biologically relevant regime limiting their biomimicry[17].

1.5.1. Biomimetic strain-stiffening hydrogels

Cells in mechanically responsive hydrogels actively exert forces generally by pulling on fibers, allowing for cellular traction and transduction of mechanical cues at various lengthscales[94,102]. Recently, strain-stiffening has been identified to enhance cell spreading and osteogenic differentiation in soft biopolymer substrates[14,103,104]. Thus, the design of biomimetic strain-stiffening hydrogels holds promising potential in a wide variety of applications, particularly in the biomedical field.

Rowan and co-workers introduced a major breakthrough in this area with the preparation of polyisocyanopeptides (PICs) polymers grafted with short oligo(ethylene glycol) (OEG) blocks[105]. PICs fold in a proteinlike fashion forming β-helices, stabilised through intramolecular peptidic hydrogen-bonds arranged parallel to the polymer backbone (Fig. 1.7). These protein mimics are soluble in cold water, yet on heating beyond the lower critical solution temperature (LCST) of the peripheral OEGs, the system undergoes a sol-gel phase transition that yields transparent hydrogels at remarkably low polymer concentration[106]. The gelation process relies on physical aggregation of individual PIC chains forming bundles of well-defined dimensions in which, the helical architecture of the polymer backbone controls the assembly process, such that, an increase of polymer length and/or concentration does not increase the aggregation number N[106,107]. Aggregation of PIC chains is essential to endow the bundles with L_p orders of magnitude higher than the typical L_p of isolated

polymer chains. Mechanically, PIC networks share crucial metrics with gels composed of neurofilament fibers –both at a single-filament and network levels– reaching, for instance, the upper limit of m = 3/2 at high stresses consistent with IF and AF networks, whose mechanics are best described by entropic stiffening models as was previously discussed in section 1.3.1. PIC gels showcase the potential of synthetic polymers to introduce a continuous variation of properties –both in linear and non-linear regimes– via modification of readily tuneable parameters[106,108]. In addition, PICs were recently combined with flexible, semi-flexible and rigid elements to form composite networks that recreate some of the synergies found between cytoskeletal and extracellular subsystems[109].

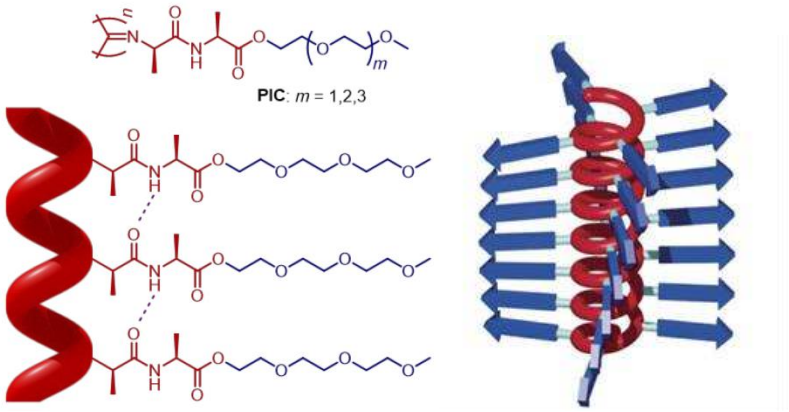

Fig. 1.6 | Molecular structure of PICs depicting the 4_1 β-sheet helical backbone stabilised via peptidic intra-chain dialanyl hydrogen bonds (dotted lines). PICs consist of a stiff polymer backbone (red) grafted with flexible oligo(ethylene glycol) chains of varying lengths (blue). Figure adapted with permission from ref. [106]. Copyright © 2013, Springer Nature.

Despite the general success of PIC gels in mimicking the strain-stiffening mechanisms of biopolymer networks, they rely on covalent polymers and their aggregation into bundles to achieve functionality and mechanical stability. By contrast, filamentous proteins realise dynamics and functionality via more structured assembly processes, allowing for structural adaptation through rapid assembly and disassembly. Along these lines, several synthetic molecules have been engineered to self-assemble into fibrous polymers in a highly specific and controlled manner, usually by introducing directional, self-recognition motifs. We argue that the so-obtained polymers are better suited to mimic the hierarchy and, particularly, the dynamic aspects of fibrous proteinaceous assemblies[110].

1.6. Fibrous supramolecular polymers in water

Supramolecular fibers consist of one-dimensional (1D) arrays of repeating subunits, linked together via non-covalent interactions leading to a rich variety of hierarchical structures, including ribbons, helices or tubes[111–113]. In contrast to classic covalent polymers, supramolecular fibers –and by extension all supramolecular polymers– are inherently dynamic with exchange rates that can be modulated by tuning the strength of the supramolecular interaction, thereby, allowing to cover multiple timescales. In water, bio- and synthetic supramolecular monomers polymerize via five fundamental types of non-covalent interactions, namely hydrophobic effects, hydrogen bonds, hydrophilic, coulombic and van der Waals interactions[114]. Because of its directionality and specificity, H-bonding motifs play a pivotal role in the rational design of fiber-forming monomers, generally, accommodated within a hydrophobic envelope that shields the motif from competing H-bonding with the surrounding water molecules –which otherwise would weaken or solvate the assemblies–[115].

Common fiber-forming monomers based on H-bonding motifs include ureido-pyrimidinone (UPy)[116–118], benzene tricarboxamide (BTA)[119–123], bis(ureas)[124–127], various examples of engineered amphiphilic peptides[128–131]. More recently, the squaramide synthon was introduced in the context of supramolecular polymers. Squaramide-based polymers were shown to harness the synergy between aromatic gain and H-bonding to produce very robust, high aspect ratio nanofibers[132]. Henceforth, we will focus exclusively on the bis-urea motif and, more specifically, on OEG-flanked bis-urea bola-amphiphiles, which self-assemble in water into long, persistent fibers that provide an excellent platform to mimic filamentous proteins.

1.7. Bis-urea bolaamphiphiles

The synthesis of urea in 1828 marks the birth of synthetic organic chemistry[133]. Ever since, ureas have found widespread use in many areas of organic as well as supramolecular chemistry due to their ability to form strong, bifurcated hydrogen bonds[134,135]. The term bis-urea refers to two urea groups placed in the vicinity within the same molecule, forming pairs of bifurcated H-bonds arranged parallel or anti-parallel relative to each other. In this context, bis-ureas have been extensively utilized in a variety of systems, including gels –both organo- and hydrogels–[126,127,136–138],

surfaces[139], thermoplastic elastomers[140–143] or supramolecular polymers[125,144–148], in which strong, 1 D assembly is required. Typically, self-assembling molecules based on the bis-urea synthon incorporate phenylene[149,150], tolylene[147,148], cyclohexylene[137,144,151] or aliphatic spacers[124,125,144,152] placed in between urea groups.

As mentioned before in section 1.9, one particularly interesting group of bis-urea-based molecules are OEG-flanked bisurea bolaamphiles (UnU) (Fig. 1.7.a). These type of non-ionic amphiphiles incorporate short alkyl spacers of variable length – constituted by 'n' methylene groups– placed in between the two urea groups. These molecules are, moreover, equipped with long hydrophobic spacers that minimise the interaction of water with the H-bonding array. Thus, when dissolved in water, UnU's stack on top of each other through a combined interplay of intermolecular urea-urea H-bonds and hydrophobic interactions (Fig. 1.7.b). The so-formed assemblies can be regarded as a densely packed hydrophobic core, surrounded by a swollen corona of solvated OEG segments (Fig. 1.7.b). More recently, UnU´s as well as other bolaamphiphic constructs have been found to exist in water as multiple stacks (or ribbons) interacting mainly through hydrophobic effects perpendicular to the fiber axis (Fig. 1.7.c)[132,146]. Ultimately, semi-flexibility in these assemblies arises from the tight packing of monomers in the parallel direction, in combination with their tendency to bundle in the lateral direction of the fiber.

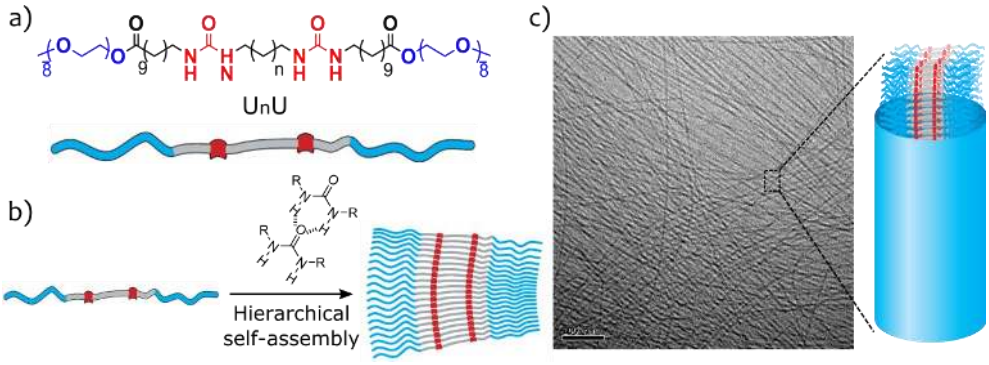

Fig. 1.7 | (a) Molecular structure of OEG-flanked (blue) bis-urea bolaamphiphiles UnU. The index n designates the number of methylenes between urea groups (red). (b) Hierarchical self-assembly through bifurcated urea-urea H-bonding and hydrophobic effects. (c) cryo-EM micrograph showing the fibers formed upon assembly of U3U in water at 1 mg mL^{-1}. Scale bar: 100 nm. Proposed fiber architecture integrating multiple ribbons arranged perpendicularly relative to the fiber axis.

Previous work showed, moreover, how continuous variation of molecular parameters could be actively used to tune the morphological features of UnU fibers[124]. Concurrently, Pal *et al.* showed that, although the morphology of fibers containing slightly different central alkyl spacers is similar, they tend to self-sort in solution due to mismatch of the self-assembling bis-urea motifs, thereby, giving rise to separated micellar populations[125,144]. This feature was later used to optimise the mechanical properties of gels constituted from UnU fibers.

1.8. Bis-urea bolaamphile-based hydrogels

As previously described in section 1.6.1, UnU fibers recapitulate some critical features of filamentous proteins, *i.e.* they form dynamic, stiff, high-aspect-ratio fibers through hierarchical self-assembly while, at the same time, integrate multiple ribbons per fiber. This combination of properties makes them attractive building blocks to construct biomimetic strain-stiffening gels. In contrast to PIC polymers, however (section 1.5)[106,108], UnU fibers do not form entangled networks on their own, requiring the synthesis of specifically designed cross-linkers.

To this end, previous work sought to cross-link UnU fibers using linear segmented copolymers[127]. Such copolymers bear multiple bis-urea hard segments interconnected by long poly(ethylene oxide) (PEO) linkers. Gelation in these systems relies on the formation of physical crosslinks, where the bis-urea hard segments of the copolymers incorporate into the matching hydrophobic core of UnU rods by means of urea-urea H-bonding and hydrophobic interactions. Note that, this is an inherently indiscriminate crosslinking strategy, *i.e.* the same copolymer can either connect two different micellar rods (active crosslink) or form intramicellar loops (inactive crosslink). The gels obtained following this approach featured both shear-thinning and self-healing properties, being able to flow through the narrow gauge of a needle and reform once the shear stress is removed.

Subsequent attempts to improve the network connectivity were conceived on the basis of self-sorting[126]. Along these lines, hetero (6×4) and homo-crosslinkers (6×6) composed of two of the bis-urea motifs also found in the bolaamphiphiles were synthesized (Fig. 1.8.a). Hence, adding (6×6) to an aqueous solution of U6U can, in analogy to the previous example, give rise to the formation of both, active and inactive crosslinks. Conversely, adding (6×4) to a mixture of self-sorted U4U and U6U minimises the probability to form inactive loops (Fig. 1.8.b). Indeed, suppression of

inactive loops led to hydrogels characterised by moduli 10 times higher than those formed through indiscriminate cross-linking strategies at the same bolaamphiphile concentration (Fig. 1.8.c).

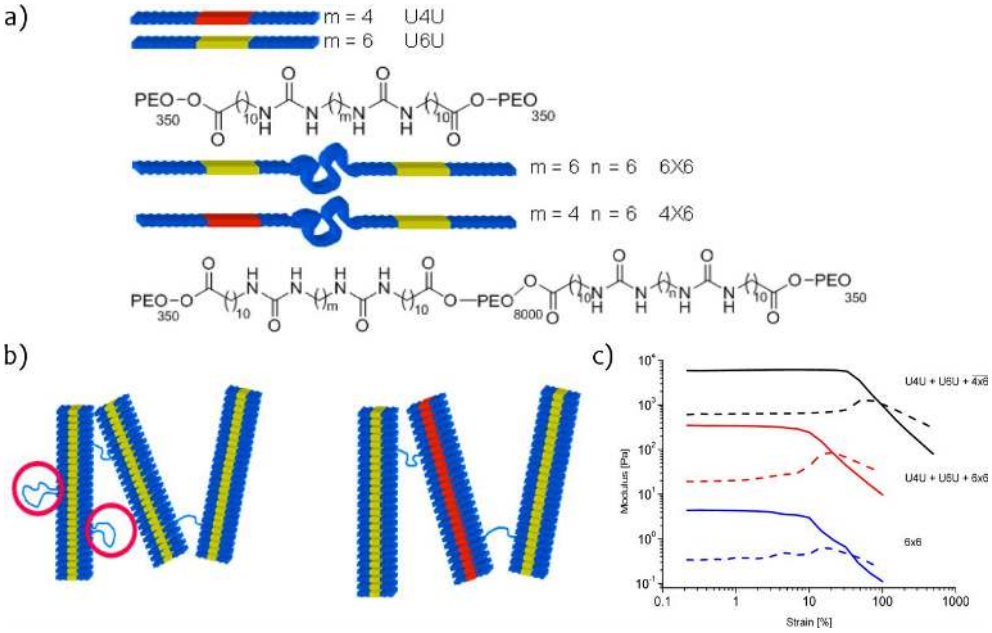

Fig. 1.8 | (a) Structures of the bolaamphiphiles (UmU) and cross-linkers (mXn). The numbers m and n designate the number of methylenes between urea groups. (b) Indiscriminate crosslinking strategy characterised by the formation of both, active and inactive crosslinks (left); suppression of loop formation in a system of self-sorted bolaamphiphiles and hetero-crosslinkers (right). (c) Strain-dependent storage (solid line) and loss (dotted line), showing the effect of homo- and hetero-crosslinking at a fixed concentration. Figure adapted with permission from ref. [126]. Copyright © 2014, American Chemical Society.

Despite the general success in forming stable, self-healing hydrogels by physically crosslinking UnU fibers, the absence (or strongly delayed onset) of strain-stiffening in these materials (Fig. 1.8.c) might be rooted in the following assumptions: (1) The use of long, polymeric PEO (Mw = 8 KDa) linkers dominate the elasticity at low-to-intermediate strains, preventing the network to rapidly enter its nonlinear extensional regime. (2) The inherently weak physical connections that impart mechanical stability to the network yield at strains below the critical strain needed to access the nonlinear deformation regime. An approach to circumvent the former would consist in replacing the long PEG linkers by short oligomeric segments as theoretically

hypothesized[153,154], while strain-yielding due to failure of the supramolecular interactions could be resolved by reinforcing the fibers with covalent bonds.

1.9. Fiber reinforcement through diacetylene cross-polymerization

Since the appearance of the seminal work of Wegner *et al.* by which the reactivity of certain unsubstituted diacetylenes (DA) was rationalised in terms of a polymerization reaction, polydiacetylene (PDA) research has rapidly evolved spanning across multiple disciplines[155].

DAs are known to photo-polymerize in the solid state as well as in solution, provided DA monomers are pre-organized at a specific orientation and distance of 4.9 Å, which corresponds to the repeat distance of the final PDA polymer[156]. PDAs possess an alternating ene-yne conjugated backbone. Thus, owing to extensive electron delocalisation within the linear π-conjugated framework, they strongly absorb light in the visible spectral region and exhibit in most cases blue color[157,158]. Moreover, one of the hallmarks of PDAs is their responsiveness towards multiple environmental stimuli leading to intense colorimetric transformations. This feature has been extensively utilized to develop chromatic sensors in a wide range of systems, including vesicles[159,160], thermoplastic elastomers[161,162], peptide amphiphiles[163–166], Langmuir monolayers[167–169], or self-assembled films[170,171]. In these systems, changes in the π-conjugated framework produce a visible change in colour, usually from blue to red as the polydiacetylenic backbone becomes less structured resulting in shorter delocalization lengths. In supramolecular assemblies, DA polymerization has proven to be a useful technique to freeze or reinforce certain morphologies[172].

Bis-ureas are also able to pre-organize diacetylenic monomers, both at the right distance and orientation (Fig. 1.9). This has enabled covalent fixation of bis-urea-based supramolecular polymers in the solid state or assembled in solution[162,173]. In our group, several analogue bis-urea bolaamphiphiles containing a photo-polymerizable DA unit in between ureas (Fig. 1.10.a) were synthesized, and the molecular parameters required to achieve a good compromise between water-compatibility and DA-polymerization were optimized[174]. In analogy to UnU's, DA monomers formed semi-flexible fibers in water while, at the same time, undergo covalent fixation under UV exposure, leading to high degrees of polymerization as well as full retention of the fiber morphology (Fig. 1.10.c).

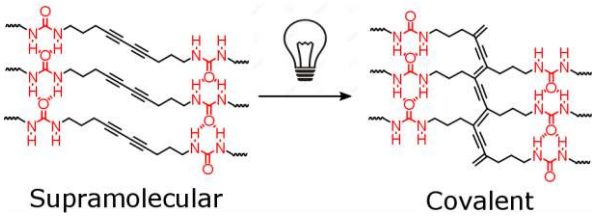

Fig. 1.9 | Diacetylene topochemical photo-polymerization, pre-organized via bis-urea self-assembly and the resulting ene-yne conjugated backbone.

As alluded to earlier, PDA research has, almost exclusively, focused on the outstanding chromatic and/or semi-conducting properties of these π-conjugated polymers. However, the role of covalent fixation on general mechanics and, in particular, on the mechanical properties of supramolecular hydrogels is an area that, to the best of our knowledge, remains largely overlooked.

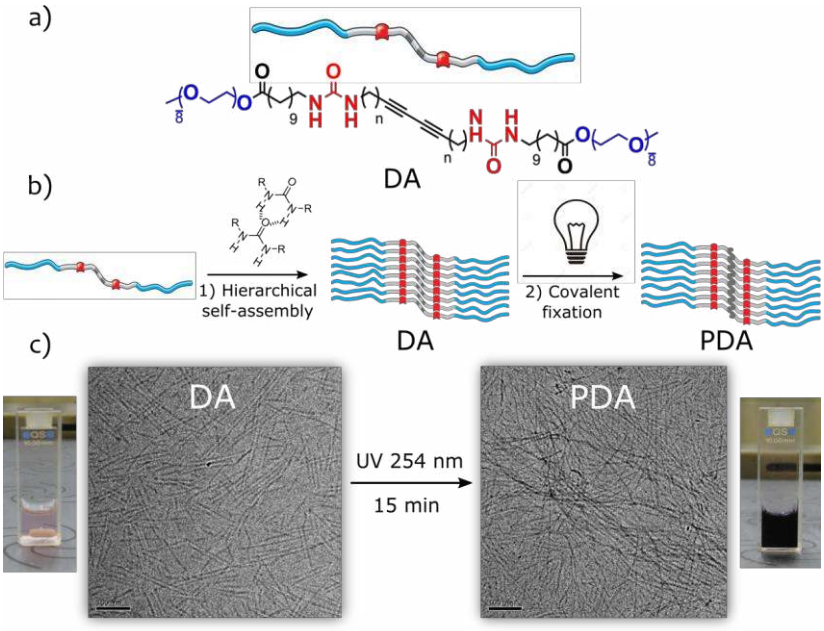

Fig. 1.10 | (a) Molecular structure of the diacetylene bis-urea bolaamphiphile. (b) Hierarchical self-assembly through bifurcated H-bonding and hydrophobic effects, followed by covalent fixation via photo-polymerization of the stacked diacetylenes. (c) cryo-TEM micrographs of DA and PDA at 1 mg mL^{-1} before and after UV (254 nm) exposure, showing no changes in morphology upon covalent fixation. Scale bar: 100 nm. The figure also illustrates the changes in optical properties resulting from the formation of π-conjugated ene-yne backbone. Cryo-EM micrographs adapted with permission from ref. [174]. Copyright © 2013, Royal Society of Chemistry.

1.10. Aim and outline of this thesis

Within the scope of this thesis, we seek to develop fully synthetic strain-stiffening hydrogels based on diacetylene bis-urea bolaamphiphiles able to mimic the mechanics of biopolymer networks in nearly all relevant senses. Unlike previously reported biomimetic PIC hydrogels (section 1.5.1), herein, the crucial fiber-forming step relies on a hierarchical, self-assembly process that harnesses the specificity and directionality of the bis-urea self-recognition motif.

In a more fundamental sense, this manuscript intends to address three major questions: (1) Is it possible to create robust, strain-stiffening hydrogels from dynamic, supramolecular fibers. In other words: Can stability coexist with stimuli responsiveness? (2) What is the role of fiber covalent fixation on the mechanics of biomimetic hydrogels? (3) Can we emulate complex biological functions, such as stiffening through internal stress generation –in analogy to myosin motor proteins– using fully synthetic building blocks?

In **Chapter 2**, we present a strategy based on click chemistry to chemically crosslink covalently fixated (PDA) fibers, while supressing the formation of inactive loops. The so-formed hydrogels feature strain-stiffening with unusual, yet universal stress-strain response. We show, moreover, how the structure of the gels mirrors that of the fibers in solution with no increase in fiber size upon gelation (*i.e.* no bundling).

In **Chapter 3**, self-assembled DA fibers are chemically crosslinked without previous covalent fixation step. In solution, DA fibers are in dynamic equilibrium with exchange rates that span several days, thereby, indicative of strong intermolecular interactions. DA fibers dissociate into smaller fragments under sonication and self-heal to recover their length at equilibrium. Chemical crosslinking of the fibers yields strain-stiffening gels with highly tuneable mechanical properties.

Chapter 4 addresses the role of fiber internal and external covalent fixation (*i.e.* along the hydrophilic corona of the fibers). We find, for instance, that internal fiber fixation through DA-polymerization imparts sufficient mechanical stability to the fibers enabling them to withstand prolonged exposure to ultrasonication. Macroscopically, gels constituted from internally and externally reinforced fibers stiffen under applied stress by nearly 100-fold before rupture. Such stiffening ranges are reminiscent of many biopolymer gels as well as PIC networks (Section 1.5.1),

where mechanical responsiveness and stability are realised by making use of covalent polymers.

Chapter 5 presents an alternative method to crosslink PDA fibers using a thermo-responsive, linear polymer. By heating above the LCST of the polymer we are able to induce internal contractile stresses in the PDA fibrous scaffold, leading to a macroscopic stiffening that increases by up to 3 orders of magnitude. Pre-stressed PDA gels share, moreover, crucial metrics with actin networks pre-stressed by myosin II molecular motors as well as pre-stressed fibroblasts.

1.11. References

1. White, C. R. & Frangos, J. A. The shear stress of it all: the cell membrane and mechanochemical transduction. *Philos. Trans. R. Soc. B Biol. Sci.* **362,** 1459–1467 (2007).
2. Huiskes, R., Ruimerman, R., van Lenthe, G. H. & Janssen, J. D. Effects of mechanical forces on maintenance and adaptation of form in trabecular bone. *Nature* **405,** 704–706 (2000).
3. Sumpio, B. E., Banes, A. J., Levin, L. G. & Johnson, G. Mechanical stress stimulates aortic endothelial cells to proliferate. *J. Vasc. Surg.* **6,** 252–256 (1987).
4. Friedl, P. & Wolf, K. Plasticity of cell migration: a multiscale tuning model. *J. Cell Biol.* **188,** 11–19 (2010).
5. Lecuit, T. & Lenne, P.-F. Cell surface mechanics and the control of cell shape, tissue patterns and morphogenesis. *Nat. Rev. Mol. Cell Biol.* **8,** 633–644 (2007).
6. Rodriguez, O. C. *et al.* Conserved microtubule–actin interactions in cell movement and morphogenesis. *Nat. Cell Biol.* **5,** 599–609 (2003).
7. Chung, B.-M., Rotty, J. D. & Coulombe, P. A. Networking galore: intermediate filaments and cell migration. *Curr. Opin. Cell Biol.* **25,** 600–612 (2013).
8. Chang, L. & Goldman, R. D. Intermediate filaments mediate cytoskeletal crosstalk. *Nat. Rev. Mol. Cell Biol.* **5,** 601–613 (2004).
9. Huber, F., Boire, A., López, M. P. & Koenderink, G. H. Cytoskeletal crosstalk: when three different personalities team up. *Curr. Opin. Cell Biol.* **32,** 39–47 (2015).
10. Laurens, N., Koolwijk, P. & De Maat, M. P. M. Fibrin structure and wound healing. *J. Thromb. Haemost.* **4,** 932–939 (2006).
11. Gelse, K., Pöschl, E. & Aigner, T. Collagens—structure, function, and biosynthesis. *Adv. Drug Deliv. Rev.* **55,** 1531–1546 (2003).
12. Claessens, M. M. a. E., Semmrich, C., Ramos, L. & Bausch, A. R. Helical twist controls the thickness of F-actin bundles. *Proc. Natl. Acad. Sci.* **105,** 8819–8822 (2008).
13. Rudnicki, M. S. *et al.* Nonlinear Strain Stiffening Is Not Sufficient to Explain How Far Cells Can Feel on Fibrous Protein Gels. *Biophys. J.* **105,** 11–20 (2013).
14. Winer, J. P., Oake, S. & Janmey, P. A. Non-Linear Elasticity of Extracellular Matrices Enables Contractile Cells to Communicate Local Position and Orientation. *PLOS ONE* **4,** e6382 (2009).
15. Huber, F. *et al.* Emergent complexity of the cytoskeleton: from single filaments to tissue. *Adv. Phys.* (2013).
16. Kasza, K. E. *et al.* The cell as a material. *Curr. Opin. Cell Biol.* **19,** 101–107 (2007).
17. Storm, C., Pastore, J. J., MacKintosh, F. C., Lubensky, T. C. & Janmey, P. A. Nonlinear elasticity in biological gels. *Nature* **435,** 191–194 (2005).
18. Kang, H. *et al.* Nonlinear Elasticity of Stiff Filament Networks: Strain Stiffening, Negative Normal Stress, and Filament Alignment in Fibrin Gels†. *J. Phys. Chem. B* **113,** 3799–3805 (2009).

19. Janmey, P. A. *et al.* Negative normal stress in semiflexible biopolymer gels. *Nat. Mater.* **6,** 48–51 (2007).
20. Piechocka, I. K. *et al.* Multi-scale strain-stiffening of semiflexible bundle networks. *Soft Matter* **12,** 2145–2156 (2016).
21. Kurniawan, N. A., Grimbergen, J., Koopman, J. & Koenderink, G. H. Factor XIII stiffens fibrin clots by causing fiber compaction. *J. Thromb. Haemost.* **12,** 1687–1696 (2014).
22. Yamauchi, M. & Sricholpech, M. Lysine post-translational modifications of collagen. *Essays Biochem.* **52,** 113–133 (2012).
23. Pritchard, R. H., Huang, Y. Y. S. & Terentjev, E. M. Mechanics of biological networks: from the cell cytoskeleton to connective tissue. *Soft Matter* **10,** 1864–1884 (2014).
24. Anseth, K. S., Bowman, C. N. & Brannon-Peppas, L. Mechanical properties of hydrogels and their experimental determination. *Biomaterials* **17,** 1647–1657 (1996).
25. Wen, Q., Basu, A., Janmey, P. A. & Yodh, A. G. Non-affine deformations in polymer hydrogels. *Soft Matter* **8,** 8039–8049 (2012).
26. MacKintosh, F. C., Käs, J. & Janmey, P. A. Elasticity of Semiflexible Biopolymer Networks. *Phys. Rev. Lett.* **75,** 4425–4428 (1995).
27. Onck, P. R., Koeman, T., van Dillen, T. & van der Giessen, E. Alternative Explanation of Stiffening in Cross-Linked Semiflexible Networks. *Phys. Rev. Lett.* **95,** 178102 (2005).
28. Lieleg, O., Claessens, M. M. a. E., Heussinger, C., Frey, E. & Bausch, A. R. Mechanics of Bundled Semiflexible Polymer Networks. *Phys. Rev. Lett.* **99,** 088102 (2007).
29. Licup, A. J. *et al.* Stress controls the mechanics of collagen networks. *Proc. Natl. Acad. Sci.* **112,** 9573–9578 (2015).
30. Broedersz, C. P. *et al.* Measurement of nonlinear rheology of cross-linked biopolymer gels. *Soft Matter* **6,** 4120–4127 (2010).
31. Gardel, M. L. *et al.* Elastic Behavior of Cross-Linked and Bundled Actin Networks. *Science* **304,** 1301–1305 (2004).
32. Gardel, M. L. *et al.* Stress-Dependent Elasticity of Composite Actin Networks as a Model for Cell Behavior. *Phys. Rev. Lett.* **96,** 088102 (2006).
33. Basu, A. *et al.* Nonaffine Displacements in Flexible Polymer Networks. *Macromolecules* **44,** 1671–1679 (2011).
34. Legant, W. R. *et al.* Measurement of mechanical tractions exerted by cells in three-dimensional matrices. *Nat. Methods* **7,** 969–971 (2010).
35. Lin, Y.-C. *et al.* Origins of Elasticity in Intermediate Filament Networks. *Phys. Rev. Lett.* **104,** 058101 (2010).
36. The Three-Dimensional Dynamics of Actin Waves, a Model of Cytoskeletal Self-Organization. *Biophys. J.* **96,** 2888–2900 (2009).
37. Swaney, K. F., Huang, C.-H. & Devreotes, P. N. Eukaryotic Chemotaxis: A Network of Signaling Pathways Controls Motility, Directional Sensing, and Polarity. *Annu. Rev. Biophys.* **39,** 265–289 (2010).
38. Gittes, F., Mickey, B., Nettleton, J. & Howard, J. Flexural rigidity of microtubules and actin filaments measured from thermal fluctuations in shape. *J. Cell Biol.* **120,** 923–934 (1993).
39. Cooper, G. M. Structure and Organization of Actin Filaments. (2000).
40. Gardel, M. L. *et al.* Prestressed F-actin networks cross-linked by hinged filamins replicate mechanical properties of cells. *Proc. Natl. Acad. Sci. U. S. A.* **103,** 1762–1767 (2006).
41. Ruddies, R., Goldmann, W. H., Isenberg, G. & Sackmann, E. The viscoelasticity of entangled actin networks: the influence of defects and modulation by talin and vinculin. *Eur. Biophys. J.* **22,** 309–321 (1993).
42. Head, D. A., Levine, A. J. & MacKintosh, F. C. Deformation of Cross-Linked Semiflexible Polymer Networks. *Phys. Rev. Lett.* **91,** 108102 (2003).

43. Liu, J., Koenderink, G. H., Kasza, K. E., MacKintosh, F. C. & Weitz, D. A. Visualizing the Strain Field in Semiflexible Polymer Networks: Strain Fluctuations and Nonlinear Rheology of F-Actin Gels. *Phys. Rev. Lett.* **98,** 198304 (2007).
44. Lieleg, O., Claessens, M. M. A. E. & Bausch, A. R. Structure and dynamics of cross-linked actin networks. *Soft Matter* **6,** 218–225 (2010).
45. Schmoller, K. M., Lieleg, O. & Bausch, A. R. Structural and Viscoelastic Properties of Actin/Filamin Networks: Cross-Linked versus Bundled Networks. *Biophys. J.* **97,** 83–89 (2009).
46. Mücke, N. *et al.* Assessing the Flexibility of Intermediate Filaments by Atomic Force Microscopy. *J. Mol. Biol.* **335,** 1241–1250 (2004).
47. Windoffer, R., Beil, M., Magin, T. M. & Leube, R. E. Cytoskeleton in motion: the dynamics of keratin intermediate filaments in epithelia. *J. Cell Biol.* **194,** 669–678 (2011).
48. Herrmann, H. & Aebi, U. Intermediate Filaments: Molecular Structure, Assembly Mechanism, and Integration Into Functionally Distinct Intracellular Scaffolds. *Annu. Rev. Biochem.* **73,** 749–789 (2004).
49. Kreplak, L., Bär, H., Leterrier, J. F., Herrmann, H. & Aebi, U. Exploring the Mechanical Behavior of Single Intermediate Filaments. *J. Mol. Biol.* **354,** 569–577 (2005).
50. Janmey, P. A., Euteneuer, U., Traub, P. & Schliwa, M. Viscoelastic properties of vimentin compared with other filamentous biopolymer networks. *J. Cell Biol.* **113,** 155–160 (1991).
51. Köster, S., Weitz, D. A., Goldman, R. D., Aebi, U. & Herrmann, H. Intermediate filament mechanics in vitro and in the cell: from coiled coils to filaments, fibers and networks. *Curr. Opin. Cell Biol.* **32,** 82–91 (2015).
52. Bertaud, J., Qin, Z. & Buehler, M. J. Intermediate filament-deficient cells are mechanically softer at large deformation: A multi-scale simulation study. *Acta Biomater.* **6,** 2457–2466 (2010).
53. Wang, N. *et al.* Cell prestress. I. Stiffness and prestress are closely associated in adherent contractile cells. *Am. J. Physiol. - Cell Physiol.* **282,** C606–C616 (2002).
54. Pampaloni, F. *et al.* Thermal fluctuations of grafted microtubules provide evidence of a length-dependent persistence length. *Proc. Natl. Acad. Sci.* **103,** 10248–10253 (2006).
55. Mandelkow, E. M., Mandelkow, E. & Milligan, R. A. Microtubule dynamics and microtubule caps: a time-resolved cryo-electron microscopy study. *J. Cell Biol.* **114,** 977–991 (1991).
56. Lin, Y.-C., Koenderink, G. H., MacKintosh, F. C. & Weitz, D. A. Viscoelastic Properties of Microtubule Networks. *Macromolecules* **40,** 7714–7720 (2007).
57. Brangwynne, C. P., Koenderink, G. H., MacKintosh, F. C. & Weitz, D. A. Nonequilibrium Microtubule Fluctuations in a Model Cytoskeleton. *Phys. Rev. Lett.* **100,** 118104 (2008).
58. Bai, M., Missel, A. R., Klug, W. S. & Levine, A. J. The mechanics and affine–nonaffine transition in polydisperse semiflexible networks. *Soft Matter* **7,** 907–914 (2011).
59. Etienne-Manneville, S. Microtubules in Cell Migration. *Annu. Rev. Cell Dev. Biol.* **29,** 471–499 (2013).
60. Gordon, M. K. & Hahn, R. A. Collagens. *Cell Tissue Res.* **339,** 247 (2010).
61. Robins, S. P. & Bailey, A. J. The chemistry of the collagen cross-links. Characterization of the products of reduction of skin, tendon and bone with sodium cyanoborohydride. *Biochem. J.* **163,** 339–346 (1977).
62. Buehler, M. J. Nanomechanics of collagen fibrils under varying cross-link densities: Atomistic and continuum studies. *J. Mech. Behav. Biomed. Mater.* **1,** 59–67 (2008).
63. Heussinger, C. & Frey, E. Role of architecture in the elastic response of semiflexible polymer and fiber networks. *Phys. Rev. E* **75,** 011917 (2007).
64. Arevalo, R. C., Urbach, J. S. & Blair, D. L. Size-Dependent Rheology of Type-I Collagen Networks. *Biophys. J.* **99,** L65–L67 (2010).
65. Stein, A. M., Vader, D. A., Weitz, D. A. & Sander, L. M. The micromechanics of three-dimensional collagen-I gels. *Complexity* **16,** 22–28 (2011).
66. Vader, D., Kabla, A., Weitz, D. & Mahadevan, L. Strain-Induced Alignment in Collagen Gels. *PLOS ONE* **4,** e5902 (2009).

67. Weisel, J. W. & Litvinov, R. I. Mechanisms of fibrin polymerization and clinical implications. *Blood* **121,** 1712–1719 (2013).
68. Ariëns, R. A. S., Lai, T.-S., Weisel, J. W., Greenberg, C. S. & Grant, P. J. Role of factor XIII in fibrin clot formation and effects of genetic polymorphisms. *Blood* **100,** 743–754 (2002).
69. Shen, L. & Lorand, L. Contribution of fibrin stabilization to clot strength. Supplementation of factor XIII-deficient plasma with the purified zymogen. *J. Clin. Invest.* **71,** 1336–1341 (1983).
70. Collet, J.-P., Shuman, H., Ledger, R. E., Lee, S. & Weisel, J. W. The elasticity of an individual fibrin fiber in a clot. *Proc. Natl. Acad. Sci. U. S. A.* **102,** 9133–9137 (2005).
71. Hategan, A., Gersh, K. C., Safer, D. & Weisel, J. W. Visualization of the dynamics of fibrin clot growth 1 molecule at a time by total internal reflection fluorescence microscopy. *Blood* **121,** 1455–1458 (2013).
72. Shah, J. V. & Janmey, P. A. Strain hardening of fibrin gels and plasma clots. *Rheol. Acta* **36,** 262–268 (1997).
73. Wen, Q. & Janmey, P. A. Effects of non-linearity on cell–ECM interactions. *Exp. Cell Res.* **319,** 2481–2489 (2013).
74. Voter, W. A., Lucaveche, C. & Erickson, H. P. Concentration of protein in fibrin fibers and fibrinogen polymers determined by refractive index matching. *Biopolymers* **25,** 2375–2384 (1986).
75. Carr, M. E. & Hermans, J. Size and Density of Fibrin Fibers from Turbidity. *Macromolecules* **11,** 46–50 (1978).
76. Brown, A. E. X., Litvinov, R. I., Discher, D. E., Purohit, P. K. & Weisel, J. W. Multiscale Mechanics of Fibrin Polymer: Gel Stretching with Protein Unfolding and Loss of Water. *Science* **325,** 741–744 (2009).
77. Piechocka, I. K., Bacabac, R. G., Potters, M., MacKintosh, F. C. & Koenderink, G. H. Structural Hierarchy Governs Fibrin Gel Mechanics. *Biophys. J.* **98,** 2281–2289 (2010).
78. Liu, W. *et al.* Fibrin Fibers Have Extraordinary Extensibility and Elasticity. *Science* **313,** 634–634 (2006).
79. Place, E. S., Evans, N. D. & Stevens, M. M. Complexity in biomaterials for tissue engineering. *Nat. Mater.* **8,** 457–470 (2009).
80. Peppas, N. A., Hilt, J. Z., Khademhosseini, A. & Langer, R. Hydrogels in Biology and Medicine: From Molecular Principles to Bionanotechnology. *Adv. Mater.* **18,** 1345–1360 (2006).
81. Wichterle, O. & Lím, D. Hydrophilic Gels for Biological Use. *Nature* **185,** 117–118 (1960).
82. Knipe, J. M. & Peppas, N. A. Multi-responsive hydrogels for drug delivery and tissue engineering applications. *Regen. Biomater.* **1,** 57–65 (2014).
83. Hoare, T. R. & Kohane, D. S. Hydrogels in drug delivery: Progress and challenges. *Polymer* **49,** 1993–2007 (2008).
84. Qiu, Y. & Park, K. Environment-sensitive hydrogels for drug delivery. *Adv. Drug Deliv. Rev.* **53,** 321–339 (2001).
85. Annabi, N. *et al.* 25th Anniversary Article: Rational Design and Applications of Hydrogels in Regenerative Medicine. *Adv. Mater.* **26,** 85–124 (2014).
86. Kopeček, J. Hydrogel biomaterials: A smart future? *Biomaterials* **28,** 5185–5192 (2007).
87. Malda, J. *et al.* 25th Anniversary Article: Engineering Hydrogels for Biofabrication. *Adv. Mater.* **25,** 5011–5028 (2013).
88. Hunt, J. A., Chen, R., Veen, T. van & Bryan, N. Hydrogels for tissue engineering and regenerative medicine. *J. Mater. Chem. B* **2,** 5319–5338 (2014).
89. Slaughter, B. V., Khurshid, S. S., Fisher, O. Z., Khademhosseini, A. & Peppas, N. A. Hydrogels in Regenerative Medicine. *Adv. Mater.* **21,** 3307–3329 (2009).
90. Lutolf, M. P. & Blau, H. M. Artificial Stem Cell Niches. *Adv. Mater.* **21,** 3255–3268 (2009).
91. Shin, H., Jo, S. & Mikos, A. G. Biomimetic materials for tissue engineering. *Biomaterials* **24,** 4353–4364 (2003).
92. Engler, A. J., Sen, S., Sweeney, H. L. & Discher, D. E. Matrix Elasticity Directs Stem Cell Lineage Specification. *Cell* **126,** 677–689 (2006).

93. Trappmann, B. *et al.* Extracellular-matrix tethering regulates stem-cell fate. *Nat. Mater.* **11,** 642–649 (2012).
94. Saez, A., Ghibaudo, M., Buguin, A., Silberzan, P. & Ladoux, B. Rigidity-driven growth and migration of epithelial cells on microstructured anisotropic substrates. *Proc. Natl. Acad. Sci.* **104,** 8281–8286 (2007).
95. Yeung, T. *et al.* Effects of substrate stiffness on cell morphology, cytoskeletal structure, and adhesion. *Cell Motil. Cytoskeleton* **60,** 24–34 (2005).
96. Calvet, D., Wong, J. Y. & Giasson, S. Rheological Monitoring of Polyacrylamide Gelation: Importance of Cross-Link Density and Temperature. *Macromolecules* **37,** 7762–7771 (2004).
97. Vatankhah-Varnosfaderani, M. *et al.* Mimicking biological stress–strain behaviour with synthetic elastomers. *Nature* **549,** nature23673 (2017).
98. Erk, K. A., Henderson, K. J. & Shull, K. R. Strain Stiffening in Synthetic and Biopolymer Networks. *Biomacromolecules* **11,** 1358–1363 (2010).
99. Pellens, L., Corrales, R. G. & Mewis, J. General nonlinear rheological behavior of associative polymers. *J. Rheol. 1978-Present* **48,** 379–393 (2004).
100. Suzuki, S., Uneyama, T., Inoue, T. & Watanabe, H. Nonlinear Rheology of Telechelic Associative Polymer Networks: Shear Thickening and Thinning Behavior of Hydrophobically Modified Ethoxylated Urethane (HEUR) in Aqueous Solution. *Macromolecules* **45,** 888–898 (2012).
101. Seitz, M. E. *et al.* Fracture and large strain behavior of self-assembled triblock copolymer gels. *Soft Matter* **5,** 447–456 (2009).
102. Jansen, K. A., Bacabac, R. G., Piechocka, I. K. & Koenderink, G. H. Cells Actively Stiffen Fibrin Networks by Generating Contractile Stress. *Biophys. J.* **105,** 2240–2251 (2013).
103. Wen, Q. & Janmey, P. A. Effects of non-linearity on cell–ECM interactions. *Exp. Cell Res.* **319,** 2481–2489 (2013).
104. Das, R. K., Gocheva, V., Hammink, R., Zouani, O. F. & Rowan, A. E. Stress-stiffening-mediated stem-cell commitment switch in soft responsive hydrogels. *Nat. Mater.* **15,** 318–325 (2016).
105. Cornelissen, J. J. L. M. *et al.* β-Helical Polymers from Isocyanopeptides. *Science* **293,** 676–680 (2001).
106. Kouwer, P. H. J. *et al.* Responsive biomimetic networks from polyisocyanopeptide hydrogels. *Nature* **493,** 651–655 (2013).
107. Jaspers, M. *et al.* Bundle Formation in Biomimetic Hydrogels. *Biomacromolecules* **17,** 2642–2649 (2016).
108. Jaspers, M. *et al.* Ultra-responsive soft matter from strain-stiffening hydrogels. *Nat. Commun.* **5,** 5808 (2014).
109. Jaspers, M. *et al.* Nonlinear mechanics of hybrid polymer networks that mimic the complex mechanical environment of cells. *Nat. Commun.* **8,** ncomms15478 (2017).
110. Picu, R. C. Mechanics of random fiber networks—a review. *Soft Matter* **7,** 6768–6785 (2011).
111. Zayed, J. M., Nouvel, N., Rauwald, U. & Scherman, O. A. Chemical complexity—supramolecular self-assembly of synthetic and biological building blocks in water. *Chem. Soc. Rev.* **39,** 2806–2816 (2010).
112. W. Elemans, J. A. A., E. Rowan, A. & M. Nolte, R. J. Mastering molecular matter. Supramolecular architectures by hierarchical self-assembly. *J. Mater. Chem.* **13,** 2661–2670 (2003).
113. Rest, C., Kandanelli, R. & Fernández, G. Strategies to create hierarchical self-assembled structures via cooperative non-covalent interactions. *Chem. Soc. Rev.* **44,** 2543–2572 (2015).
114. Krieg, E., Bastings, M. M. C., Besenius, P. & Rybtchinski, B. Supramolecular Polymers in Aqueous Media. *Chem. Rev.* **116,** 2414–2477 (2016).
115. Hirschberg, J. H. K. K. *et al.* Helical self-assembled polymers from cooperative stacking of hydrogen-bonded pairs. *Nature* **407,** 167–170 (2000).

116. Dankers, P. Y. W. *et al.* Hierarchical Formation of Supramolecular Transient Networks in Water: A Modular Injectable Delivery System. *Adv. Mater.* **24,** 2703–2709 (2012).
117. Pape, A. C. H. *et al.* Mesoscale Characterization of Supramolecular Transient Networks Using SAXS and Rheology. *Int. J. Mol. Sci.* **15,** 1096–1111 (2014).
118. Bastings, M. M. C. *et al.* A Fast pH-Switchable and Self-Healing Supramolecular Hydrogel Carrier for Guided, Local Catheter Injection in the Infarcted Myocardium. *Adv. Healthc. Mater.* **3,** 70–78 (2014).
119. Lou, X. *et al.* Dynamic diversity of synthetic supramolecular polymers in water as revealed by hydrogen/deuterium exchange. *Nat. Commun.* **8,** ncomms15420 (2017).
120. Cantekin, S., Greef, T. F. A. de & Palmans, A. R. A. Benzene-1,3,5-tricarboxamide: a versatile ordering moiety for supramolecular chemistry. *Chem. Soc. Rev.* **41,** 6125–6137 (2012).
121. Besenius, P. *et al.* Controlling the growth and shape of chiral supramolecular polymers in water. *Proc. Natl. Acad. Sci.* **107,** 17888–17893 (2010).
122. Smulders, M. M. J., Schenning, A. P. H. J. & Meijer, E. W. Insight into the Mechanisms of Cooperative Self-Assembly: The "Sergeants-and-Soldiers" Principle of Chiral and Achiral C3-Symmetrical Discotic Triamides. *J. Am. Chem. Soc.* **130,** 606–611 (2008).
123. Gillissen, M. A. J. *et al.* Triple Helix Formation in Amphiphilic Discotics: Demystifying Solvent Effects in Supramolecular Self-Assembly. *J. Am. Chem. Soc.* **136,** 336–343 (2014).
124. Chebotareva, N., Bomans, P. H. H., Frederik, P. M., Sommerdijk, N. & Sijbesma, R. P. Morphological control and molecular recognition by bis-urea hydrogen bonding in micelles of amphiphilic tri-block copolymers. *Chem. Commun.* 4967–4969 (2005). doi:10.1039/b507171b
125. Pal, A., Karthikeyan, S. & Sijbesma, R. P. Coexisting Hydrophobic Compartments through Self-Sorting in Rod-like Micelles of Bisurea Bolaamphiphiles. *J. Am. Chem. Soc.* **132,** 7842–+ (2010).
126. Koenigs, M. M. E. *et al.* Tuning Cross-Link Density in a Physical Hydrogel by Supramolecular Self-Sorting. *Macromolecules* **47,** 2712–2717 (2014).
127. Pawar, G. M. *et al.* Injectable Hydrogels from Segmented PEG-Bisurea Copolymers. *Biomacromolecules* **13,** 3966–3976 (2012).
128. Greenfield, M. A., Hoffman, J. R., Olvera de la Cruz, M. & Stupp, S. I. Tunable Mechanics of Peptide Nanofiber Gels. *Langmuir* **26,** 3641–3647 (2010).
129. Hartgerink, J. D., Beniash, E. & Stupp, S. I. Self-Assembly and Mineralization of Peptide-Amphiphile Nanofibers. *Science* **294,** 1684–1688 (2001).
130. Baral, A. *et al.* Assembly of an Injectable Noncytotoxic Peptide-Based Hydrogelator for Sustained Release of Drugs. *Langmuir* **30,** 929–936 (2014).
131. Löwik, D. W. P. M. & Hest, J. C. M. van. Peptide based amphiphiles. *Chem. Soc. Rev.* **33,** 234–245 (2004).
132. Saez Talens, V. *et al.* Aromatic Gain in a Supramolecular Polymer. *Angew. Chem. Int. Ed.* **54,** 10502–10506 (2015).
133. Wöhler, F. Ueber künstliche Bildung des Harnstoffs. *Ann. Phys.* **87,** 253–256 (1828).
134. Estroff, L. A., Huang, J. S. & Hamilton, A. D. Fiber formation in water by a mono-urea dicarboxylic acid. *Chem. Commun.* **0,** 2958–2959 (2003).
135. Jadzyn, J., Stockhausen, M. & Zywucki, B. Structure of hydrogen-bonded sym-dialkylureas in nonpolar organic media. *J. Phys. Chem.* **91,** 754–757 (1987).
136. Brinksma, J., Feringa, B. L., Kellogg, R. M., Vreeker, R. & van Esch, J. Rheology and Thermotropic Properties of Bis-Urea-Based Organogels in Various Primary Alcohols. *Langmuir* **16,** 9249–9255 (2000).
137. de Loos, M., van Esch, J., Kellogg, R. M. & Feringa, B. L. Chiral Recognition in Bis-Urea-Based Aggregates and Organogels through Cooperative Interactions. *Angew. Chem. Int. Ed.* **40,** 613–616 (2001).

138. van Esch, J., De Feyter, S., Kellogg, R. M., De Schryver, F. & Feringa, B. L. Self-Assembly of Bisurea Compounds in Organic Solvents and on Solid Substrates. *Chem. – Eur. J.* **3,** 1238–1243 (1997).
139. De Feyter, S. *et al.* Supramolecular Control of Two-Dimensional Phase Behavior. *Chem. – Eur. J.* **9,** 1198–1206 (2003).
140. Wisse, E. *et al.* Segmental Orientation in Well-Defined Thermoplastic Elastomers Containing Supramolecular Fillers. *Macromolecules* **42,** 524–530 (2009).
141. Wisse, E. *et al.* Molecular Recognition in Poly(ε-caprolactone)-Based Thermoplastic Elastomers. *Biomacromolecules* **7,** 3385–3395 (2006).
142. Karthikeyan, S. & Sijbesma, R. P. Probing Strain in Thermoplastic Elastomers Using Fluorescence Resonance Energy Transfer. *Macromolecules* **42,** 5175–5178 (2009).
143. Botterhuis, N. E., Karthikeyan, S., Veldman, D., Meskers, S. C. J. & Sijbesma, R. P. Molecular recognition in bisurea thermoplastic elastomers studied with pyrene-based fluorescent probes and atomic force microscopy. *Chem. Commun.* **0,** 3915–3917 (2008).
144. Pal, A., Besenius, P. & Sijbesma, R. P. Self-Sorting in Rodlike Micelles of Chiral Bisurea Bolaamphiphiles. *J. Am. Chem. Soc.* **133,** 12987–12989 (2011).
145. Lortie, F. *et al.* Structural and Rheological Study of a Bis-urea Based Reversible Polymer in an Apolar Solvent. *Langmuir* **18,** 7218–7222 (2002).
146. Obert, E. *et al.* Both Water- and Organo-Soluble Supramolecular Polymer Stabilized by Hydrogen-Bonding and Hydrophobic Interactions. *J. Am. Chem. Soc.* **129,** 15601–15605 (2007).
147. Brocorens, P. *et al.* Conformational Plasticity of Hydrogen Bonded Bis-urea Supramolecular Polymers. *J. Phys. Chem. B* **117,** 5379–5386 (2013).
148. Ribagnac, P. *et al.* Fluorescent Labeling of a Bisurea-Based Supramolecular Polymer. *J. Phys. Chem. B* **117,** 1958–1966 (2013).
149. Meazza, L. *et al.* Halogen-bonding-triggered supramolecular gel formation. *Nat. Chem.* **5,** 42–47 (2013).
150. Foster, J. A. *et al.* Anion-switchable supramolecular gels for controlling pharmaceutical crystal growth. *Nat. Chem.* **2,** 1037–1043 (2010).
151. Loos, M. de, Friggeri, A., Esch, J. van, Kellogg, R. M. & Feringa, B. L. Cyclohexane bis-urea compounds for the gelation of water and aqueous solutions. *Org. Biomol. Chem.* **3,** 1631–1639 (2005).
152. Lloyd, G. O., Piepenbrock, M.-O. M., Foster, J. A., Clarke, N. & Steed, J. W. Anion tuning of chiral bis(urea) low molecular weight gels. *Soft Matter* **8,** 204–216 (2011).
153. Broedersz, C. P., Storm, C. & MacKintosh, F. C. Effective-medium approach for stiff polymer networks with flexible cross-links. *Phys. Rev. E* **79,** 061914 (2009).
154. Broedersz, C. P., Storm, C. & MacKintosh, F. C. Nonlinear elasticity of composite networks of stiff biopolymers with flexible linkers. *Phys. Rev. Lett.* **101,** 118103 (2008).
155. Baughman, R. H. Solid-state polymerization of diacetylenes. *J. Appl. Phys.* **43,** 4362–4370 (1972).
156. Petruschke, M. Advances in polymer science. Vol. 63. Polydiacetylenes. Hg. von H.-J. CANTOW. ISBN 3-540-13414-X. Berlin/Heidelberg/New York/Tokyo: Springer-Verlag 1984. 149 S., 87 Abb., 11 Tab., DM 98,–. *Acta Polym.* **36,** 644–644 (1985).
157. Chance, R. R. Chromism in Polydiacetylene Solutions and Crystals. *Macromolecules* **13,** 396–398 (1980).
158. Tieke, B. Polymerization of butadiene and butadiyne (diacetylene) derivatives in layer structures. in *Analysis/Reactions/Morphology* 79–151 (Springer, Berlin, Heidelberg, 1985). doi:10.1007/3-540-15482-5_8
159. Charych, D. H., Nagy, J. O., Spevak, W. & Bednarski, M. D. Direct colorimetric detection of a receptor-ligand interaction by a polymerized bilayer assembly. *Science* **261,** 585–588 (1993).
160. Okada, S., Peng, S., Spevak, W. & Charych, D. Color and Chromism of Polydiacetylene Vesicles. *Acc. Chem. Res.* **31,** 229–239 (1998).

161. Nallicheri, R. A. & Rubner, M. F. Thermal and mechanical properties of polyurethane-diacetylene segmented copolymers. I. Molecular weight and annealing effects. *Macromolecules* **23,** 1005–1016 (1990).
162. Koevoets, R. A., Karthikeyan, S., Magusin, P. C. M. M., Meijer, E. W. & Sijbesma, R. P. Cross-Polymerization of Hard Blocks in Segmented Copoly(ether urea)s. *Macromolecules* **42,** 2609–2617 (2009).
163. Hsu, L., Cvetanovich, G. L. & Stupp, S. I. Peptide amphiphile nanofibers with conjugated polydiacetylene backbones in their core. *J. Am. Chem. Soc.* **130,** 3892–3899 (2008).
164. Löwik, D. W. P. M. *et al.* A Highly Ordered Material from Magnetically Aligned Peptide Amphiphile Nanofiber Assemblies. *Adv. Mater.* **19,** 1191–1195 (2007).
165. Asdonk, P. van der, Keshavarz, M., Christianen, P. C. M. & Kouwer, P. H. J. Directed peptide amphiphile assembly using aqueous liquid crystal templates in magnetic fields. *Soft Matter* **12,** 6518–6525 (2016).
166. van den Heuvel, M. *et al.* Patterns of Diacetylene-Containing Peptide Amphiphiles Using Polarization Holography. *J. Am. Chem. Soc.* **131,** 15014–15017 (2009).
167. Biesalski, M. A., Knaebel, A., Tu, R. & Tirrell, M. Cell adhesion on a polymerized peptide–amphiphile monolayer. *Biomaterials* **27,** 1259–1269 (2006).
168. Kajzar, F., Messier, J., Zyss, J. & Ledoux, I. Nonlinear interferometry in Langmuir-Blodgett multilayers of polydiacetylene. *Opt. Commun.* **45,** 133–137 (1983).
169. Batchelder, D. N., Cheng, C., Müller, W. & Smith, B. J. E. A compact Raman microprobe/microscope: Analysis of polydiacetylene Langmuir and Langmuir-Blodgett films. *Makromol. Chem. Macromol. Symp.* **46,** 171–179 (1991).
170. Carpick, R. W., Sasaki, D. Y. & Burns, A. R. First Observation of Mechanochromism at the Nanometer Scale. *Langmuir* **16,** 1270–1278 (2000).
171. Spevak, W., Nagy, J. O. & Charych, D. H. Molecular assemblies of functionalized polydiacetylenes. *Adv. Mater.* **7,** 85–89 (1995).
172. Rondeau-Gagné, S. *et al.* Topochemical Polymerization of Phenylacetylene Macrocycles: A New Strategy for the Preparation of Organic Nanorods. *J. Am. Chem. Soc.* **135,** 110–113 (2013).
173. Yoon, B. *et al.* Inkjet Printing of Conjugated Polymer Precursors on Paper Substrates for Colorimetric Sensing and Flexible Electrothermochromic Display. *Adv. Mater.* **23,** 5492–5497 (2011).
174. Pal, A. *et al.* Topochemical polymerization in self-assembled rodlike micelles of bisurea bolaamphiphiles. *Soft Matter* **10,** 952–956 (2014).

Chapter 2:

Strain-stiffening gels through self-assembly and covalent fixation of semi-flexible fibers†

Abstract: *Biomimetic, strain-stiffening materials are reported, made through self-assembly and covalent fixation of small building blocks to form fibrous hydrogels that are able to stiffen by an order of magnitude in response to applied stress. The gels consist of semi-flexible rodlike micelles of bisurea bolaamphiphiles with oligo(ethylene oxide) (EO) outer blocks and a polydiacetylene (PDA) backbone. The micelles are fibers, composed of 9–10 ribbons. A gelation method based on Cu-catalyzed azide–alkyne cycloaddition (CuAAC), was developed and shown to lead to strain-stiffening hydrogels with unusual, yet universal, linear and nonlinear stress–strain response. Upon gelation, the X-ray scattering profile is unchanged, suggesting that crosslinks are formed at random positions along the fiber contour without fiber bundling. The work expands current knowledge about the design principles and chemistries needed to achieve fully synthetic, biomimetic soft matter with on-demand, targeted mechanical properties.*

†This Chapter is based on published work:

M. Fernandez-Castano Romera, M.; René P. M. Lafleur, Clément Guibert, Ilja K. Voets, Cornelis Storm, and Rint P. Sijbesma. Strain Stiffening Hydrogels through Self-Assembly and Covalent Fixation of Semi-Flexible Fibers. *Angew. Chem. Int. Ed.* **56,** 8771–8775 (2017). DOI: 10.1002/anie.20170404

2.1. Introduction

Many natural soft tissues respond to small strains with a large change in mechanical properties. A particularly advantageous response of natural materials is to stiffen when exposed to small strains. This behaviour can counteract large deformations, which otherwise might compromise their integrity. Such complex, nonlinear mechanical response is shared by a number of proteins arranged into network architectures, including actin[1,2], collagen[3–5], fibrin[6–8], and all types of intermediate filaments[9,10]. However, this type of adaptivity is unmatched in the vast majority of synthetic materials, including many artificial extracellular matrices.

Considerable effort has gone into the creation of synthetic materials that are mechanically indistinguishable from natural systems, for potential application in tissue engineering or regenerative medicine. In this context, a variety of theoretical models has been proposed to establish the fundamental design principles of synthetic biogels[1,11–16]. Early theoretical work[11] suggests that strain-stiffening is inherent to any connected mesh of semi-flexible filaments. In later work[13], it was shown that even for stiff polymers, stiffening is universally expected for generic, geometric reasons. For all its ubiquity in natural materials, the general absence of strong strain-stiffening in synthetic gels is perhaps all the more remarkable. The reason for this, primarily, has been the difficulty to obtain semi-flexible or even stiff polymers (synthetic polymers are generally very flexible) with strong crosslinks or long-lived entanglements which can, moreover, remain intact at sufficiently large stresses to permit the polymers to enter their nonlinear extensional regimes.

Recent work of Kouwer *et al.*[17,18] on entangled networks of bundled polyisocyanopeptides (PICs), presented the first synthetic system mimicking the strain-stiffening mechanisms of biopolymer networks and showed considerable potential to further exploit the high degree of control over design parameters in synthetic molecules. In this chapter, we introduce a novel approach, complementary to the PIC strategy, to create strain stiffening gels. In our system, actual crosslinking is incorporated rather than relying on physical entanglements for connectivity. This approach provides with control over the mesh size, one of the key structural parameters of network gels and crucially implicated in their mechanical response. We use a combination of self-assembly, covalent fixation and click chemistry to develop a novel class of materials that responds to very low stresses. The strategy towards these

gels is shown in Scheme 2.2.a and entails the use of a set of three oligo(EO)-grafted bis-urea bolaamphiphiles (DA, DA-AC and DA-N_3, Fig. 2.1) containing a topochemically polymerizable diacetylene unit in between ureas[19]. In water, these molecules aggregate into elongated, rodlike micelles through urea hydrogen-bonding and hydrophobic interactions. In previous work, we demonstrated that when the fibers are covalently fixated by topochemical polymerization of the diacetylene groups to gain mechanical strength, no gelation takes place[19].

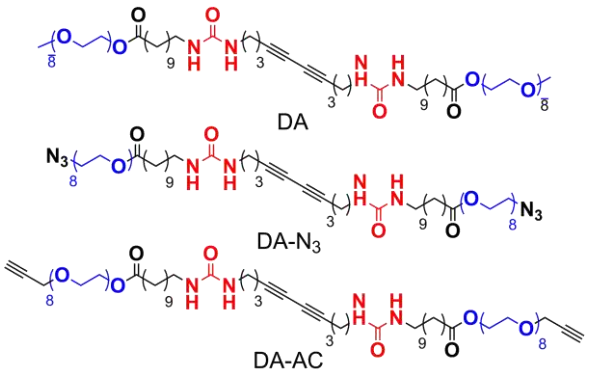

Fig. 2.1 | Molecular structure of the diacetylene bis-urea bolaamphile DA and its functionalized analogues DA-AC and DA-N_3.

In the current work, gels are obtained by a Cu-catalyzed click reaction of azide and acetylene groups that crosslinks fibers without affecting their size (Scheme 2.2.a). The solubility of DA bis-urea bolaamphiphiles in water combined with precise control over the crosslink density allows us to finely tune the network stiffness to access a broad range of storage modulus G' values.

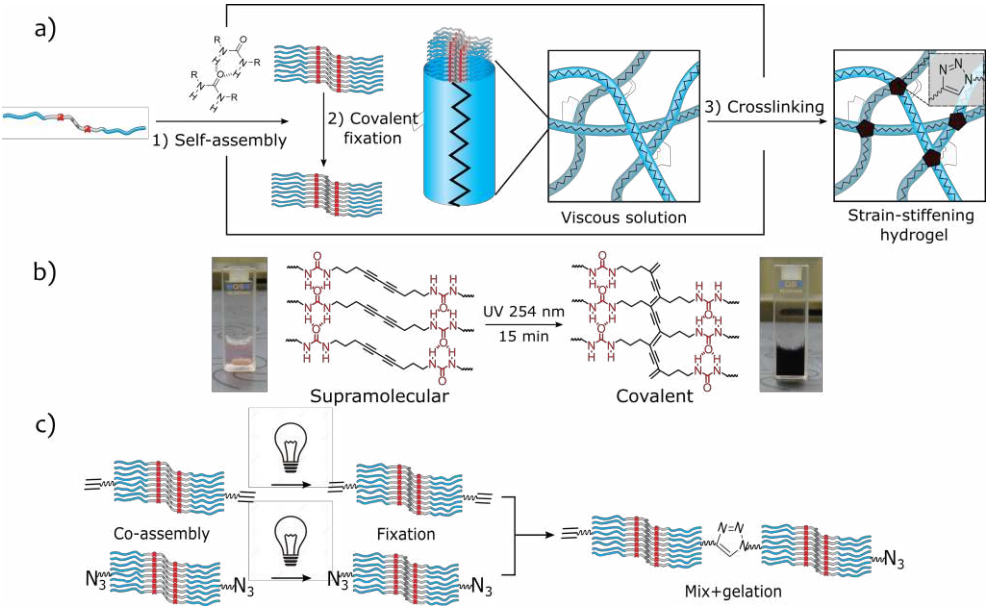

Scheme 2.2 | (a) Hierarchical self-assembly through intermolecular H-bonding and hydrophobic interactions of diacetylene bis-urea bolaamphiphiles followed by topochemical polymerization of the stacked diacetylenes. Aggregation of 9–10 ribbons into semi-flexible fibers followed by covalent crosslinking into strain-stiffening networks. (b) Photo-polymerization of the assembled diacetylene groups (i.e. covalent fixation) and the resulting PDAs. (c) Gel preparation method involving separate co-assembly and covalent fixation of DA-AC and DA-N_3 analogues with DA followed by mixing and gelation through CuAAC cycloaddtion reaction.

2.2. Results and discussion

Morphological analysis of the fibers

Polydiacetylene PDA was selected due to its previously reported high DP and its tendency to form long semi-flexible rods in water both before and after topochemical polymerization[19]. To determine the average values of the contour length L_c and the persistence length L_p in their native environment, a series of cryo-EM images of PDA fibers (Figs. 2.3.a-c) were subjected to statistical analysis. From a set of micrographs with 84 rods, L_c and L_p were determined and compared to those of neurofilaments (NFs) (Table 2.4). We found that the persistence length of PDA fibers is on the order of 280 nm, comparable to typical NFs, although NFs vary in length across several microns[20,21], while the PDA fibers have an average length of 0.16 μm.

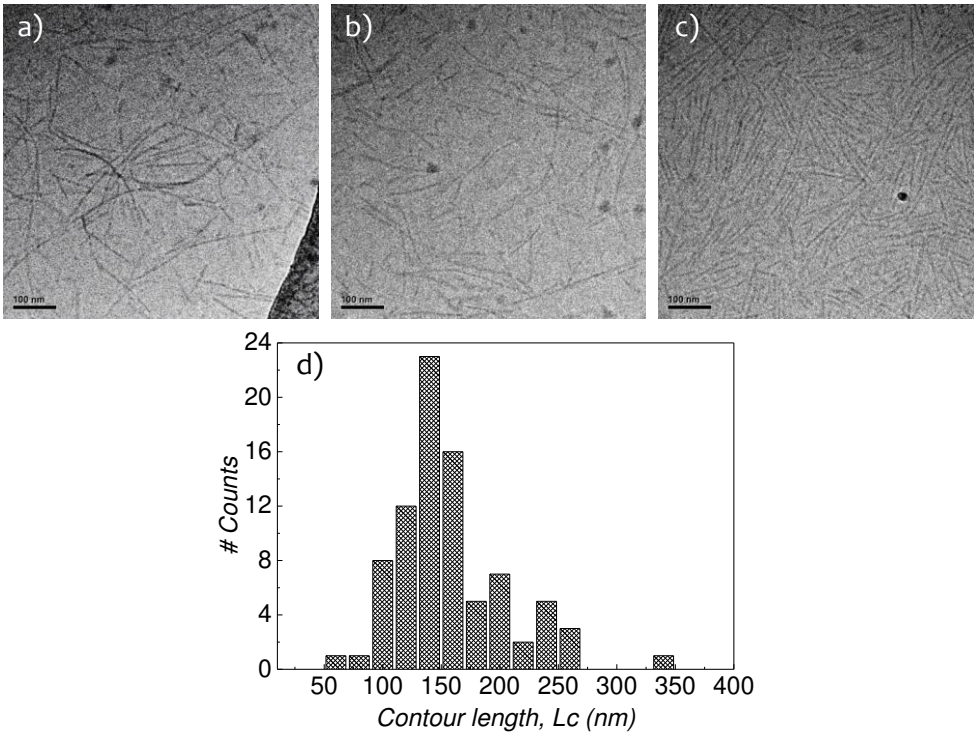

Fig. 2.3 | (a-c) Cryo-EM images of PDA in water (1 mM). Scale bars: 100 nm. (d) Histogram of contour length distribution calculated for a sample of N = 84 fibers taken from the micrographs shown in Figs. 2.3.a-c.

Table 2.4 | Comparison of PDA gels with neurofilaments.

Characteristic network parameter	**PDA**	**NFs**[10,22,23]
Crosslink distance	50-80[a]	300
Contour length, L_c [nm]	157[b]	2000-10000
Persistence length, l_p [nm]	280[b]	200
Concentration [mg mL^{-1}]	10-30	0.2-5
G_0 [Pa]	4-4000	0.5-30
Critical stress (σ_c) [Pa]	1-86	0.1-4
High stress regime	$K' \propto \sigma^1$	$K' \propto \sigma^1$
Fibre diameter [nm]	6.6[b]	10

[a] Determined from modeling detailed in methods section [b] Calculated from cryo-EM graphical analysis.

SAXS analysis of the fibers

The structure of DA and PDA rods was further investigated with small-angle X-ray scattering (SAXS). The scattering profiles of both objects displayed in Fig. 2.5 overlap over the whole *q*-range indicating no structural changes upon topochemical polymerization. Furthermore, in the low *q*-regime the slope is close to unity, indicative of high aspect-ratio scatterers with lengths beyond the resolution of the experiment (given by $q_{min}^{-1} \approx 30$ nm). These results are consistent with those derived from cryo-EM[19], showing rodlike micelles whose morphology is retained when undergoing photochemical polymerization of the assembled diacetylene groups. By fitting the scattering data (Fig. S2.7), a fiber radius of 3.1 nm and a cross-sectional mass per unit length (M_L) of 4.70×10^{-13} g cm^{-1} was calculated, indicating that each fiber is composed of 9-10 ribbons, on average. Similar aggregation numbers have been reported for other bolaamphiphile wormlike micelles and have been ascribed to the hydrophobic segregation of their micellar cores[24,25]. In the methods section, we provide a detailed analysis of the fitting procedures and calculation of the number of ribbons per fiber.

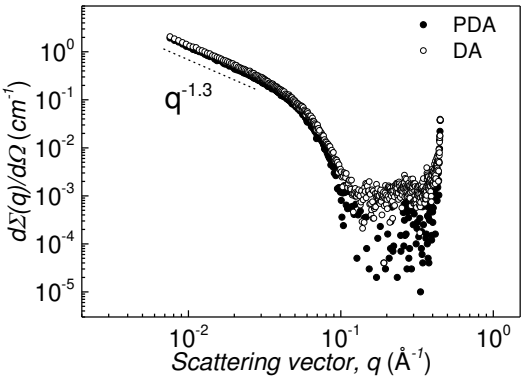

Fig. 2.5 | Small-angle X-ray scattering profiles of DA aqueous solutions (1 mg mL^{-1}) before and after photo-polymerization of the diacetylene unit.

Cu-catalyzed crosslinking reaction

As previously reported, rodlike micelles of bis-urea bolaamphiphiles do not form elastic gels on their own[26,27]. In order to induce gelation by covalent crosslinking, DA-AC and DA-N_3, (analogues of DA with matching hydrophobic domains and octaethylene glycol segments functionalized with acetylene and azide end-groups) were incorporated into the rods. These groups undergo a highly efficient cycloaddition reaction at low substrate concentrations using Cu^I catalysts with accelerating ligands[28,29]. In a protocol that was used to suppress reactions within fibers (Scheme 2.2.c), DA-N_3 and DA-AC (10 mol%) were separately blended with DA in chloroform. After allowing the solvent to evaporate overnight, DA/DA-N_3 and DA/DA-AC mixtures were dissolved in water and exposed to UV-light (254 nm)[19] with the rapid evolution of a dark purple color (Scheme 2.2.b) due to extensive π-electron delocalization along the polydiacetylenic backbone. After covalent fixation, the solutions were mixed ensuring equimolar azide/acetylene (5 mol%) ratios while preventing monomer exchange between micelles. Crosslinking of the rods was performed using a slightly modified standard protocol (methods section)[29], and after 2–3 h resulted in the formation of elastic gels able to support their own weight upon tilting the vials (Fig. 2.6.a). Gel formation was further monitored with oscillatory rheology in which storage (G') and loss (G") moduli were followed over time (Fig. 2.6.b), requiring as much as 19 h before G' and G" reached a plateau. To test the assumption that reduction of Cu^{II} to Cu^I is essential for the gelation process, we performed a crosslinking experiment of an aqueous solution of 2 wt% PDA co-assembled with DA-N_3/ DA-AC (5 mol%) in the absence of Na-ascorbate. Fig. 2.6.c shows that without generation of Cu^I ions no measurable changes in moduli are observed.

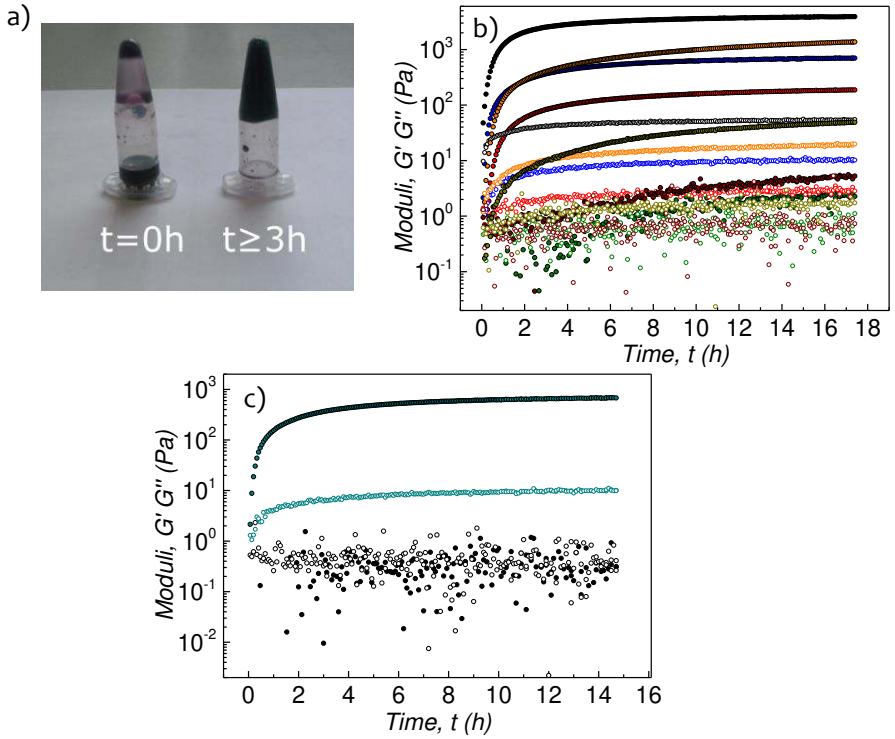

Fig. 2.6 | (a) Aqueous solutions of PDA before and 3 h after addition of the catalyst mixture illustrate gelation. (b) Time course of storage G' (solid dots) and loss moduli G" (open dots) during Cu-catalyzed crosslinking reaction of PDA mixtures containing 5 mol% DA-AC and DA-N_3 measured at constant strain amplitudes (1 %) and angular frequencies (6.28 rad s^{-1}) for different concentrations (in mg mL^{-1}): 10 (olive), 13 (wine), 14 (dark yellow), 15 (red), 20 (blue), 25 (orange) and 30 (black). (c) Time course of moduli for PDA mixtures (20 mg mL^{-1}) containing 5 mol% DA-AC and DA-N_3 in the presence (cyan) and absence (black) of Na-ascorbate in the catalyst mixture.

Nonlinear mechanics of PDA gels

To learn more about the mechanical properties of the gels, a well-established pre-stress protocol was applied[30], which records the differential modulus K' (defined as the derivative of stress σ with respect to the shear strain γ, $K' = \delta\sigma/\delta\gamma$) as a function of the applied stress. The typical elastic response observed in crosslinked biopolymer networks, as well as synthetic PIC gels, features two distinct regimes: A linear, low stress regime where K' is defined by the plateau storage modulus ($K' = G'_0$) and a stress-stiffening regime at higher stresses where the magnitude of K' increases as a power law $K' \propto \sigma^m$. The power m is known as the stiffening index and is a direct measure of the degree of mechanical responsiveness of the material. In addition, we

define σ_c to be the critical stress at which the modulus begins to depart from its linear behaviour. For biopolymer networks, σ_c typically lies between 0.5 Pa $\leq \sigma_c \leq$10 Pa, in line with the stresses that cells impart to their surrounding matrix[11].

To probe the mechanical properties of the PDA hydrogels, a concentration series of PDA was prepared while keeping the relative content of functionalized (DA-N_3 and DA-AC) to unfunctionalized DA constant (i.e. 5 mol%). Fig. 2.7.a shows a strong concentration dependence of the linear response G_0. The value of K' in the low-stress regime ranges over nearly 3 decades. Fig. 2.7.a shows, moreover, a universal high-stress asymptote characterised by a stiffening exponent m = 1. Similar indices have been reported by Rammensee *et al.*[22] for in vitro NFs and, most notably, for reconstituted collagen type I networks which are known to exhibit highly unusual nonlinear mechanics[31]. In the PIC gels, m = 1 is typically seen close to the critical stress; interestingly the PDA gels seem not to cross over to the characteristic m= 3/2 associated with the terminal scaling of semi-flexible networks. We speculate that the origin of the absence (or strongly delayed onset) of this regime is the relatively high density of the networks; previous work on aggrecan gels[32], suggests that at increased concentrations m may be decreased to values as low as 0.6. In biological m = 1 networks, the stress response is argued to be dominated by the release of mesoscopic bending of the fibrils in contrast to F-Actin or intermediate filaments where the upper limit of m = 3/2, associated to the stretching out of thermal undulations at short length scales, is typically accessible at high stress[1,10]. The PDA networks all have m = 1, but the extent of this responsive regime is far larger at lower concentrations, where the broadest range of stiffening is observed. If, as we hypothesize, this stiffening originates from the exhaustion of very soft bending modes (which may involve clusters of fibers, rather than single fibers) we can understand that increasing the concentration strongly increases the modulus, but at the same time the increased confinement suppresses those soft modes and the stiffening range decreases. Figs. 2.7.a and b summarize the findings: PDA networks exhibit a universal m = 1 stiffening at large strains. Upon rescaling the stresses and moduli, a universal stiffening curve is obtained highlighting the common origins of linear and nonlinear elasticity in these materials. In the methods section, we present further analysis of the scaling behaviour of the critical stress and the modulus.

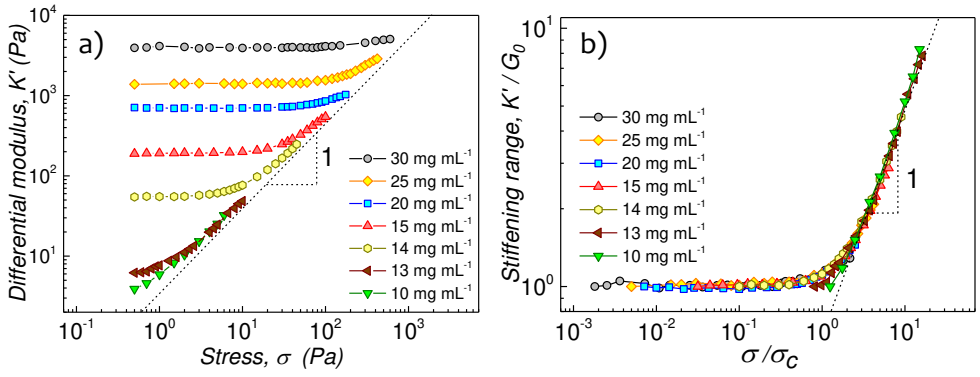

Fig. 2.7 | (a) Differential modulus K' vs stress σ of PDA containing 5 mol% DA-AC and DA-N_3 at different concentrations. (b) Scaling of K' with G_0 and σ with σ_c with the collapse into a master curve showing a $K' \propto \sigma^1$ dependency at high σ and low c.

Structure of the gels

SAXS scattering profiles of PDA were measured before and after gelation. To this end, 2.5 wt% aqueous solutions of PDA containing 5 mol% DA-N_3 and DA-AC were recorded before, and 24h after, the addition of Na-ascorbate (Fig. 2.8). Gelation through bundle formation is a common feature of PIC gels[17,18,33] as well as certain biopolymers, such as fibrin[34] or actin[35,36]. By contrast, PDA gels follow a rather different gelation mechanism: there, the formation of covalent links occurs at random positions along the fiber contour (Scheme 2.2.a). In that case, there is no net increase of the bundle diameter as inferred from SAXS data that show similar forward scattering intensities while completely retaining the shape of the scattering profiles as the system undergoes gelation. In other words, the structure of the gels mirrors that of the fibers in solution with restricted mobility due to permanent covalent crosslinking.

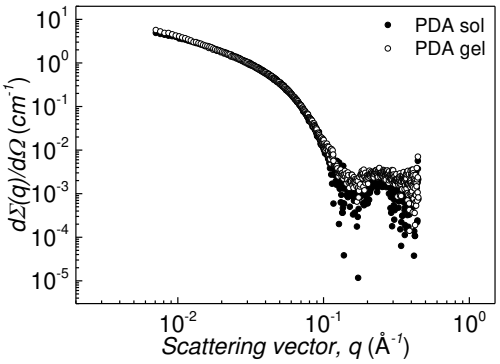

Fig. 2.8 | Small-angle X-ray scattering profiles PDA (2.5 wt%) containing DA-AC and DA-N_3 (5 mol%) recorded before (solution) and 24 h after addition of Na-ascorbate (gel).

2.3. Conclusions

In summary, we present a novel approach towards biomimetic strain-stiffening gels. Implementing requisite features of natural materials—semi-flexible polymers and strong links—the bisurea bolaamphihiles covalently fixated into rodlike micelles with a conjugated PDA backbone represent the first synthetic system that just like natural protein materials relies on self-assembly for the crucial step of fiber formation. The self-assembled rodlike micelles exist in water as bundled structures containing multiple ribbons, which we argue is essential to endow fibers with the necessary high persistence lengths. In future work, control over bundling may be leveraged to gain control over the persistence length. The supramolecular nature of the rods, moreover, allows for the controlled incorporation of a variety of functional analogues which can be subsequently immobilized via covalent fixation. Here, this advantage is exploited to suppress the formation of inactive loops along the same rod. The hydrogelation process, as inferred from SAXS analysis, occurs without an increase in fiber dimensions. In other words, the structure of the constituent rods remains intact as the system undergoes gelation, with superior control over the network architecture.

The ability to control both the stiffness and the degree of connectivity between networks of semi-flexible rods breaks ground for genuinely biomimetic materials; indeed we show that in the first incarnation presented here the network shares crucial dimensional and elastic metrics with gels composed of neurofilament fibers. However, where nature is limited by properties of the fibrillar proteins at its disposal, the current synthetic route in principle allows for continuous variation of properties, opening up a

class of transnatural, bio-inspired materials that not only mimic but conceivably outperform biological matter.

2.4. Experimental section

Materials

All solvents used were of reagent grade quality or better and purchased from Biosolve, Sigma-Aldrich or Actu-All Chemicals. THF and DCM were dried using molecular sieves (3 Å). All chemicals were purchased from Sigma-Aldrich, TCI Europe, Acros or Fluka at the highest purity available and used without further purification unless otherwise stated. Flash chromatography was performed on a Reveleris X2 system using 40μm mesh silica gel cartdriges. Reactions were followed by thin-layer chromatography (precoated 0.25 mm, 60-F254 silica plate purchased from Merck). Tetraethylene glycol monopropargyl ether (**1**), azido-tetraethylene glycol (**2**)[37], N-(*ter*tbutyloxycarbonyl)-11-aminoundecanoic acid (Boc-AUDA)[38], 1,12-diisocyanatodeca-4,6-diyne[19], and DA[19] were prepared according to literature procedures.

General methods

NMR spectra were recorded on a 400 MHz Varian Mercury Vx (100 MHz for ^{13}C-NMR) or 400 MHz Bruker UltraShield Magnet (100 MHz for ^{13}C-NMR). Chemical shifts (δ) are reported in parts per million (ppm) using residual solvent signal or tetramethylsilane (TMS) as internal standards[39]. Splitting patterns are labelled as singlet (s), doublet (d), double doublet (dd), triplet (t), quartet (q), pentet (p) and multiplet (m). Infrared spectra were measured on a Perkin Elmer 1600FT-IR equipped with a Perkin Elmer Universal ATR Sampler Accesory. Matrix-assisted laser desorption ionization time-of-flight (MALDI-TOF) measurements were carried out on a Perseptive DE PRO Voyager mass spectrometer using α-cyano-4-hydroxycinnamic acid as the calibration matrix. (LC-MS).

Vitrified films were prepared in a 'Vitrobot' instrument (PC controlled vitrification robot, patent applied, Frederik *et al.* 2002, patent licensed to FEI) at 22 ^{o}C and at a relative humidity of 100%. In the preparation chamber of the 'Vibrobot', 3 μL sample was applied on a Quantifoil grid (R 2/2, Quantifoil Micro Tools GmbH), which was surface plasma treated just prior use (Cressington 208 carbon coater operation at 5

mA for 40 s). Vitrified films were transferred to a cryoholder (Gatan 626) and observed at -170 ^{o}C in a Tecnai Sphera microscope operating at 200 kV. The images were recorded using a 1k × 1k Gatan CCD camera.

Small angle X-Ray scattering (SAXS) profiles were recorded on SAXLAB GANESHA 300 XL SAXS equipped with a GeniX 3D Cu Ultra Low Divergence micro focus sealed tube source producing X-rays with a wavelength λ = 1.54 Å at a flux of 1×10^{8} ph/s and a Pilatus 300 K silicon pixel detector with 487 × 619 pixels of 172 × 172 μm^2 in size placed a three sample-to-detector distances of 113, 713, and 1513 mm respectively to cover a q-range of $0.07 \leq q \leq 3.0$ nm^{-1} with $q = 4\pi/\lambda(\sin\theta/2)$. Silver behenate was used for calibration of the beam centre as well as the q-range. Samples were measured within 2 mm quartz capillaries (Hilgenberg GmbH, Germany). The two-dimensional SAXS patterns were brought to an absolute intensity scale using the calibrated detector response function, known sample-to-detector distance, measured incident and transmitted beam intensities, and azimuthally averaged to obtain one-dimensional SAXS profiles. The scattering curves of the fibers were obtained by subtraction of the scattering contribution of the solvent and quartz cell.

The mechanical properties of the hydrogels were tested by oscillatory rheology. Dynamic viscoelastic measurements were conducted on a stress-controlled Anton Paar, Physicia MCR 501 rheometer equipped with a 25-mm stainless steel sand-blasted plate-plate geometry to prevent slippage of the sample. Measurements were performed at a fixed temperature of 20 ^{o}C sealed by placing mineral oil around the sample to minimize evaporation at a fixed plate-to-plate gap of 800 μm. After addition of the catalyst, gelation was monitored by continuous oscillations with a strain amplitude of 0.1 % and an angular frequency of 6.28 rad/s. To probe the elasticity of the gels, we applied a steady prestress, σ_0 on which an oscillatory $\sigma(t) = \delta\sigma e^{iwt}$ was superimposed with an amplitude at most 10% of σ_0 and at an angular frequency of ω = 6.28 rad s^{-1}.

Synthetic procedures

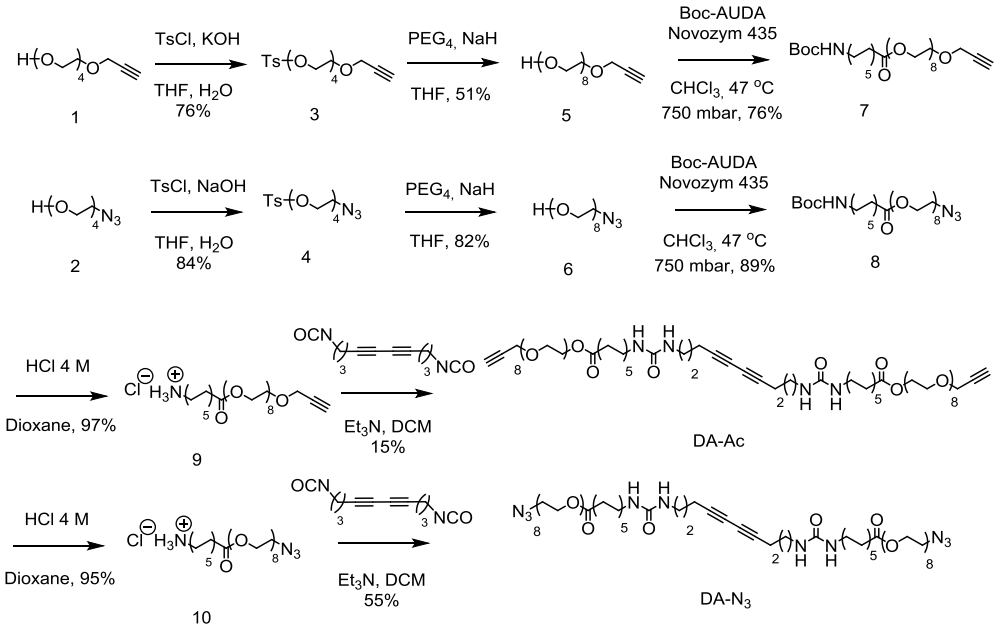

Scheme S2.1 | Synthetic route towards DA-AC and DA-N_3 analogues

Tetraethylene glycol monopropargyl ether tosylate (3)

Tetraethylene glycol monopropargyl ether (**1**) (12.85 g, 55.35 mmol), tosyl chloride (12.63 g, 66.24 mmol) and THF (250 mL) were placed in a round-bottomed flask, and the mixture was chilled in an ice bath. At this temperature, an aqueous solution of KOH 16 M (12.54 g, 0.22 mol) was added dropwise, and the reaction mixture was allowed to stir overnight at room temperature. At the conclusion of the reaction, the mixture was poured into ice H_2O (150 mL) and the aqueous layer extracted three times with DCM (150 mL). The organic extracts were combined and washed twice with 3% HCl (150 mL) and once with brine (150 mL), dried over $MgSO_4$ and concentrated under reduced pressure. The resultant crude product was purified by flash chromatography (silica gel, DCM/EtOH, 99:1 v/v) to yield **3** (16.31 g, 42.24 mmol, 76%) as a faintly yellow oil.

^{1}H-NMR (400 MHz, $CDCl_3$, T = 295K): δ = 7.76 (d, 2H, J=8. Hz, Ar), 7.31 (d, 2H, J = 8.0 Hz, Ar), 4.16 (d, 2H, J=2.4 Hz, C$\underline{H}_2$C≡H), 4.13 (t, 2H, J = 4.0 Hz, C$\underline{H}_2$tosyl), 3.66-3.55 (m, 14H, C$\underline{H}_2$O), 2.41 (m, 4H, tosylC$\underline{H}_3$ + CH_2C≡$\underline{H}$).

^{13}C-NMR (400 MHz, $CDCl_3$, T = 295K): δ = 144.84, 133.02, 129.86, 127.99, 79.70, 74.61, 70.74-70.41, 69.31, 69.13, 68.69, 58.41, 21.67.

MALDI-TOF-MS: calculated Mw = 386.14 g/mol, found m/z [M+Na^+] = 409.33, m/z [M+NH_4^+] = 404.25, [M+H^+] = 387.17.

Azido-tetraethylene glycol tosylate (4)

Azido-tetraethylene glycol (**2**) (6.84 g, 31.21 mmol), tosyl chloride (6.70 g, 35.16 mmol) and THF (140 mL) were placed in a round-bottomed flask, and the mixture was cooled to 0 °C in an ice bath. At this temperature, an aqueous solution of NaOH 4.8 M (4.81 g, 0.12 mol) was added dropwise, and the reaction mixture was stirred overnight at room temperature. At the conclusion of the reaction, the mixture was chilled in an ice bath and quenched with HCl 1M (150 mL). The organic layer was removed by rotary evaporation and the remaining aqueous solution extracted thrice with DCM (150 mL). The organic extracts were combined and washed twice with 10% Na_2CO_3 (150 mL), H_2O (150 mL) and dried over $MgSO_4$. The final product was evaporated to dryness to afford **4** (9.76g, 26.16 mmol, 84%) which was used in subsequent steps without further purification.

^{1}H-NMR (400 MHz, $CDCl_3$, T = 295K): δ = 7.76 (d, 2H, J = 8.4 Hz, Ar), 7.32 (d, 2H, J = 8.4 Hz, Ar), 4.14 (t, 2H, J = 4.7 Hz, C*H*$_2$tosyl), 3.68-3.57 (m, 12H, C*H*$_2$O), 3.36 (t, 2H, J = 5.2 Hz, CH_2N_3), 2.43 (s, 3H, tosylC*H*$_3$).

^{13}C-NMR (400 MHz, $CDCl_3$, T = 295K): δ = 144.89, 133.05, 129.89, 128.02, 70.80-70.65, 70.09, 69.33, 68.73, 50.74, 21.70.

MALDI-TOF-MS: calculated Mw = 373.13 g/mol, found m/z [M+Na^+] = 396.25, m/z [M+NH_4^+] = 391.17, [M+H^+] = 373.92.

Octaethylene glycol monopropargyl ether (5)

Tetraethylene glycol (PEG_4) (48.97 g, 0.253 mol) in anhyd. THF (200 mL) was placed in a round-bottom flask and chilled in an ice bath under an atmosphere of argon. To the resultant solution, sodium hydride (NaH) (60% dispersion in mineral oil, 2.65 g, 66.34 mmol) was added in three portions over a period of 30 mins, and the reaction mixture was allowed to warm to r.t. followed by the addition of **3** (16.31 g, 42.24 mmol) in dry THF (10 mL) by syringe pump over 7h. The reaction mixture was further stirred for 2d under an atmosphere of argon. At the conclusion of the reaction, brine (150 mL) was added and to quench the excess of NaH and the organic

layer was evaporated under reduced pressure. The resultant aqueous slurry was extracted thrice with CH_2Cl_2 (150 mL) and the combined organic extracts were collected, washed with 10 wt% aqueous solution of $KHPO_4$ (150 mL), H_2O (150 mL), dried over anhyd. $MgSO_4$ and concentrated *in vacuo*. The crude product was subjected to flash column chromatography (silica gel, DCM/EtOH 97:3 v/v) to afford **5** (8.80 g, 21.56 mmol, 51%) as a faint yellow viscous oil.

^{1}H-NMR (400 MHz, $CDCl_3$, T = 295K): δ = 4.19 (d, 2H, J = 3.2 Hz, C$\underline{H}_2$C≡CH), 3.64-3.51 (m, 32H, C$\underline{H}_2$O), 2.40 (t, 1H, J = 2.4 Hz, C≡C$\underline{H}$).

^{13}C-NMR (400 MHz, $CDCl_3$, T = 295K): δ = 79.59, 74.60, 72.48, 70.51-70.45, 70.31, 70.25, 69.00, 61.56, 58.30.

MALDI-TOF-MS: calculated Mw = 408.28 g/mol, found m/z [M+Na$^+$] = 431.50, m/z [M+H$^+$] = 409.42.

Azido-octaethylene glycol (6)

4 (9.76 g, 26.16 mmol) was reacted following the same procedure as described for **5**. The crude product obtained after liquid-liquid extraction was subjected to column chromatography (silica gel, gradients DCM/EtOH, 99:1 to 19:1 v/v) to yield **6** (8.53 g, 21.58 mmol, 82%) as a faintly yellow viscous oil.

^{1}H-NMR (400 MHz, $CDCl_3$, T = 295K): δ = 3.69-3.65 (m, 30H, C$\underline{H}_2$O), 3.39 (t, 2H, J = 4.0 Hz, C$\underline{H}_2$N$_3$).

^{13}C-NMR (400 MHz, $CDCl_3$, T = 295K): δ = 72.42, 70.49-70.35, 70.14, 69.86, 61.44, 50.48.

MALDI-TOF-MS: calculated Mw = 395.23 g/mol, found m/z [M+Na$^+$] = 418.42, m/z [M+H$^+$] = 396.33.

N-(*tert*-butyloxycarbonyl)-11-aminoundecanoyl-(octaethyleneglycol monopropargyl ether)-ester (7)

N-(*tert*butyloxycarbonyl)-11-aminoundecanoic acid (Boc-AUDA) (4.45 g, 14.76 mmol), **5** (5.05 g, 12.37 mmol) and Novozym 435 (2.85 g, 30 wt%) in $CHCl_3$ (50 mL) were placed in a round bottom flask and the reaction mixture was stirred at 47 °C and 750 mbar in a rotavap apparatus for 5 h. To the resultant solution, molecular sieves were added and the mixture was allowed to react overnight. The suspension was filtered off, and the filtrate dried by rotary evaporation. The product was purified

using flash column chromatography (silica gel, CH_2Cl_2/Ethanol 23:2 v/v) yielding **7** (6.49 g, 9.386 mmol, 76%) as a viscous colourless oil.

^{1}H-NMR (400 MHz, $CDCl_3$, T = 295K): δ = 4.60 (bs, 1H, N*H*), 4.12 (t, 2H, J = 4.76 Hz, C*H*$_2$OCO), 4.10 (d, 2H, J = 2.4 Hz, C*H*$_2$C≡CH), 3.60-3.56 (m, 30H, OC*H*$_2$), 2.99 (q, 2H, J = 6.48 Hz, C*H*$_2$N), 2.38 (t, 1H, J = 2.36 Hz, C≡C*H*), 2.23 (t, 2H, J = 7.48 Hz C*H*$_2$-CO) 1.56-1.47 (m, 2H, C*H*$_2$CH$_2$CO), 1.34 (s, 9H, C(C*H*$_3$)$_3$), 1.24-1.13 (m, 14H, C*H*$_2$).

^{13}C-NMR (400 MHz, $CDCl_3$, T = 295K): δ = 173.64, 155.87, 79.53, 78.71, 74.57, 70.49-70.42, 70.28, 69.06, 68.96, 63.24, 58.26, 40.48, 34.05, 29.95, 29.35-28.97, 28.34, 26.67, 24.76.

MALDI-TOF-MS: calculated Mw = 691.45 g/mol, found m/z [M+Na$^+$] = 714.47.

N-(*tert*-butyloxycarbonyl)-11-aminoundecanoyl-(azido-octaethyleneglycol)-ester (8)

6 (4.00 g, 10.12 mmol) was reacted following the same experimental procedure as described for **7** to give **8** (6.15 g, 9.06 mmol, 89%) as a transparent oil.

^{1}H-NMR (400 MHz, $CDCl_3$, T = 295K): δ = 4.54 (bs, 1H, N*H*), 4.12 (t, 2H, J = 4.80 Hz, C*H*$_2$OCO), 3.66-3.61 (m, 30H, OC*H*$_2$), 3.55 (t, 2H, J = 5.24 Hz, C*H*$_2$N$_3$), 3.05 (q, 2H, J = 6.20 Hz, C*H*$_2$N), 2.28 (t, 2H, J = 7.48 Hz C*H*$_2$CO), 1.64-1.50 (m, 2H, C*H*$_2$CH$_2$CO), 1.40 (s, 9H, C(C*H*$_3$)$_3$), 1.32-1.15 (m, 14H, C*H*$_2$).

^{13}C-NMR (400 MHz, $CDCl_3$, T = 295K): δ = 173.75, 155.95, 78.85, 70.64-70.50, 70.00, 69.14, 63.32, 50.62, 40.56, 34.13, 30.01, 29.42-29.05, 28.40, 26.74, 24.84.

MALDI-TOF-MS: calculated Mw = 678.44 g/mol, found m/z [M+Na$^+$] = 701.44.

11-aminoundecanoyl-(octaethyleneglycol monopropargyl ether)-ester-HCl salt (9)

A solution of HCl 4 M in dioxane (35 mL) was chilled to 0 °C in an ice bath. At this temperature, **7** (6.49 g, 9.39 mmol) in dioxane (35 mL) was added dropwise under atmosphere of argon and the reaction mixture was stirred for 4 hours at r.t. At the conclusion of the reaction, the volatiles were removed *in vacuo* and **9** (5.72 g, 9.12 mmol, 97%) was isolated as a faintly yellow waxy solid.

^{1}H-NMR (400 MHz, $CDCl_3$, T = 295K): δ = 8.10 (bs, 3H, CH$_2$N*H*$_3$), 4.13-4.11 (m, 4H, C*H*$_2$C≡CH +C*H*$_2$OCO), 3.61-3.56 (m, 30H, OC*H*$_2$), 2.87 (m, 2H, C*H*$_2$NH$_3$), 2.39

(t, 1H, J = 2.36 Hz, C≡C*H*), 2.22 (t, 2H, J = 7.52 Hz, C*H*$_2$CO), 1.66 (m, 2H, C*H*$_2$NH$_3$), 1.51 (m, 2H, CH$_2$CH$_2$CO) 1.24-1.17 (m, 12H, CH$_2$).

^{13}C-NMR (400 MHz, $CDCl_3$, T = 295K): δ = 173.33, 79.53, 74.66, 70.42-70.37, 70.22, 69.05, 68.91, 63.22, 58.28, 39.90, 34.05, 29.05-28.91, 27.44, 26.50, 24.75.

MALDI-TOF-MS: calculated Mw = 591.78 g/mol, found m/z [M+H$^+$] = 592.75.

11-aminoundecanoyl-(azido-octaethyleneglycol)-ester-HCl salt (10)

8 (6.15 g, 9.06 mmol) was reacted following the same experimental procedure as described for **9** yielding **10** (5.26 g, 8.57 mmol, 95%) as a slightly yellow waxy solid.

^{1}H-NMR (400 MHz, $CDCl_3$, T = 295K): δ = 8.12 (bs, 3H, CH$_2$N*H*$_3$), 4.17 (m, 2H, C*H*$_2$OCO), 3.66-3.61 (m, 28H, OC*H*$_2$), 3.55 (t, 2H, J = 5.0 Hz, C*H*$_2$N$_3$), 2.92 (m, 2H, C*H*$_2$NH$_3$), 2.27 (t, 2H, J = 7.52 Hz, C*H*$_2$CO), 1.71 (m, 2H, C*H*$_2$NH$_3$), 1.56 (m, 2H, CH$_2$CH$_2$CO) 1.31-1.22 (m, 12H, CH$_2$).

^{13}C-NMR (400 MHz, $CDCl_3$, T = 295K): δ = 173.80, 70.66-70.53, 70.02, 69.31, 63.35, 50.68, 40.00, 34.18, 29.31-28.98, 27.61, 26.55, 24.87.

MALDI-TOF-MS: calculated Mw = 578.75 g/mol, found m/z [M+Na$^+$] = 601.50, m/z [M+H$^+$] = 579.75.

DA-AC

9 (1.98 g, 3.12 mmol), triethlylamine (0.84 g, 8.33 mmol) and anhyd. CH_2Cl_2 (15 mL) were placed in a round bottomed flask under argon atmosphere and the mixture was cooled to 0 °C in an ice bath, followed by the dropwise addition of 1,12-diisocyanatodeca-4,6-diyne (0.31 g, 1.44 mmol) in dry CH_2Cl_2 (5 mL). The reaction was stirred for 1 hour at r.t, after which the crude product was concentrated under reduced pressure and purified using flash column chromatography (silica gel, CH_2Cl_2/Ethanol 97:3 v/v) to afford **DA-AC** (0.29 g, 0.21 mmol, 15%) as a white waxy solid that turned faintly pink under prolonged exposure to stray light.

^{1}H-NMR (400 MHz, $CDCl_3$, T = 295K): δ = 5.04 (t, 2H, J = 5.36 Hz, NH), 4.88 (t, 2H, J = 4.84 Hz, NH), 4.21 (m, 8H, C*H*$_2$OCO+C*H*$_2$C≡H), 3.70-3.60 (m, 60H, OC*H*$_2$), 3.25 (q, 4H, J = 6.24 Hz, C*H*$_2$NH), 3.11 (q, 4H, J = 6.32 Hz, NHC*H*$_2$), 2.43 (t, 2H, J = 2.08 Hz, C≡C*H*), 2.31 (m, 8H, C*H*$_2$CO+C*H*$_2$C≡C), 1.69, (quint, 4H, J = 6.68 Hz, NHCH$_2$C*H*$_2$CH$_2$CO), 1.60 (p, 4H, J = 6.88 Hz, C*H*$_2$CH$_2$CO), 1.45 (p, 4H, J = 6.32 Hz, C*H*$_2$CH$_2$NH), 1.30-1.25 (m, 24H, C*H*$_2$).

^{13}C-NMR (400 MHz, $CDCl_3$, T = 295K): δ = 147.01, 158.77, 79.75, 74.71, 70.71-70.67, 70.51, 69.31, 69.21, 66.03, 63.49, 58.51, 40.55, 39.27, 34.31, 30.34, 29.57, 29.43, 29.30, 29.17, 28.15, 27.02, 24.99, 16.76.

MALDI-TOF-MS: calculated Mw = 1398.89 g/mol, found m/z [M+Na^+] = 1421.88, m/z [M+K^+] = 1437.86.

FT-IR (ATR) υ (cm^{-1}): 3334, 2921, 2851, 1731, 1614, 1579, 1101, 621.

DA-N_3

10 (1.57 g, 2.56 mmol) was reacted following the same procedure as described for the synthesis of **DA-AC** to yield **DA-N_3** (0.28 g, 0.20 mmol, 53%) as a white waxy solid that turned slightly purple under prolonged exposure to stray light.

^{1}H-NMR (400 MHz, $CDCl_3$, T = 295K): δ = 5.01 (t, 2H, J = 5.8 Hz, N<u>H</u>), 4.85 (t, 2H, J = 5.48 Hz, N<u>H</u>), 4.85 (t, 4H, J = 4.8 Hz, C<u>*H*$_2$</u>OCO), 3.69-3.62 (m, 60H, OC<u>*H*$_2$</u>), 3.35 (t, 4H, J = 5.24 Hz, C<u>*H*$_2$</u>N_3), 3.25 (q, 4H, J = 6.2 Hz, C<u>*H*$_2$</u>NH), 3.12 (q, 4H, J = 6.12 Hz, NHC<u>*H*$_2$</u>), 2.31 (m, 8H, C<u>*H*$_2$</u>CO+C<u>*H*$_2$</u>-C≡C), 1.69, (quint, 4H, J = 6.72 Hz, $NHCH_2$C<u>*H*$_2$</u>CH_2CO), 1.60 (p, 4H, J = 7.08 Hz, C<u>*H*$_2$</u>CH_2CO), 1.44 (p, 4H, J = 6.56 Hz, C<u>*H*$_2$</u>CH_2NH), 1.31-1.25 (m, 24H, C<u>*H*$_2$</u>).

^{13}C-NMR (400 MHz, $CDCl_3$, T = 295K): δ = 174.01, 158.75, 70.81-70.68, 70.15, 69.31, 66.04, 63.49, 50.80, 40.57, 39.28, 34.31, 30.47, 29.57, 29.43, 29.31, 29.17, 28.90, 27.02, 24.99, 16.76.

MALDI-TOF-MS: calculated Mw = 1372.87 g/mol, found m/z [M+Na^+] = 1395.89, m/z [M+K^+] = 1411.87.

FT-IR (ATR) υ (cm^{-1}): 3328, 2919, 2849, 2099, 1731, 1615, 1580, 1096, 608.

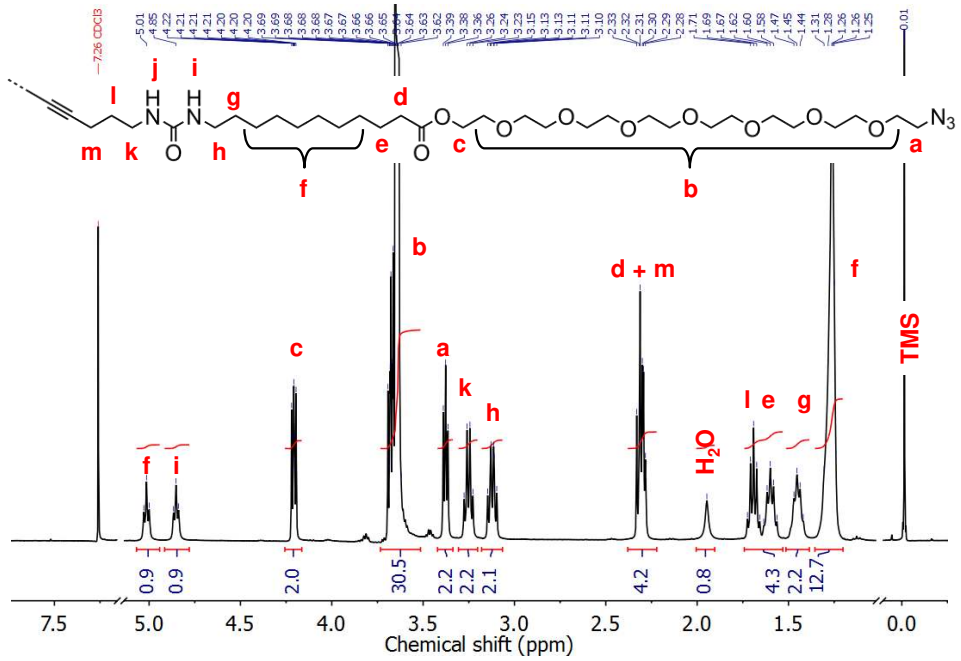

Fig. S2.2 | ^{1}H-NMR spectrum of DA-N_3.

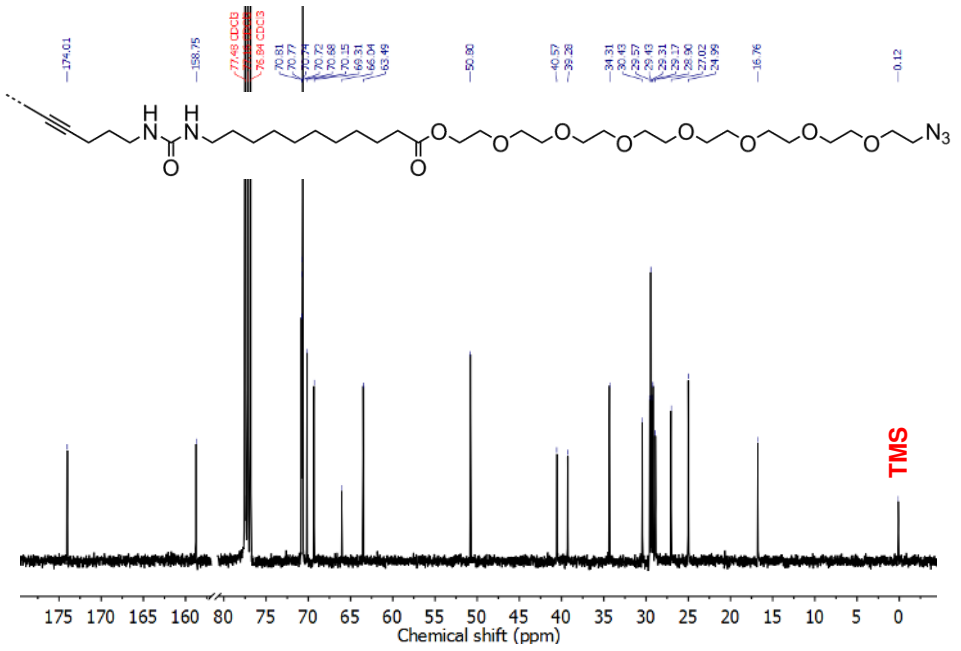

Fig. S2.3 | ^{13}C-NMR spectrum of DA-N_3.

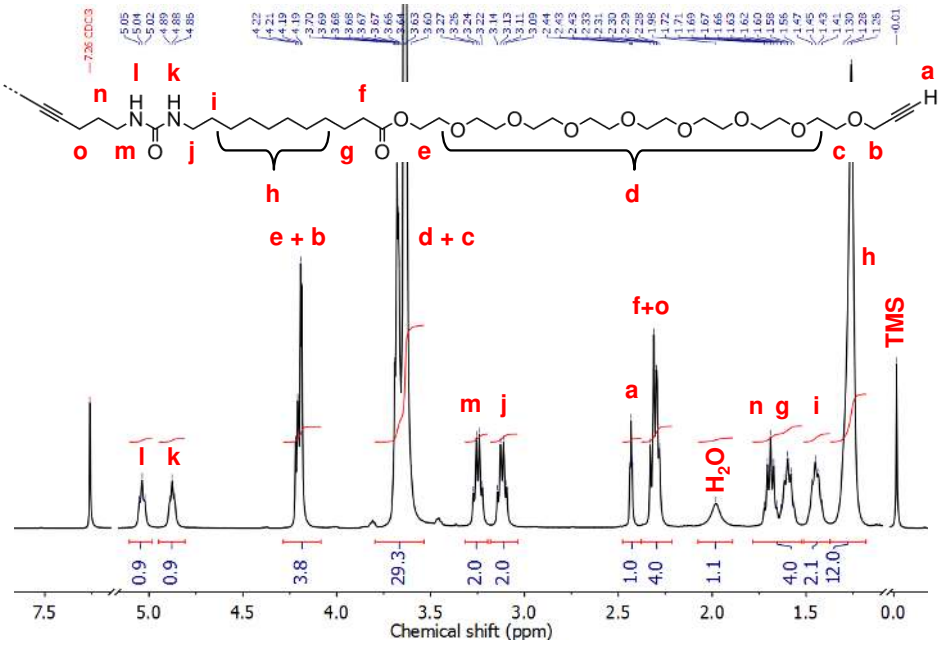

Fig. S2.4 | ^{1}H-NMR spectrum of DA-AC.

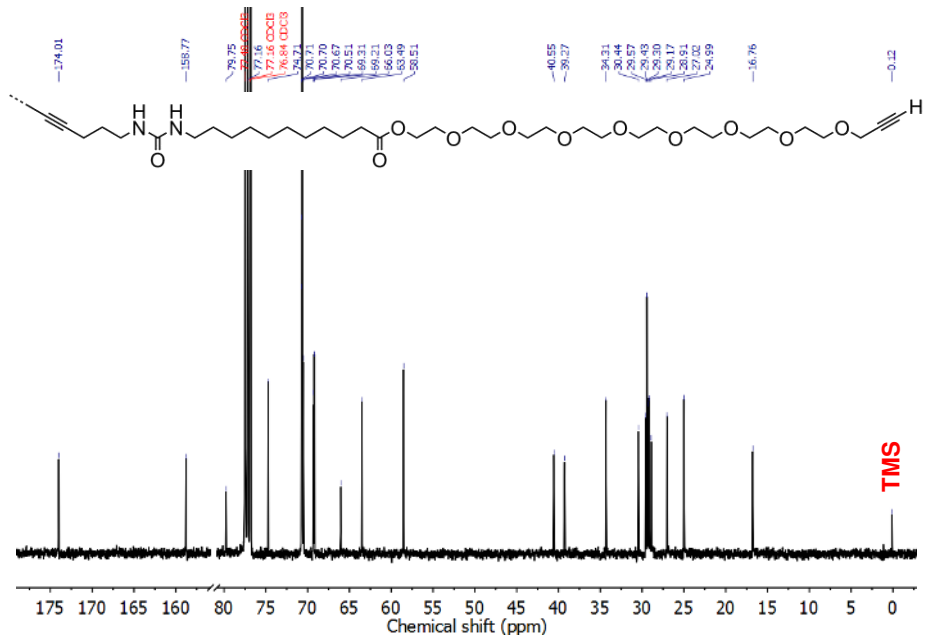

Fig. S2.5 | ^{13}C-NMR spectrum of DA-AC.

Contour and persistence length calculation

DA was weighed in the solid state and dissolved in ca. 300 μL chloroform. The solvent was allowed to evaporate overnight and the remaining solid re-dissolved in mili-Q water to a concentration of 20 mg mL^{-1}. The micelles were allowed to grow for 2h, after which, the solution was transferred to a quartz cuvette (1×1 cm) where photo-polymerization was performed by irradiating at 254 nm for 15 min under continuous stirring using a Luzchem photoreactor (model LCZ 4V) equipped with 7.2 W UV-C lamps. Solutions were diluted with water to 1 mM prior imaging. The sample vitrification procedure was carried out using an automated vitrification robot (PC controlled vitrification robot, patent applied, Frederik *et al.* 2002, patent licensed to FEI) at 22 ^{o}C and a relative humidity of 100%. Quantifoil electron microscopy grids, purchased from Quantifoil Micro Tools GmbH (R 2/2), were surface plasma treated using a Cressington 208 carbon coater operating at 5 mA for 40 s just prior use. In the preparation chamber of the 'Vibrobot', a 3 μL sample was applied to the Quantifoil grid and the excess sample removed by blotting using filter paper for 3 s at 3 mm. The thin film thus formed was plunged (acceleration about 3 g) into liquid ethane just above its freezing point. After transferring the grids to a cryoholder (Gatan 626), the vitrified films were observed using an FEI Tecnai 20, type Sphera (www.cryotem.nl). The LaB_6 filament was operated at 200 kV. Micrographs were taken at low dose conditions, using a typical defocus value of 40 μm at 6500 magnification, and defocus values of 2, 5 and 10 μm at 25000 magnification.

To calculate L_c and L_p, the micrographs of Figs. 2.3.a-c were first processed using Fiji[40], whereby the background of the images was inverted and the high-frequency noise smoothed using a Gaussian blur filter. The calculation of L_c distribution was done using the Curve Tracing plugin from Fiji wherein a total sample of 84 fibers was subjected to statistical analysis. The calculation of L_p was performed using Easyworm using the procedure detailed by Lamour *et al.*[41].

Calculation of number of ribbons per fiber

Small angle X-Ray scattering was used to determine the number of ribbons per fiber of pre-polymerized self-assembled PDA rods. Density measurements of water and PDA aqueous solutions were performed using an Anton Paar DMA 5000M.

First, the specific volume (υ) of PDA rods at a concentration of 10 mg mL^{-1} was determined by measuring the density (D) of DA aqueous solutions over the concentration range indicated in Fig. S2.6 and assuming that the density of the system does not change upon topochemical polymerization:

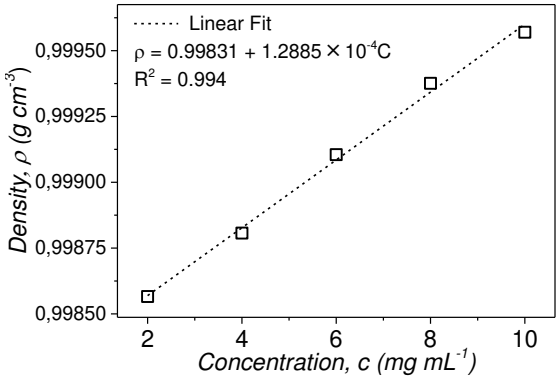

Fig. S2.6 | Plot of ϱ vs c of DA in mili-Q water measured at 20 °C including linear regression.

Thus, the density of a 0.01 g cm^{-3} PDA aqueous solution was calculated to be D_{PDA} = 0.99960 g cm^{-3}. The specific volume was then obtained as:

$$\upsilon = \frac{1}{D_{water}}\left(1-\frac{D_{PDA}-D_{water}}{c}\right) = \frac{1}{0.99820\ \text{g cm}^{-3}}\left(1-\frac{0.99960-0.99820\ \text{g cm}^{-3}}{0.01\ \text{g cm}^{-3}}\right) =$$

$$= 0.86205\ \text{cm}^3\text{g}^{-1}$$

To fit the experimental data with a nonlinear least squares procedure implemented in Igor Pro, we used a model that calculates the form factor of a flexible cylinder with a uniform scattering length density (ρ_{cyl}) and cross-sectional radial polydispersity which is averaged over a Schultz distribution of cylinder radii. The non-negligible diameter of the cylinder is included by accounting for excluded volume interactions within the walk of a single cylinder. Inter-cylinder interactions are not included.

We then proceeded to fix the values of volume fraction (ϕ = 0.00862) and use the values of contour length (L_c = 157 nm) and Kuhn length (b = 2×l_p = 560 nm) as derived from cryo-EM analysis. The tabulated value of ρ_{water} = 9.37 × 10^{10} cm^{-2} was used.

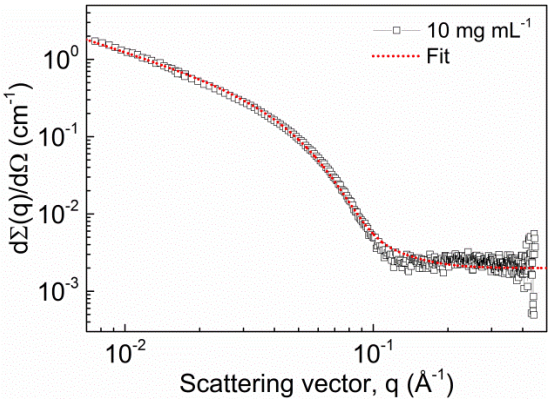

Fig. S2.7 | Small angle X-Ray profile (black squares) and form factor fit (dashed red line) of PDA solution in mili-Q water recorded at a concentration of 10 mg mL^{-1}.

Fitting of the scattering data with the model (Fig. S2.7) gave a value of 3.1 ± 0.1 nm for the radius, consistent with the value of 3.3 nm measured in cryo-EM. The fitting procedure also provided a value for ρ_{cyl} = (10.43 ± 0.01) × 10^{10} cm^{-2}. The scattering contrast was then calculated as:

$$\Delta\varrho = \varrho_{cyl} - \varrho_{water} = (10.43\text{-}9.37) \times 10^{10} cm^{-2} = 1.06 \times 10^{10}\ cm^{-2}$$

The electron length density difference ($\Delta\varrho_M$) can be now determined as:

$$\Delta\varrho_M = \Delta\varrho \times \upsilon = 1.06 \times 10^{10}\ cm^{-2} \times 0.86\ cm^3 g^{-1} = 9.12 \times 10^9\ cm\ g^{-1}$$

The overall scattered intensity for elongated scatterers originates from two separate contributions: A part arising from the cross-section ($I_{cs}(q)$) and a part resulting from the elongated structure. To calculate the cross-sectional mass per unit length (M_L) we used a Cassasa-Holtzer plot of the data and extrapolated the curve with the parameters obtained from the fitting procedure (Fig. S2.7). This gave the height of the plateau as indicated by the value of the product $[d\Sigma(q)/d\Omega]\times q = 1.23 \times 10^6\ cm^{-2}$.

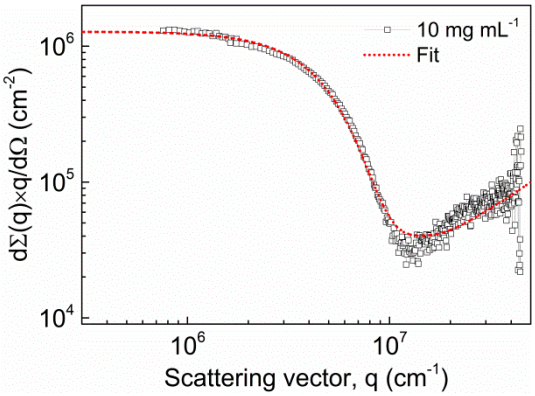

Fig. S2.8 | Casassa-Holtzer plot of the scattering profile of PDA at 10 mg mL^{-1}. The value of the Holtzer plateau obtained by extrapolation of the experimental data with the best-fit parameters as indicated by the dashed red line.

Now, the cross-sectional scattered intensity ($I_{cs}(0)$) was calculated according to the following expression:

$$I_{cs}\ (0) = \frac{[d\Sigma(q)/d\Omega] \times q}{\pi} = 3.91 \times 10^{5}\ \text{cm}^{-2}$$

M_L was subsequently obtained using the equation below:

$$M_L = \frac{I_{CS}(0)}{C \times (\Delta\varrho_M)^2} = \frac{3.91 \times 10^{5}\ \text{cm}^{-2}}{0.01\ \text{g cm}^{-3} \times \left(9.12 \times 10^{9}\ \text{cm g}^{-1}\right)^2} = 4.70 \times 10^{-13}\ \text{g cm}^{-1}$$

Finally, an estimate for the number of ribbons per fiber can be obtained assuming that the distance between molecules along the fiber axis is determined by the repeat distance of the urea-urea hydrogen bonding motif:

$$\frac{\text{Molecule}}{\text{H-H}} = \frac{\text{H-H}_{distance} \times M_L \times N_A}{M_W} =$$

$$= \frac{4.6 \times 10^{-8}\text{cm} \times 4.70 \times 10^{-13}\text{g cm}^{-1} \times 6.02 \times 10^{23}\text{mol}^{-1}}{1350.9\ \text{g mol}^{-1}} = 9.6\ \text{molecules}$$

$\text{H-H}_{distance}$ being the distance between urea groups along the stack, N_A Avogadro's number and M_W the molecular weight of DA.

Gel preparation method

Samples were prepared by weighing DA along with DA-AC or DA-N_3 (10 mol%) in the solid state followed by the addition of ca. 300 μL chloroform. The solvent was allowed to evaporate overnight. The remaining solid was subsequently re-dissolved in mili-Q water assisted by applying combined cycles of sonication (30 min) and vortex (1 min) until the full dissolution of the solid material. The micelles were then allowed to grow for additional 2 d and the solutions transferred to quartz cuvettes (1 × 1 cm) followed by irradiation with UV-light (254 nm) for 15 min under continuous stirring using a Luzchem photoreactor (model LCZ 4V) equipped with 7.2 W UV-C lamp. Equal volumes of polymerized PDA/DA-Ac and PDA/DA-N_3 mixtures were mixed ensuring equimolar acetylene/azide ratios (5 mol%) with subsequent addition of premixed aqueous solutions of $CuSO_4$/Tris(3-hydroxypropyltriazolylmethyl)amine (THPTA) and a solution of sodium ascorbate (Na-Ascorbate) to a final concentration of 0.1, 0.5 and 10 mM respectively. The reaction mixture was immediately transferred to the rheometer where gelation was monitored by oscillatory rheometry.

Scaling relationships and crosslinking length determination

In order to establish the origins of the observed nonlinear elastic response, we have individually plotted the scaling of the plateau modulus (G_0) and the critical stress (σ_c) with concentration; see Figs. S2.9.a and b. In both cases, the double-logarithmic plots clearly reveal two regimes; below the 15 mg mL^{-1} concentration point, the dependence of either quantity on concentration is different from that above 15 mg mL^{-1}. In addition, the observed power laws are far stronger than those generically expected for semi-flexible polymers. This we attribute to the short, stiff rods in our system combined with the high density. As far as we are aware, no generic scaling prediction exist for this regime.

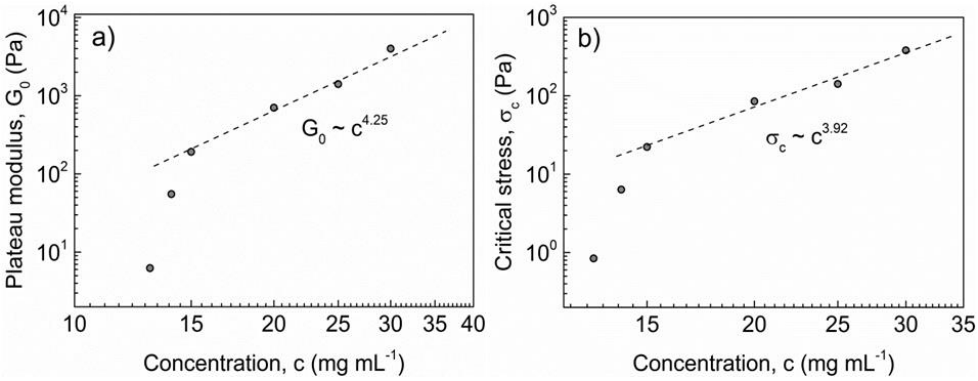

Fig. S2.9 | (a) Dependence of G_0 on concentration showing two regimes, separated at c of about 15 mg mL^{-1} dropping the point at 10 mg mL^{-1}. (b) σ_c vs concentration with two distinct regimes, separated at c of about 15 mg mL^{-1} dropping the point at 10 mg mL^{-1}.

The distinct high- and low-density regimes might appear to make it all the more surprising that the nonlinear curves do collapse, but this is incorrect; the values of σ_c and G_0 were chosen such that the rheology curves collapse, and therefore the two observations are not independent. The universal power-law m = 1 at high strains is, however, independent. The fact that it is preserved in both the low- and high-density regime suggests a common, strain-prompted nonlinear origin of the stiffening.

Remarkably, across the range of concentrations considered, there is a universal interdependency among concentration, G_0 and σ_c. Following the suggestions in Yao *et al.*[9], we plot in Fig. S2.10 the square root of concentration times the modulus versus the critical concentration, and find - over more than two decades of scaling - a power-law relation with a slope very close to 3/2, observed and predicted for intermediate filaments[9].

The crosslinking length for the material was estimated by generating coarse-grained networks of stiff rods with a length of 152 nm, and determining how many of the putative crosslinking groups are within a crosslinking distance (12 nm) of each other, assuming a random arrangement. While we find that for the high volume fractions (4%) of these systems a significant portion of all crosslinks is expected to be engaged, these links have a strong tendency to cluster around sites of particularly close rod proximity. On average, we estimate from these simulations that 2-3 such clustered connections exist per rod (see Fig. S2.11), which brings the crosslinking length estimate to 50-80 nm

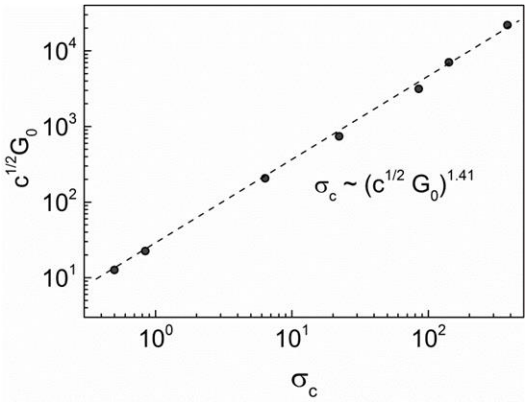

Fig. S2.10 | Dependence of $c^{1/2}G_0$ on σ_c. The dashed line is the result of a regression fit to the data and depicts an exponent of 1.41. The scaling appears to agree with the affine thermal model, which predicts an exponent of 3/2.

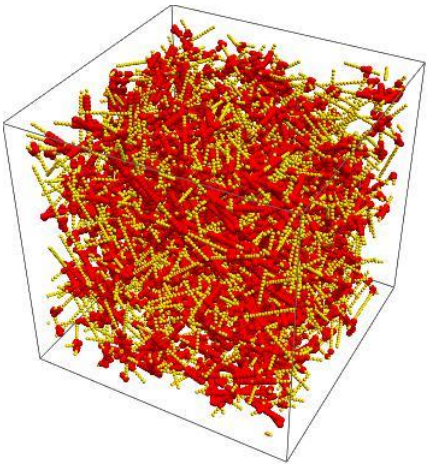

Fig. S2.11 | A sample simulated network configuration: 1500 rods of length 152 nm and diameter 6.6 nm in a 500x500x500nm box. Volume fraction (after deleting segments outside of the box) is 3.7%. For this network, 54% of all available crosslinking sites is within crosslinking distance (12nm, sites coloured red) of another site, and 2-3 clusters of links occur per rod.

2.5. References

1. Gardel, M. L. *et al.* Elastic Behavior of Cross-Linked and Bundled Actin Networks. *Science* **304,** 1301–1305 (2004).
2. Gardel, M. L. *et al.* Scaling of F-Actin Network Rheology to Probe Single Filament Elasticity and Dynamics. *Phys. Rev. Lett.* **93,** 188102 (2004).
3. Motte, S. & Kaufman, L. J. Strain stiffening in collagen I networks. *Biopolymers* **99,** 35–46 (2013).
4. Kurniawan, N. A., Wong, L. H. & Rajagopalan, R. Early Stiffening and Softening of Collagen: Interplay of Deformation Mechanisms in Biopolymer Networks. *Biomacromolecules* **13,** 691–698 (2012).
5. Licup, A. J. *et al.* Stress controls the mechanics of collagen networks. *Proc. Natl. Acad. Sci.* **112,** 9573–9578 (2015).
6. Brown, A. E. X., Litvinov, R. I., Discher, D. E., Purohit, P. K. & Weisel, J. W. Multiscale Mechanics of Fibrin Polymer: Gel Stretching with Protein Unfolding and Loss of Water. *Science* **325,** 741–744 (2009).
7. Piechocka, I. K. *et al.* Multi-scale strain-stiffening of semiflexible bundle networks. *Soft Matter* **12,** 2145–2156 (2016).
8. Piechocka, I. K., Bacabac, R. G., Potters, M., MacKintosh, F. C. & Koenderink, G. H. Structural Hierarchy Governs Fibrin Gel Mechanics. *Biophys. J.* **98,** 2281–2289 (2010).
9. Yao, N. Y. *et al.* Elasticity in Ionically Cross-Linked Neurofilament Networks. *Biophys. J.* **98,** 2147–2153 (2010).
10. Lin, Y.-C. *et al.* Origins of Elasticity in Intermediate Filament Networks. *Phys. Rev. Lett.* **104,** 058101 (2010).
11. Storm, C., Pastore, J. J., MacKintosh, F. C., Lubensky, T. C. & Janmey, P. A. Nonlinear elasticity in biological gels. *Nature* **435,** 191–194 (2005).
12. Erk, K. A., Henderson, K. J. & Shull, K. R. Strain Stiffening in Synthetic and Biopolymer Networks. *Biomacromolecules* **11,** 1358–1363 (2010).
13. Onck, P. R., Koeman, T., van Dillen, T. & van der Giessen, E. Alternative Explanation of Stiffening in Cross-Linked Semiflexible Networks. *Phys. Rev. Lett.* **95,** 178102 (2005).
14. Lieleg, O., Claessens, M. M. a. E., Heussinger, C., Frey, E. & Bausch, A. R. Mechanics of Bundled Semiflexible Polymer Networks. *Phys. Rev. Lett.* **99,** 088102 (2007).
15. Broedersz, C. P., Storm, C. & MacKintosh, F. C. Effective-medium approach for stiff polymer networks with flexible cross-links. *Phys. Rev. E* **79,** 061914 (2009).
16. Broedersz, C. P., Storm, C. & MacKintosh, F. C. Nonlinear elasticity of composite networks of stiff biopolymers with flexible linkers. *Phys. Rev. Lett.* **101,** 118103 (2008).
17. Kouwer, P. H. J. *et al.* Responsive biomimetic networks from polyisocyanopeptide hydrogels. *Nature* **493,** 651–655 (2013).
18. Jaspers, M. *et al.* Bundle Formation in Biomimetic Hydrogels. *Biomacromolecules* **17,** 2642–2649 (2016).
19. Pal, A. *et al.* Topochemical polymerization in self-assembled rodlike micelles of bisurea bolaamphiphiles. *Soft Matter* **10,** 952–956 (2014).
20. Kasza, K. E. *et al.* The cell as a material. *Curr. Opin. Cell Biol.* **19,** 101–107 (2007).
21. Yuan, A., Rao, M. V., Veeranna & Nixon, R. A. Neurofilaments at a glance. *J Cell Sci* **125,** 3257–3263 (2012).
22. Rammensee, S., Janmey, P. A. & Bausch, A. R. Mechanical and structural properties of in vitro neurofilament hydrogels. *Eur. Biophys. J.* **36,** 661–668 (2007).
23. Dogic, Z. *et al.* Elongation and Fluctuations of Semiflexible Polymers in a Nematic Solvent. *Phys. Rev. Lett.* **92,** 125503 (2004).
24. Saez Talens, V. *et al.* Aromatic Gain in a Supramolecular Polymer. *Angew. Chem. Int. Ed.* **54,** 10502–10506 (2015).

25. Obert, E. *et al.* Both Water- and Organo-Soluble Supramolecular Polymer Stabilized by Hydrogen-Bonding and Hydrophobic Interactions. *J. Am. Chem. Soc.* **129,** 15601–15605 (2007).
26. Koenigs, M. M. E. *et al.* Tuning Cross-Link Density in a Physical Hydrogel by Supramolecular Self-Sorting. *Macromolecules* **47,** 2712–2717 (2014).
27. Pawar, G. M. *et al.* Injectable Hydrogels from Segmented PEG-Bisurea Copolymers. *Biomacromolecules* **13,** 3966–3976 (2012).
28. Hong, V., Presolski, S. I., Ma, C. & Finn, M. G. Analysis and Optimization of Copper-Catalyzed Azide–Alkyne Cycloaddition for Bioconjugation. *Angew. Chem. Int. Ed.* **48,** 9879–9883 (2009).
29. Presolski, S. I., Hong, V., Cho, S.-H. & Finn, M. G. Tailored Ligand Acceleration of the Cu-Catalyzed Azide−Alkyne Cycloaddition Reaction: Practical and Mechanistic Implications. *J. Am. Chem. Soc.* **132,** 14570–14576 (2010).
30. Broedersz, C. P. *et al.* Measurement of nonlinear rheology of cross-linked biopolymer gels. *Soft Matter* **6,** 4120–4127 (2010).
31. Licup, A. J. *et al.* Stress controls the mechanics of collagen networks. *Proc. Natl. Acad. Sci.* **112,** 9573–9578 (2015).
32. Meechai, N., Jamieson, A. M., Blackwell, J., Carrino, D. A. & Bansal, R. Viscoelastic properties of aggrecan aggregate solutions: Dependence on aggrecan concentration and ionic strength. *J. Rheol.* (2002). doi:10.1122/1.1463419
33. Jaspers, M. *et al.* Ultra-responsive soft matter from strain-stiffening hydrogels. *Nat. Commun.* **5,** 5808 (2014).
34. Piechocka, I. K. *et al.* Multi-scale strain-stiffening of semiflexible bundle networks. *Soft Matter* (2016). doi:10.1039/C5SM01992C
35. Schmoller, K. M., Lieleg, O. & Bausch, A. R. Structural and Viscoelastic Properties of Actin/Filamin Networks: Cross-Linked versus Bundled Networks. *Biophys. J.* **97,** 83–89 (2009).
36. Claessens, M. M. a. E., Semmrich, C., Ramos, L. & Bausch, A. R. Helical twist controls the thickness of F-actin bundles. *Proc. Natl. Acad. Sci.* **105,** 8819–8822 (2008).
37. Goswami, L. N., Houston, Z. H., Sarma, S. J., Jalisatgi, S. S. & Hawthorne, M. F. Efficient synthesis of diverse heterobifunctionalized clickable oligo(ethylene glycol) linkers: potential applications in bioconjugation and targeted drug delivery. *Org. Biomol. Chem.* **11,** 1116–1126 (2013).
38. Baral, A. *et al.* Assembly of an Injectable Noncytotoxic Peptide-Based Hydrogelator for Sustained Release of Drugs. *Langmuir* **30,** 929–936 (2014).
39. Fulmer, G. R. *et al.* NMR Chemical Shifts of Trace Impurities: Common Laboratory Solvents, Organics, and Gases in Deuterated Solvents Relevant to the Organometallic Chemist. *Organometallics* **29,** 2176–2179 (2010).
40. Schindelin, J. *et al.* Fiji: an open-source platform for biological-image analysis. *Nat. Methods* **9,** 676–682 (2012).
41. Lamour, G., Kirkegaard, J. B., Li, H., Knowles, T. P. & Gsponer, J. Easyworm: an open-source software tool to determine the mechanical properties of worm-like chains. *Source Code Biol. Med.* **9,** 16 (2014).

Chapter 3:

Strain-stiffening hydrogels made from supramolecular polymers*

Abstract: *The cytoskeleton is a highly adaptive network of filamentous proteins capable of robustly stiffening under stress while, at the same time, collectively assemble/disassemble with turnover rates on the order of minutes. Synthetic biomimetic materials that combine reversibility and strain-stiffening properties remain unexplored. Here, strain-stiffening gels that have dynamic fibrous polymers as their main structural components are reported. The fibers form via hierarchical self-assembly of oligoethlylene diacetylene bis-urea bolaamphiphiles (DA). In water, DA-based fibers integrate multiple ribbons, that aggregate perpendicular to the fiber axis. The monomers exchange slowly in solution with dynamics that span a few days, reflecting their strong intermolecular interactions. Sonication of the fibers disrupts the supramolecular interactions breaking the fibers into smaller aggregates that recombine to recover the equilibrium length. Chemical crosslinking of the fibers yields hydrogels capable of strain-stiffening in a way that closely resembles biogels, and enables continuous variation of properties though readily modifiable parameters. The work thus demonstrates that biomimetic strain-stiffening gels are a robust and versatile motif for biomimetic and responsive materials with tunable properties.*

*Jürgen Schill is acknowledged for the cryo-EM analysis, Dr. Peter-Paul K. H. Fransen is acknowledged for the synthesis and characterization of the pentaazide linker, Gijs M. ter Huurne and Dr. Ilja K. Voets for their contribution to the SAXS analysis, Prof. Dr. Cornelis Storm is acknowledged for discussions on the interpretation of the results and modelling of the rheology data and Dr. Koen Pieterse (ICMS Animation Studio) is gratefully thanked for help with the graphics.

3.1. Introduction

Biological fibrous networks are both adaptive and robust. These seemingly conflicting responses are encoded at different lengthscales. On the one hand, the constituent fibers (actin, microtubules, collagen) are held together by often quite weak supramolecular forces, enabling dynamic structural adaptation through rapid assembly and disassembly[1–6]. On the other hand, their networks, taken as a whole, are robustly capable of 'strain stiffening'[7–12]; a strengthening that is prompted by external loading, without the need for structural changes. Clearly these contrapuntal abilities provide great functionality, which ideally one would like to reconstitute in synthetic materials.

However, while both reversibility[13–16] and strain stiffening[17–20] have been repeatedly demonstrated *separately*, there is until now no single synthetic material that possesses *both* qualities. In the current chapter, we present uniquely biomimetic, strain-stiffening hydrogels composed of crosslinked, reversibly self-assembled semi-flexible fibers that display self-healing properties that span several days.

In previous attempts to make self-assembled strain-stiffening gels, fibers formed from oligo(ethylene glycol) (OEG)-bisurea bolaamphiphiles were physically crosslinked using, polymeric, flexible crosslinkers[21,22]. The absence (or strongly delayed onset) of strain-stiffening was ascribed to the length of the crosslinkers. In Chapter 2, (OEG)-bisurea bolaamphiphiles with a diacetylene unit embedded between urea groups (DA), were successfully introduced as building blocks to create strain-stiffening networks. In water, these molecules self-assemble into fibers composed of 9-10 aggregated ribbons with an average contour length of 157 nm, 3.3 nm radius and a persistence length of 280 nm. The molecules are held together via intermolecular urea-urea hydrogen-bonds and hydrophobic interactions. Photo-polymerization of the stacked diacetylenes produces fibers with a covalent polydiacetylene (PDA) backbone without morphological changes[23]. Moreover, as illustrated in Chapter 2, the system does not gelate in the absence of specifically designed cross-linkers, providing an opportunity to tune the rheology by chemical cross-linking. To this end, reactive bisurea analogues with azide- and acetylene moieties grafted to peripheral octaethylene glycol hydrophilic blocks were incorporated in the fibers. A Cu-catalyzed click reaction was used to crosslink fibers without affecting their size.

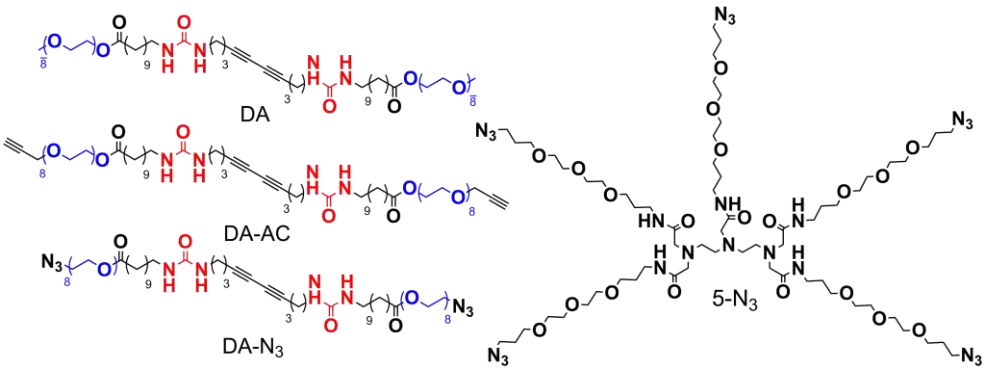

Fig. 3.1 | Molecular structure of the diacetylene bis-urea bolaamphiphile DA, its functionalized analogues DA-AC and DA-N_3 and the pentaazide 5-N_3 crosslinker.

In the current chapter we investigate strain-stiffening in gels of DA fibers which are not fixated via diacetylene cross-polymerization. We confirm the reversible nature of the fibers by showing that the amphiphiles exchange slowly between fibers, and by demonstrating that fibers re-assemble when fragmented by ultrasound. The most striking finding is that cross-linked gels of supramolecular DA fibers may exhibit strain-stiffening – the first demonstration of non-covalent, self-assembling building blocks with sufficient axial strength and orientational persistence to withstand forces high enough to support a nonlinear mechanical response. Furthermore, we demonstrate control over mechanical performance; by using a combined crosslinking-fixation strategy we significantly extend the stiffening range (*i.e.* the overall relative increase in modulus before failure).

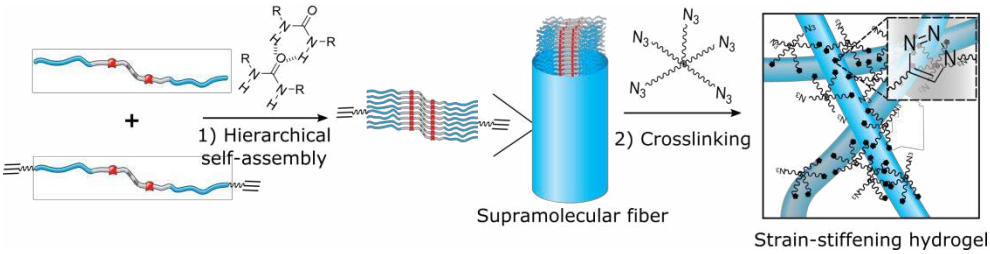

Scheme 3.2 | Hierarchical self-assembly through intermolecular H-bonding and hydrophobic interactions of functionalized (DA-AC) and unfunctionalized (DA) diacetylene bisurea bolaamphiphiles. Structure of the fibers containing 9-10 ribbons as confirmed by SAXS in Chapter 2 and covalent crosslinking with pentaazide linker (5-N_3) into strain-stiffening networks with covalent triazole linkages.

3.2. Results and discussion

Chemical crosslinking using pentaazide linker

Gelation was achieved by chemical crosslinking of solutions containing a mixture of co-assembled DA/DA-AC fibers and a pentaazide (5-N_3) (Fig. 3.1 and Scheme 3.2) consisting of short functionalized OEG blocks grafted to a diethylenetriaminepentaacetic (DTPA) core capable of forming multiple crosslinks per molecule[24,25]. Click reaction between azide and acetylene groups was initiated at room temperature upon addition of sodium ascorbate (Na-ascorbate) to an aqueous solution containing an stoichiometric ratio of acetylene/azide groups in combination with premixed $CuSO_4$ and a water-soluble tris(3-hydroxypropyltriazolylmethyl)amine (THPTA) kelating ligand widely used for bioconjugations (see methods section)[26]. ^{1}H-NMR showed high conversions of the crosslinking reaction, in which 80% of the terminal acetylene groups from DA-AC reacted with 5-N_3 during the gelation process (Fig. 3.3).

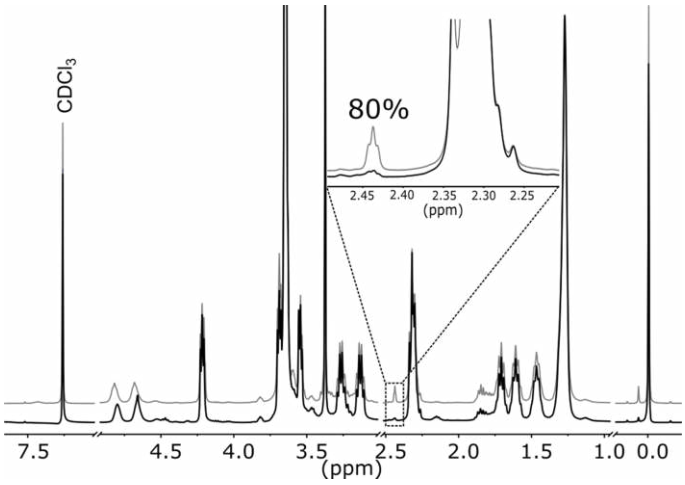

Fig. 3.3 | ^{1}H-NMR ($CDCl_3$, 25 ^{o}C) spectra of 20 mg mL^{-1} DA containing 20 mol% DA-AC, crosslinked with 5-N_3 acquired before (grey line) and 24 h after addition of the catalyst (black line) showing 80% conversion calculated by integrating the area below the curve corresponding to the terminal acetylene protons of DA-AC.

Structural characterization of the system before (sol) and after completion of the crosslinking reaction (gel) was performed by Small-Angle X-Ray scattering (SAXS). While the observed differences in slope in the low *q*-regime between sol and gel

cannot be explicitly attributed to a change in the fiber's length or rigidity solely based on SAXS (Fig. 3.4), the overlap in the high *q*-region infers that the diameter of the fibers is around 3 nm. Indeed, fitting of the scattering profiles before and after gelation gave a value for the cross-sectional radius of 3.3 ± 0.2 nm (Fig. 3.4 and experimental section). This value is consistent with the radius of 3.3 nm measured in cryo-electron microscopy (cryo-EM) as well as the value of 3.1 ± 0.1 nm obtained from fitting of the scattering profiles detailed in Chapter 2. This is in clear contrast to polyisocyanopeptide (PIC) strain-stiffening hydrogels, where gelation relies on physical aggregation of individual polymer chains with an associated increase in bundle dimensions measurable by SAXS[27].

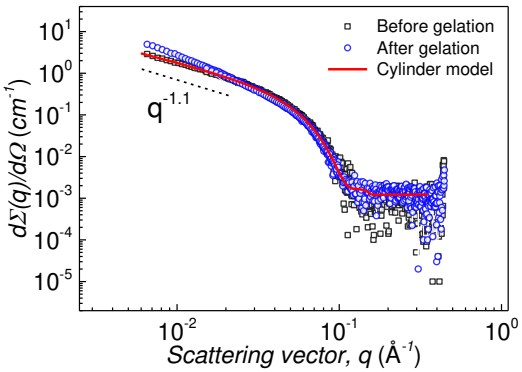

Fig. 3.4 | SAXS profiles recorded before (blue) and 24 h after (black) crosslinking of 15 mg mL^{-1} DA/DA-AC (20 mol% DA-AC) solutions with 5-N_3.

Dynamics of DA fibers in solution

The exchange dynamics of DA fibers were investigated through the mechanical properties of their gels. Thus, equal amounts of 1.6 wt% aqueous solutions of DA fibers with and without 20 mol% reactive DA-AC in the presence of 5-N_3 were mixed, and allowed to exchange in solution during a varying incubation time prior to chemical crosslinking upon addition of the catalyst mixture (Fig. 3.4.a)[26,28]. Immediately after addition of the catalyst, solutions were transferred to the rheometer, where gelation was monitored under continuous oscillatory strain until a plateau of the dynamic moduli was reached. Without exchange, only half of the fibers can be crosslinked and contribute to the network stiffness, while the dynamic exchange of amphiphilic molecules will lead to a homogeneous distribution of reactive DA-AC in all fibers at full equilibration (*i.e.* all fibers contribute to the network mechanics). The

moduli during gelation were measured after incubation times of 0, 1, 4 and 7 days. Fig. 3.5.b shows the development of the storage moduli G' after addition of the catalyst. For all incubation times, G' steadily increases and reaches a plateau after approximately 15 h. However, the plateau value of G' at the completion of the crosslinking reaction is higher by nearly a factor of 3 after incubation for 1 week relative to samples where crosslinking was initiated immediately after mixing of reactive and unreactive fibers indicating a slow dynamic equilibrium with a time constant of a few days. Similar monomer exchange rates were reported for water-soluble, synthetic supramolecular polymers with comparable-sized aliphatic cores[29] as well as biopolymer amyloid fibrils[30,31] where the hydrogen bond array, tightly packed within the fibrillar structure is efficiently shielded from interaction with water molecules.

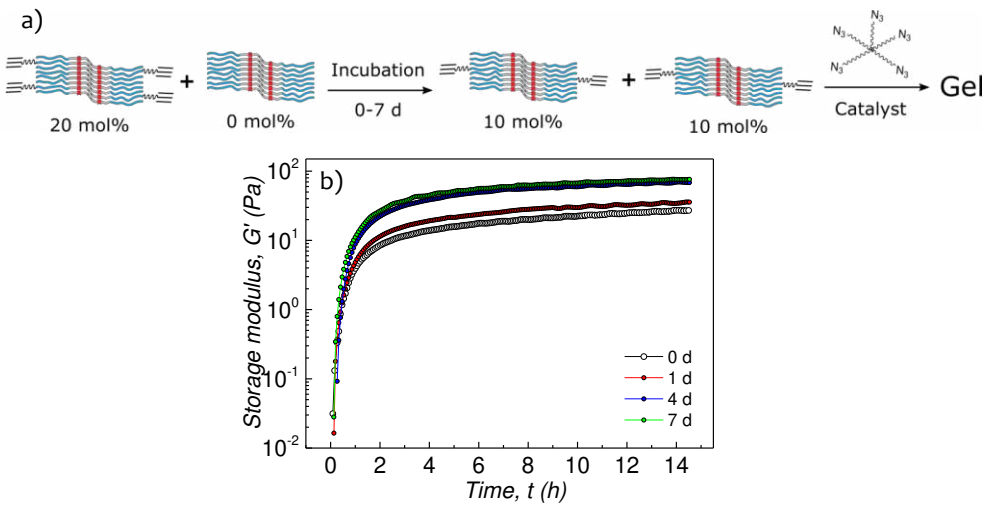

Fig. 3.5 | (a) Monomer exchange between labeled (DA/DA-AC) and unlabeled (DA) fibers followed by gelation via covalent crosslinking. Time course of storage modulus G' measured by applying oscillatory shear $\gamma = 1\%$ and $\omega = 6.28$ rad s^{-1} during Cu-catalyzed click reaction of b) 16 mg mL^{-1} DA/DA-AC (20 mol% DA-AC) mixed with 16 mg mL^{-1} DA plotted as a function of incubation time.

The reversibility of DA aggregates was further probed by sonication of fiber solutions. Similar to experiments reported by Talens *et al.* [32] involving analogous squaramide-based bolaamphiphiles, cryo-EM of fibers before and after sonication for 1h (Figs. 3.6.a-c) provide direct evidence that the fibers are fragmented by sonication but recover their original length after equilibration for 2 days (Fig. 3.6.c). Similar

disassembly processes into much shorter ensembles have been observed in solutions of amyloid fibrils subjected to sonication[33].

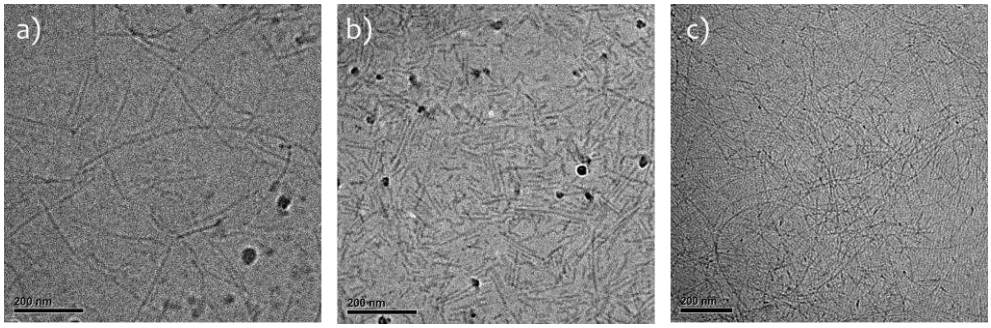

Fig. 3.6 | Cryo-EM micrographs of DA in water (1 mM): (a) Unperturbed system. (b) After 1 h of sonication. (c) After 1h of sonication followed by 2 d of re-assembly. Scale bars: 200 nm.

We found no signs of sonication-induced diacetylene polymerization after 2h, nor of polymerization due to exposure to stray light within the experimental timescales (Fig. S3.6).

Concentration dependence

In contrast to conventional synthetic hydrogels based on flexible polymers, biogels are known to stiffen at low-to-intermediate stresses[7,9–11,34,35]. DA networks were likewise found to respond to applied shear stress with an associated increase in modulus. To carefully capture linear and nonlinear regimes of crosslinked DA networks, a pre-stress protocol[36] was applied, and the differential modulus K (the elastic part of which relates the change in stress with strain $K' = \delta\sigma/\delta\gamma$) was measured by parallel superposition of an oscillatory and a steady pre-stress σ. By plotting K' against σ, two distinct regimes arise: a low-stress regime where the elastic response is linear with K' equal to the plateau modulus G_0, and a high stress regime above the critical stress σ_c where K' becomes strongly dependent on σ and scales with stress as $K' = \sigma^m$, m being the stiffening index. The combination of these parameters provide a direct measure of the network's sensitivity to applied stress; a property commonly termed responsiveness.

An effective way to change the mechanical properties of the gels is through varying the polymer concentration, c. Indeed, the linear modulus of the hydrogels G_0 is strongly dependent on DA concentration, as was determined for bolaamphiphile concentrations between 6 mg mL^{-1} and 35 mg mL^{-1} for a fixed molar ratio [DA]/[DA-

AC] of 10:1 and a stoichiometric alkyne/azide ratio. The data in Fig. 3.7.a show, that upon increasing the concentration in the hydrogels by a factor of 6, the modulus increases by nearly 3 orders of magnitude while the stress at failure σ_{max} rises by 4 decades. Concurrently, the onset of the nonlinear regime is delayed to higher critical pre-stresses σ_c at higher bolaamphiphile concentration. Over the whole concentration range explored, both G_0 and σ_c scale strongly with concentration, $G_0 \propto c^n$ and $\sigma_c \propto c^n$ with high exponents n of 3.4 and 3.6 respectively (Fig. S3.7). These values were found to be well above the exponent of n =11/5 predicted for permanently crosslinked semiflexible networks in which the elasticity is entropic in nature[37]. Nonetheless, n values as high as 2.5 for bundled actin networks[7,38] and 3 for reconstituted collagen type-I networks[39] have been experimentally reported, suggesting that the original theoretical predictions, relying on single chains to support the stresses, may need to be adjusted upward in bundled systems. We suspect such corrections to be of particular relevance in situations where there is a distribution of fiber diameters.

Upon imparting a critical stress σ_c that is concentration-dependent, all gels begin to stiffen, entering their nonlinear regime. Normalizing of K' and σ against G_0 and σ_c collapses all data onto a single master curve (Fig. 3.7.b) featuring the characteristic linear relationship between K' and σ ($K' \propto \sigma^1$) also reported in Chapter 2. The same relationship has been observed in various types biopolymer gels reconstituted from extra- and intracellular proteins including type I collagen[11], neurofilament hydrogels[34] and, more recently, branched actin networks measured under compressive forces exerted by magnetic cylinders[40]. These results highlight the common origins of elasticity in these systems where non-linearity sets in due to enhanced flexural rigidity and backbone stiffness of the constituent biopolymers[7,41]. Normalization of the curves also reveals relatively narrow stiffening ranges K'_{max}/G_0 of approximately 2.5-3-fold at this specific [DA]/[DA-AC] molar ratio, tightly coupled to the inherently weak supramolecular interactions between bolaamphiphiles. Such weak mechanical responsiveness is in stark contrast to strain-stiffening PIC hydrogels where robustness relies on the use of covalent polymers leading to K'_{max}/G_0 values well above 10[17,18].

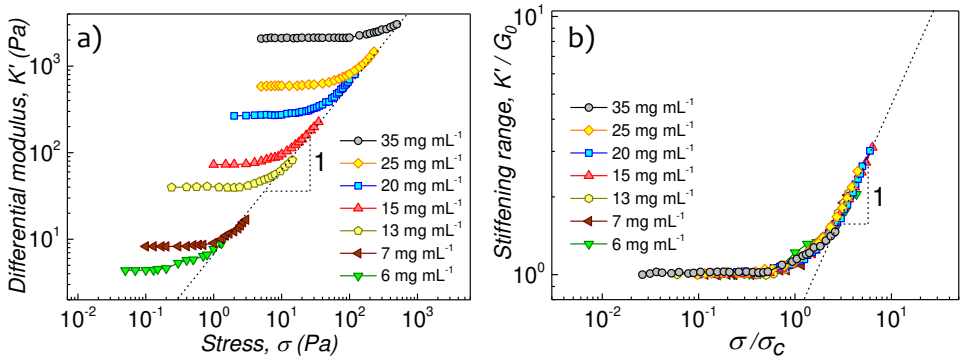

Fig. 3.7 | (a) Differential modulus K' vs. stress σ for crosslinked DA mixtures containing 10 mol% DA-AC of different concentrations. (b) Plot of K' vs stress σ with K' normalized to G_0 and σ normalized to σ_c, showing collapse onto single master curve with $K' \propto \sigma^1$ dependency at high σ.

Effect of crosslink density

The mechanical properties of hydrogels are profoundly influenced by the density of crosslinks found within the 3D meshwork. To assess the effect of crosslinking density on DA hydrogel mechanics, the degree of functionalization of the fibers was modified by blending functionalized DA-AC and unfunctionalized DA at different molar ratios prior chemical crosslinking with 5-N_3 ensuring a stoichiometric ratio of acetylene/azide groups in all experiments. Figs. 3.8.a-c summarize the findings: increased [DA-AC]/[DA] molar ratios were shown to enhance hydrogel elasticity (measured as the ratio G'/G" in the linear regime) (Fig. S3.8). Concomitantly, the stiffening range K'_{max}/G_0 of the gels dramatically increased with [DA-AC]/[DA] ratio reaching a maximum value of 8.6 at 20 mol% DA-AC beyond which a cloudy dispersion of undissolved material was observed at 25 mol% DA-AC that resulted in both decrease of G'/G" and K'_{max}/G_0 (Figs. 3.8.c and S3.8.b). The enhancement of K'_{max}/G_0 at a higher density of crosslinks can be rationalized on the basis of an external covalent reinforcement of the supramolecular fibers caused by the inherently non-selective crosslinking strategy here employed. Thus, according to this hypothesis, a single 5-N_3 molecule can either react with acetylene groups present along the same fiber (intrafiber fixation) or bridge different fibers thereby contributing to the linear modulus of the network. The formation of intrafiber crosslinks provides an external reinforcement that covalently interconnects bolaamphiphiphiles within the same fiber (Fig. 3.8.d). Now, considering the high conversion of the crosslinking reaction as

measured by NMR in Fig. 3.3 (*i.e.* ca. 80 %), the degree of functionalization of the fibers required for connectivity and that each fiber is composed of about 10 ribbons aggregated perpendicular to the fiber axis (Scheme 3.2), we can expect almost 2 acetylene groups every urea-urea repeat distance (0.46 nm)[42] along the fiber axis at a degree of functionalization above 10 mol% DA-AC. Indeed, a steeper increase in K'_{max}/G_0 is observed beyond 10 mol% corresponding to full external fixation of the fibers presumably in combination with cross-fixation of the ribbons leading to stronger fibers, capable of bearing considerably higher extensional loading at high shear stress. This allows the hydrogels to retain their integrity over a broader range of applied stress.

To compare the nonlinear rheology of our gels to that of biogels, we apply a model introduced by Shull and coworkers[43]. This phenomenological hyperelastic model is equivalent to the Fung model[44] commonly used to describe the mechanics of collagenous tissues such as those found in arteries[45,46]. In the Fung-Shull model, the stress σ as a function of the strain γ is given by:

$$\sigma = G_0 \gamma e^{(\gamma/\gamma_c)^2}$$

With σ_c the critical strain (at which nonlinearity sets in) and G_0 the plateau modulus. Taking the strain derivative of this function, eliminating γ in favour of σ from the result, and normalizing G to G_0 and σ to σ_c, respectively, yields a universal, zero-parameter stiffening curve which captures our data remarkably well (see Fig. 3.8.b). The stiffening exponent m in the Shull-Fung model is equal to 1. This agreement between biomaterial and synthetic performance again highlights the biomimetic character of our hydrogels.

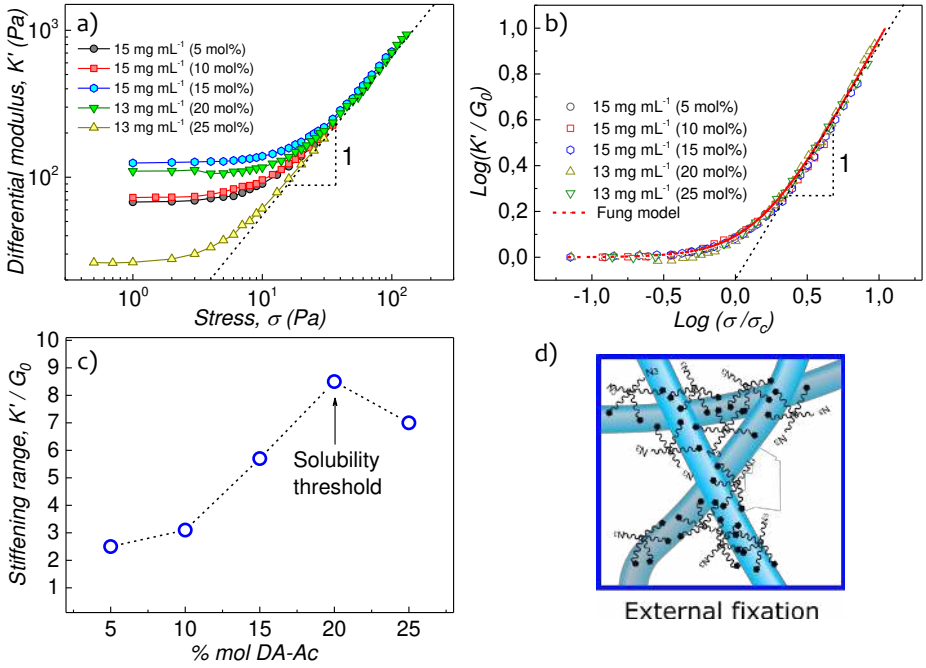

Fig. 3.8 | (a) Differential modulus K' vs stress σ for different DA/DA-AC ratios. (b) Scaling of K' with G_0 and σ with σ_c showing a collapse into single master curve with K' ∝ σ^1 dependency at high σ. Data fitted to Fung model (red line). (c) Stiffening range K'/G_0 plotted against molar percent of DA-AC with the arrow indicating the onset of fiber precipitation. d) Fiber strengthening through external covalent reinforcement.

Incubation time dependence on the nonlinear regime

In the previous section, we have illustrated how the stiffening range K'_{max}/G_0 of the hydrogels varies in line with extent of functionalization of the fibers. Accordingly, we used K'_{max}/G_0 to probe the exchange of monomer between labelled (DA/DA-AC) and unlabelled (DA) fibers as previously illustrated in Fig. 3.5. Thus, the K'_{max}/G_0 values from gels formed by chemical crosslinking of fibers previously incubated in solution were measured as a function of the incubation time. Figs. 3.8.a and b. clearly illustrate that mixtures of labelled/unlabelled fibers crosslinked without exchange, exhibit predominantly the K'_{max}/G_0 values reminiscent of networks composed of fibers with 20 mol% DA-AC. By allowing the mixture of labelled/unlabelled fibers to exchange in solution for a few days, the K'_{max}/G_0 of the resultant hydrogels gradually decreases over time approaching the values associated to networks of fibers containing 10 mol% DA-AC functionalization, suggestive of an homogeneous

distribution of DA-AC across the system at full equilibration (1 week) consistent with the timescales measured in Fig. 3.5.a. These results provide further evidence that DA fibers are in slow dynamic equilibrium and that these dynamics directly influence the rheology of their gels.

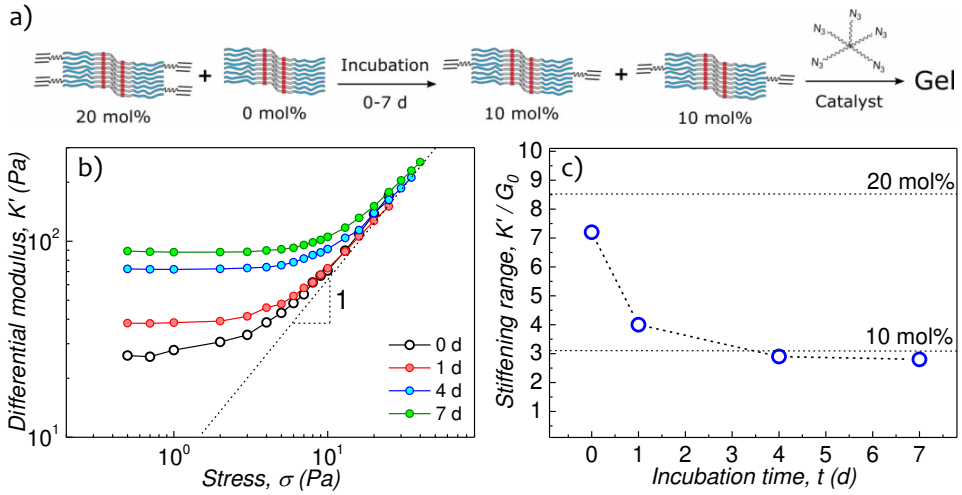

Fig. 3.9 | (a) Monomer exchange between labelled (DA/DA-AC) and unlabelled (DA-AC) fibers followed by gelation via covalent crosslinking. (b) Differential modulus K' vs stress σ obtained from gels of Fig. 3.5.b. (c) Measured change in stiffening ranges K'_{max}/G_0 as a function of fiber incubation time. Dashed lines indicate the K'_{max}/G_0 values measured for networks containing 20 and 10 mol% DA-AC as obtained from normalized curves of Fig. 3.7.b.

Suppressing external fiber fixation through selective crosslinking

So far, we have shown that strain-stiffening hydrogels are formed using supramolecular polymers after crosslinking. Nevertheless, the use of covalent, non-selective crosslinks potentially induces covalent fixation of the fibers along their hydrophilic contour in a similar fashion to fiber reinforcement through internal diacetylene cross-polymerization discussed in Chapter 2. In other words, the presence of intrafiber surface fixation conceals the contribution arising exclusively from the supramolecular network thereby augmenting its responsiveness towards applied stress. To circumvent this, an alternative crosslinking strategy was adopted that is similar to that presented in Chapter 2, where the extent of internal loop formation −and by extension that of external fiber fixation− is minimized. According to this method, co-assembled mixtures from DA/DA-AC and DA/DA-N_3 were blended in chloroform

and re-dissolved in water separately to a final concentration of 50 mg mL^{-1}. Equal volumes of azide- and acetylene-labelled fibers were mixed and the crosslinking reaction was immediately started upon addition of the catalyst mixture (Fig. 3.9.a). Herein, given the slow dynamics of exchange measured for DA monomers under no stimulus (Fig. 3.5.b), the formation of inactive loops due to insertion of DA-N_3 into a DA-AC-labelled fiber can be considered negligible within the experiment timescales (*i.e* 12-15 h). Gels formed via this procedure were subjected to a full range of applied constant pre-stress and the stiffness of the material was measured as a function of σ. Remarkably, gels formed through selective crosslinking strategies were found to exhibit stress-stiffening, where the modulus of the material is initially characterized by its plateau storage modulus G_0 at low σ yet it increases after a σ_c is imparted to the hydrogel (Fig. 3.10.b). We then proceeded to calculate the magnitude of K'_{max}/G_0 from the normalized curves and compare them with the values derived from non-selective crosslinking strategies (Fig. 3.10.c). Fig. 3.10 clearly shows the appearance of two distinct regimes: a regime characterized by lower values of K'_{max}/G_0 corresponding to the stiffening arising from the supramolecular network. Here, the magnitude of K'_{max}/G_0 is independent on the density of crosslinks (negligible effect of intrafiber fixation) and a regime where K'_{max}/G_0 is tightly coupled to the extent of external covalent fixation that continuously increases with [DA]/[DA-AC] molar ratio. Furthermore, the values of K'_{max}/G_0 of gels formed through selective and non-selective strategies converge at the point where the extent of external fixation reaches a minimum in the latter case.

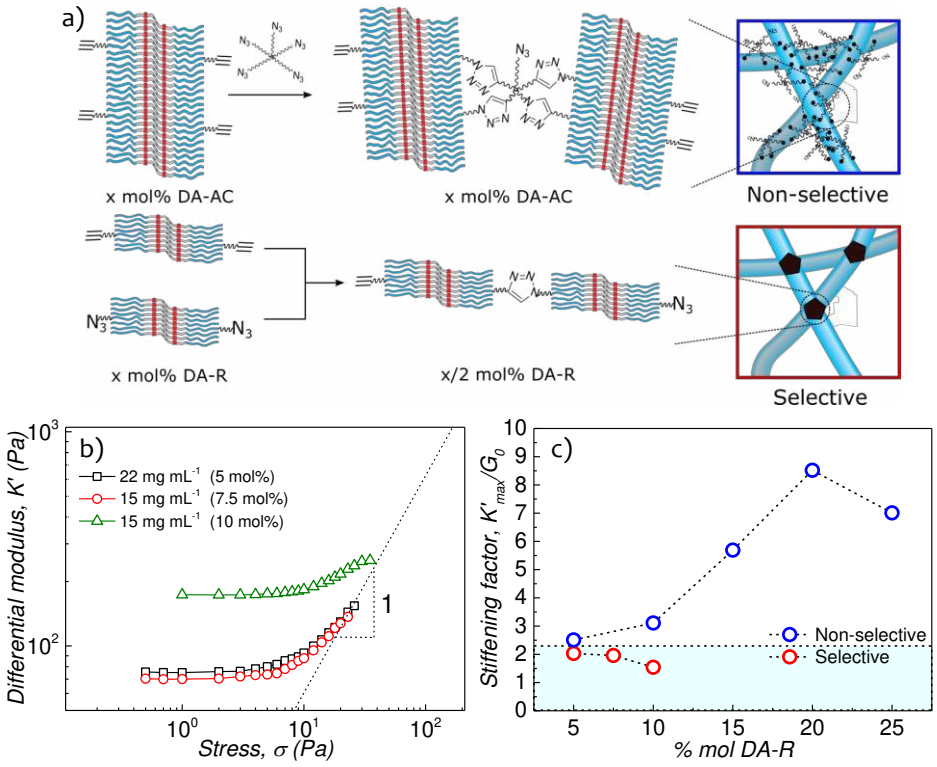

Fig. 3.10 | (a) Schematic representation of non-selective crosslinking of DA-AC labelled fibers with 5-N_3 resulting in the formation of intra- and interfiber crosslinks (upper). Suppression of intrafiber crosslinks (inactive loops) via mixing of separated solutions containing DA-AC/DA and DA-N_3/DA fibers followed by chemical crosslinking (lower). (b) Differential modulus K' vs stress σ obtained from DA gels formed through selective crosslinking strategies. (c) Stiffening range K'/G_0 plotted against molar percent of DA-R, with R = -AC or -N_3. The blue rectangle illustrates the K'_{max}/G_0 that separates the mechanics of purely supramolecular and externally fixated stress-stiffening gels.

3.3. Conclusions

In summary, fibers made through supramolecular polymerization of diacetylene bisurea bolaamphiphiles were crosslinked to form strain-stiffening gels. In contrast to the supramolecular hydrogels with long crosslinkers[21,22], the current gels do show pronounced strain-stiffening, even though the fiber backbone is not fixated like in PDA hydrogels described in Chapter 2.

The observation of strain-stiffening in the supramolecular materials yields two generally applicable principles: (1) Strain-stiffening is inherent to any connected meshwork of semi-flexible, supramolecular polymers provided that the non-covalent interactions that hold the fibers together are sufficiently strong to remain intact under stresses larger than the characteristic network critical stress. (2) Crosslinks between fibers should be short and robust, allowing the network to rapidly enter its nonlinear extensional regime and ensure that failure does not happen due to crosslinking unbinding prior to the critical stress. Thus, the crosslinking strategy crucially determines the presence or absence of strain-stiffening in gels composed of robust, semi-flexible, supramolecular polymers.

Our results critically expand current knowledge about the origins of strain-stiffening in bio- as well as synthetic polymers breaking ground for the rational design of genuinely supramolecular, biomimetic soft matter whose mechanical properties can be purposely modulated by tuning the strength of the supramolecular interactions. These novel materials are expected to mimic the dynamic mechanical environment of cells more closely and may potentially find application in the biomedical field as artificial scaffolds for cell culture or tissue engineering.

3.4. Experimental section

Materials

All solvents used were of reagent grade quality or better and purchased from Biosolve, Sigma-Aldrich or Actu-All Chemicals. DCM was dried using molecular sieves (3 Å) prior use. Diethylenetriaminepentaacetic dianhydride (DTPA) was obtained from Sigma-Aldrich (Benzotriazol-1-yloxy)tripyrrolidinophosphonium hexafluorophosphate (PyBOP) was obtained from Bachem, 1-Azido-4,7,10-trioxa-13-tridecanamine (TOTA-N_3) was obtained from Iris Biotech. DA was prepared according to literature procedures[23]. The synthesis of DA-AC has been detailed in Chapter 2.

General methods

NMR spectra were recorded 400 MHz Bruker UltraShield Magnet (100 MHz for ^{13}C-NMR). Chemical shifts (δ) are reported in parts per million (ppm) using residual solvent signal or tetramethylsilane (TMS) as internal standards.[47] Splitting patterns are labeled as singlet (s), doublet (d), double doublet (dd), triplet (t), quartet (q), pentet (p) and multiplet (m). Matrix-assisted laser desorption ionization time-of-flight (MALDI-TOF) measurements were carried out on a Perseptive DE PRO Voyager mass spectrometer using α-cyano-4-hydroxycinnamic acid as the calibration matrix. (LC-MS).

Small-Angle X-Ray scattering (SAXS) profiles were recorded on SAXLAB GANESHA 300 XL SAXS equipped with a GeniX 3D Cu Ultra Low Divergence micro focus sealed tube source producing X-rays with a wavelength $\lambda = 1.54$ Å at a flux of 1×10^8 ph/s and a Pilatus 300 K silicon pixel detector with 487 × 619 pixels of 172 × 172 μm^2 in size placed a three sample-to-detector distances of 113, 713, and 1513 mm respectively to cover a q-range of $0.07 \leq q \leq 3.0$ nm^{-1} with $q = 4\pi/\lambda(\sin\theta/2)$. Silver behenate was used for calibration of the beam centre as well as the q-range. Samples were measured within 2 mm quartz capillaries (Hilgenberg GmbH, Germany). The two-dimensional SAXS patterns were brought to an absolute intensity scale using the calibrated detector response function, known sample-to-detector distance, measured incident and transmitted beam intensities, and azimuthally averaged to obtain one-dimensional SAXS profiles. The scattering curves of the fibers

were obtained by subtraction of the scattering contribution of the solvent and quartz cell.

Ultraviolet-visible (UV-vis) absorbance spectra were recorded on a Jasco V-650 UV-vis spectrometer equipped with a Jasco ETCT-762 temperature controller. All samples were measured using quartz cuvettes (1×1 cm) at 20 °C.

The mechanical properties of the hydrogels were tested by oscillatory rheology. Dynamic viscoelastic measurements were performed on a stress-controlled Anton Paar and a Physicia MCR 501 Discovery HR-3 and TA Instruments rheometers equipped with a 25-mm stainless steel sand-blasted plate-plate geometry to prevent slippage of the sample in a temperature-controlled environment. Measurements were performed at a fixed temperature of 20 °C sealed by placing mineral oil around the sample to minimize evaporation at a fixed plate-to-plate gap of 500 μm. After addition of the catalyst, gelation was monitored by continuous oscillations with a strain amplitude of 1 % and an angular frequency of 6.28 rad/s. To probe the elasticity of the gels, we applied a steady prestress, σ on which an oscillatory stress, $\delta\sigma(t) = \delta\sigma e^{iwt}$ is superimposed with an amplitude at most 10% of σ and at an angular frequency of ω = 6.28 rad s^{-1}.

Synthetic procedures

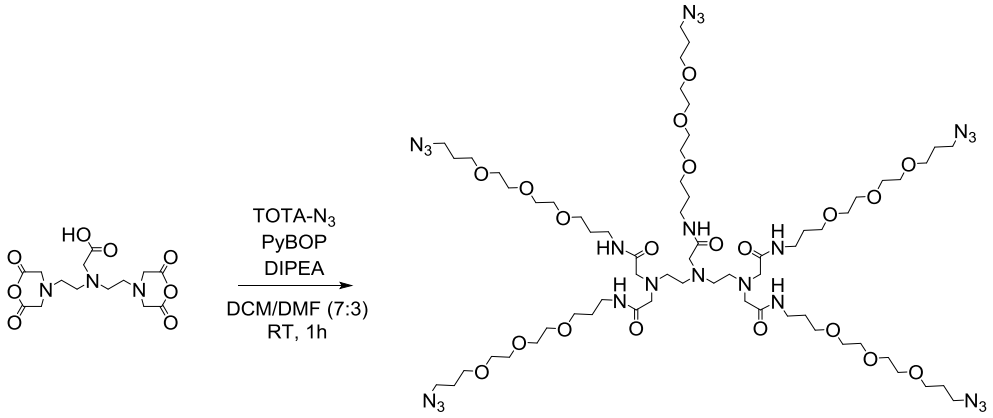

Scheme S3.1 | Synthetic route towards 5-N_3

DTPA-anhydride (26 mg, 0.074 mmol) was dissolved in 10 mL of CH_2Cl_2:DMF (7:3, v:v), solid PyBOP (127 mg, 0.24 mmol) and TOTA-N_3 (100 mg, 0.41 mmol) were added. The pH was adjusted to 8 with N,N-Diisopropylethylamine (DIPEA). After 1 h of stirring at room temperature, solvents were removed in vacuo. The

resulting crude was dissolved in 10 mL of CH_2Cl_2 and washed with 5% $NaHCO_3$ (10 mL). The organic phase was evaporated, and the resulting crude was transferred to a 15 mL tube while dissolved in CH_2Cl_2 (2 mL) and hexane (12 mL) was added. The mixture was stirred vigorously and centrifuged. The supernatant was discarded and the remaining oily precipitate corresponded to pure compound (93 mg, 82% yield).

^{1}H-NMR (400 MHz, $CDCl_3$): δ = 7.52 (t, 4H, J = 5.50 Hz, N*H*, 7.33 (t, H, J = 5.66 Hz, N*H*), 3.60 (m, 40H, OC*H*$_2$), 3.52 (m, 20H, OC*H*$_2$CH$_2$CH$_2$), 3.37 (t, 10H, J = 6.70, CH$_2$CH$_2$C*H*$_2$N$_3$), 3.32 (m, 10H, NHC*H*$_2$CH$_2$CH$_2$), 3.14 (s, 8H, NC*H*$_2$CO), 3.05 (s, 2H, NC*H*$_2$CO), 2.63 (m, 4H, NC*H*$_2$CH$_2$N), 2.57 (m, 4H, NCH$_2$C*H*$_2$N), 1.83 (m, 10 H, CH$_2$C*H*$_2$CH$_2$N$_3$), 1.77 (NHCH$_2$C*H*$_2$CH$_2$).

^{13}C-NMR (100 MHz, $CDCl_3$): δ = 170.46, 70.56, 70.49, 70.35, 70.16, 69.56, 67.94, 58.45, 53.29, 48.52, 37.64, 29.16.

MS: Theoretical mass for $[C_{64}H_{123}N_{23}O_{18}+H]^+$: 1533.93. Experimental mass detected by LC-MS: 768.08 (M+2)/2.

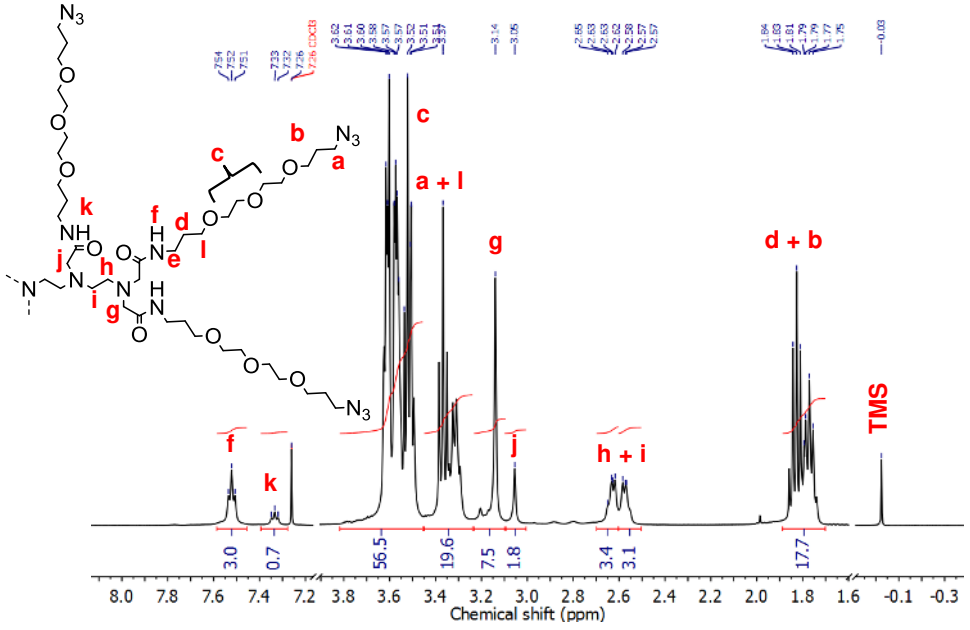

Fig. S3.2 | ^{1}H-NMR ($CDCl_3$, 25 °C) spectrum of 5-N_3

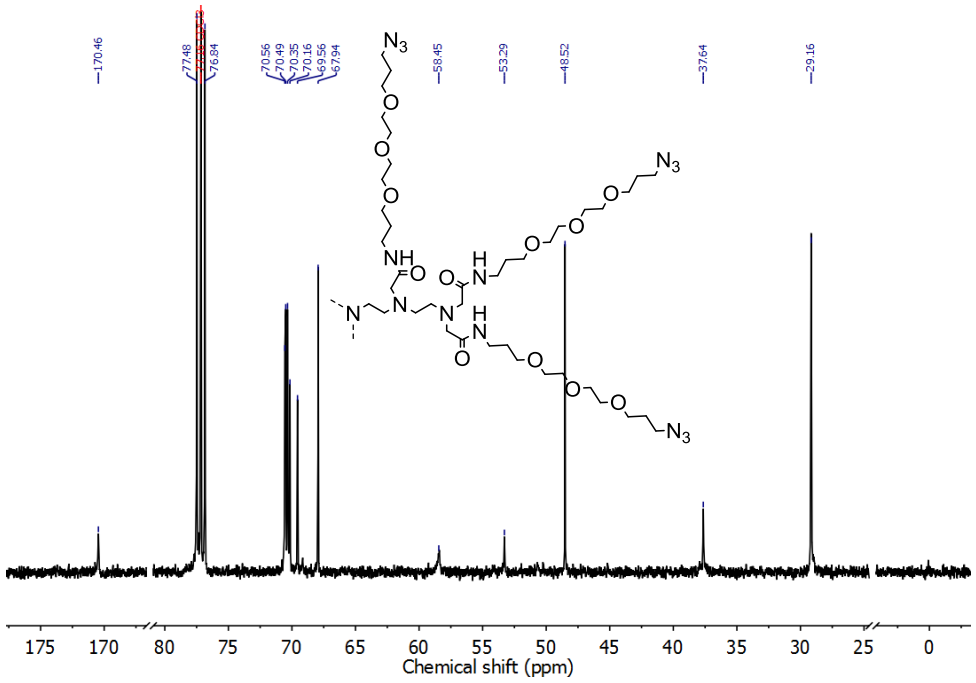

Fig. S3.3 | ^{13}C-NMR ($CDCl_3$, 25 ^{o}C) spectrum of 5-N_3

Gel preparation method

Non-selective crosslinking of DA/DA-AC fibers with 5-N_3 was performed by weighing DA and DA-AC in the solid state to the desired molar ratio followed by the addition of ca. 300 μL chloroform which was subsequently allowed to evaporate overnight. The resultant solid was dissolved in mili-Q water to a concentration of 50 mg mL^{-1} assisted by applying combined cycles of ultrasonication (ca. 30 min) and vortex until the full dissolution of the solid material. The solutions were then placed in a UV-protected environment for a minimum of 2 d. Samples were then prepared by adding mili-Q water and an aqueous solution of 5-N_3 (20 mg mL^{-1}) to the desired concentration while ensuring a stoichiometric azide/alkyne molar ratio. Chemical crosslinking was initiated upon addition of premixed aqueous solutions of $CuSO_4$/THPTA and a solution of Na-Ascorbate to a final concentration of 0.1, 0.5 and 10 mM respectively.

For selective crosslinking of DA/DA-AC and DA/DA-N_3 fibers an analogous procedure was carried out in which DA was separately blended in chloroform with

DA-AC or DA-N_3 to the desired molar ratio. After allowing the solvent to evaporate overnight, the remaining solids were dissolved in mili-Q water to a concentration of 50 mg mL^{-1} and the fibers were allowed to grow for a minimum of 2 d. Samples were then prepared by adjusting the concentration with mili-Q water followed by mixing of equal volumes of DA/DA-AC and DA/DA-N_3 and chemical crosslinking upon addition of the catalyst.

^{1}H-NMR conversion of crosslinking reaction

Self-assembled DA/DA-AC fibers were allowed to react with 5-N_3 for 24 h. The resultant hydrogel was freeze dried and the remaining solid re-dissolved in deuterated chloroform for ^{1}H-NMR analysis.

SAXS profiles

Small angle X-Ray scattering was used to determine the cross-sectional radius of DA fibers in solution and the gel state. Density measurements of water and DA aqueous solutions were performed using an Anton Paar DMA 5000M.

First, the specific volume (υ) of DA rods at a concentration of 15 mg mL^{-1} was determined by measuring the density (ϱ) of DA aqueous solutions over the concentration range indicated in Fig. S3.4.

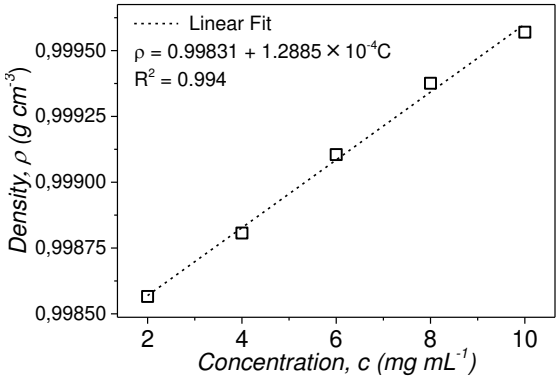

Fig. S3.4 | Plot of ϱ vs c of PDA in mili-Q water measured at 20 °C including linear regression.

Thus, the density of a 0.015 g cm^{-3} PDA aqueous solution was calculated by extrapolation of the linear fit in Fig. S3.4 D_{PDA} = 1.0002 g cm^{-3}. The specific volume was then calculated using the following equation:

$$\upsilon = \frac{1}{D_{water}}\left(1-\frac{D_{PDA}-D_{water}}{c}\right) = \frac{1}{0.9982\ g\ cm^{-3}}\left(1-\frac{1.0002-0.9982\ g\ cm^{-3}}{0.015\ g\ cm^{-3}}\right) =$$

$$= 0.8682\ cm^3 g^{-1}$$

To fit the experimental data with a non-linear least squares procedure implemented in Igor Pro, we employed a model that calculates the form factor of a flexible cylinder with a uniform scattering length density (ρ_{cyl}) and cross-sectional radial polydispersity which is averaged over a Schultz distribution of cylinder radii. The non-negligible diameter of the cylinder is included by accounting for excluded volume interactions within the walk of a single cylinder. Inter-cylinder interactions are not included.

We then proceeded to fix the values of volume fraction (ϕ = 0.00868) and use the values of contour length (L_c = 157 nm) and Kuhn length (b = 2×l_p = 560 nm) as derived from cryo-EM analysis detailed in Chapter 2. The tabulated value of ρ_{water} = 9.37 × 10^{10} cm^{-2} was used.

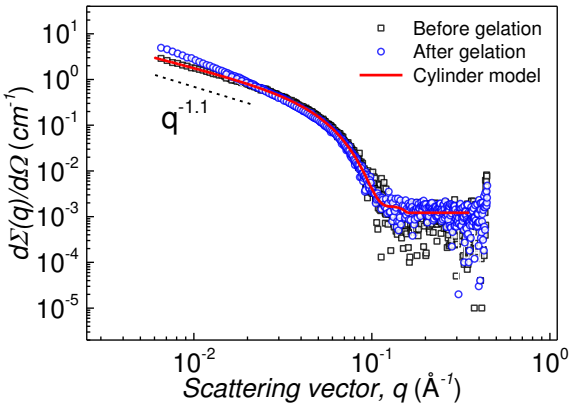

Fig. S3.5 | SAXS profiles recorded before and 24 h after crosslinking of 15 mg mL^{-1} DA/DA-AC (20 mol% DA-AC) solutions with 5-N_3.

Fitting of the scattering data with the model (Fig. S3.5) gave a value of 3.3 ± 0.2 nm for the radius, consistent with the value of 3.3 nm measured in cryo-EM. The fitting procedure also provided a value for ρ_{cyl} = (10.69 ± 0.02) × 10^{10} cm^{-2} that agrees

well with the fitting results reported in Chapter 2, where $\rho_{cyl} = (10.43 \pm 0.01) \times 10^{10}$ cm^{-2}.

Cryo-EM sample preparation

DA aqueous solutions (18 mg mL^{-1}) were placed in a sonication bath for 1 h and subsequently allowed to re-assemble for 2 d in a UV-protected environment unless otherwise noted. Samples were diluted by a factor of 1000 with mili-Q water prior imaging.

Vitrified films were prepared in an automated vitrification robot (Vitrobot™ Mark III, FEI) at 20 °C and at a relative humidity of 100%. In the preparation chamber, 3 μL sample was applied on a Quantifoil grid (carbon support film on a copper grid, typeR 2/2, Electron Microscopy Sciences), which was glow discharged prior use (Cressington 208 carbon coater operation at 5 mA for 40s). Subsequently, the samples were blotted to remove the excess of solution and vitrified in liquid ethane. The vitrified films were transferred to a cryoholder (Gatan 626) and studied in a FEI Tecnai 20 (type Sphera) microscope operating at 200 kV, equipped with a LaB_6 filament. The images were recorded using a 1k × 1k Gatan CCD camera. Gatan DigitalMicrograph was used for image analysis.

UV-Vis spectra

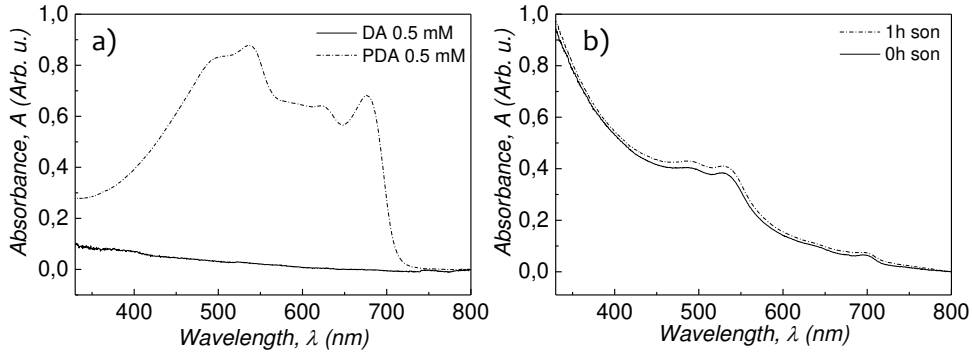

Fig. S3.6 | (a) UV-Vis spectra of aqueous PDA (dashed line) and DA (solid line) solutions (0.5 mM). Photo-polymerization was carried out by irradiating an aqueous solution of DA (18 mg mL^{-1}) with UV-light (254 nm) for 15 min under stirring. (b) UV-vis spectra of DA (18 mg mL^{-1}) in water recorded before (solid line) and after (dashed line) 2 h of sonication

Scaling relationships

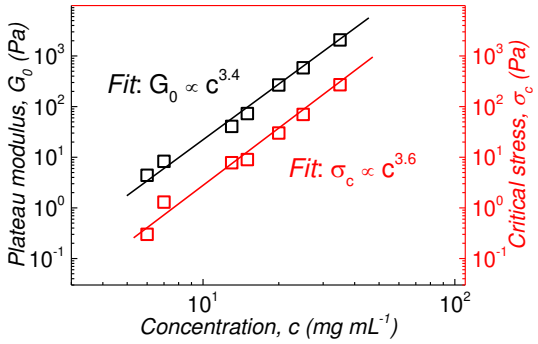

Fig. S3.7 | Plateau modulus G_0 (black) and critical stress σ_c (red) plotted against concentration with dash lines indicative of the corresponding power-law fits.

Cross-linker dependency

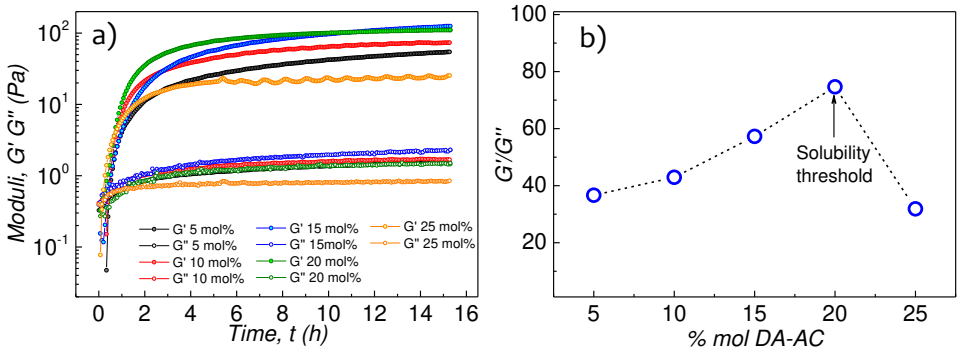

Fig. S3.8 | (a) Time course of storage G'(solid dots) and loss G" (empty dots) moduli measured at constant strain amplitude of $\gamma = 1\%$ and $\omega = 6.28$ rad s^{-1} during Cu-catalyzed click reaction of DA/DA-AC with 5-N_3 derived from gels measured in Fig. 3.8. (b) Ratio between storage G' and loss G" moduli plotted against molar percent of DA-AC with the arrow indicating the onset of fiber precipitation.

3.5. References

1. Pollard, T. D. & Borisy, G. G. Cellular Motility Driven by Assembly and Disassembly of Actin Filaments. *Cell* **112,** 453–465 (2003).
2. Helfand, B. T. *et al.* Vimentin organization modulates the formation of lamellipodia. *Mol. Biol. Cell* **22,** 1274–1289 (2011).
3. Kirschner, M. & Mitchison, T. Beyond self-assembly: From microtubules to morphogenesis. *Cell* **45,** 329–342 (1986).
4. Swaney, K. F., Huang, C.-H. & Devreotes, P. N. Eukaryotic Chemotaxis: A Network of Signaling Pathways Controls Motility, Directional Sensing, and Polarity. *Annu. Rev. Biophys.* **39,** 265–289 (2010).
5. The Three-Dimensional Dynamics of Actin Waves, a Model of Cytoskeletal Self-Organization. *Biophys. J.* **96,** 2888–2900 (2009).
6. Windoffer, R., Beil, M., Magin, T. M. & Leube, R. E. Cytoskeleton in motion: the dynamics of keratin intermediate filaments in epithelia. *J. Cell Biol.* **194,** 669–678 (2011).
7. Gardel, M. L. *et al.* Elastic Behavior of Cross-Linked and Bundled Actin Networks. *Science* **304,** 1301–1305 (2004).
8. Lin, Y.-C. *et al.* Origins of Elasticity in Intermediate Filament Networks. *Phys. Rev. Lett.* **104,** 058101 (2010).
9. Yao, N. Y. *et al.* Elasticity in Ionically Cross-Linked Neurofilament Networks. *Biophys. J.* **98,** 2147–2153 (2010).
10. Piechocka, I. K. *et al.* Multi-scale strain-stiffening of semiflexible bundle networks. *Soft Matter* **12,** 2145–2156 (2016).
11. Licup, A. J. *et al.* Stress controls the mechanics of collagen networks. *Proc. Natl. Acad. Sci.* **112,** 9573–9578 (2015).
12. Brown, A. E. X., Litvinov, R. I., Discher, D. E., Purohit, P. K. & Weisel, J. W. Multiscale Mechanics of Fibrin Polymer: Gel Stretching with Protein Unfolding and Loss of Water. *Science* **325,** 741–744 (2009).
13. Phadke, A. *et al.* Rapid self-healing hydrogels. *Proc. Natl. Acad. Sci.* **109,** 4383–4388 (2012).
14. Tuncaboylu, D. C., Sari, M., Oppermann, W. & Okay, O. Tough and Self-Healing Hydrogels Formed via Hydrophobic Interactions. *Macromolecules* **44,** 4997–5005 (2011).
15. Cui, J. & Campo, A. del. Multivalent H-bonds for self-healing hydrogels. *Chem. Commun.* **48,** 9302–9304 (2012).
16. Zhu, D., Ye, Q., Lu, X. & Lu, Q. Self-healing polymers with PEG oligomer side chains based on multiple H-bonding and adhesion properties. *Polym. Chem.* **6,** 5086–5092 (2015).
17. Kouwer, P. H. J. *et al.* Responsive biomimetic networks from polyisocyanopeptide hydrogels. *Nature* **493,** 651–655 (2013).
18. Jaspers, M. *et al.* Ultra-responsive soft matter from strain-stiffening hydrogels. *Nat. Commun.* **5,** 5808 (2014).
19. Jaspers, M. *et al.* Nonlinear mechanics of hybrid polymer networks that mimic the complex mechanical environment of cells. *Nat. Commun.* **8,** ncomms15478 (2017).
20. Fernandez-Castano Romera, M. *et al.* Strain Stiffening Hydrogels through Self-Assembly and Covalent Fixation of Semi-Flexible Fibers. *Angew. Chem. Int. Ed.* **56,** 8771–8775 (2017).
21. Pawar, G. M. *et al.* Injectable Hydrogels from Segmented PEG-Bisurea Copolymers. *Biomacromolecules* **13,** 3966–3976 (2012).
22. Koenigs, M. M. E. *et al.* Tuning Cross-Link Density in a Physical Hydrogel by Supramolecular Self-Sorting. *Macromolecules* **47,** 2712–2717 (2014).
23. Pal, A. *et al.* Topochemical polymerization in self-assembled rodlike micelles of bisurea bolaamphiphiles. *Soft Matter* **10,** 952–956 (2014).

24. Fransen, P. *et al.* High Control, Fast Growth OEG-Based Dendron Synthesis via a Sequential Two-Step Process of Copper-Free Diazo Transfer and Click Chemistry. *Macromolecules* **47,** 2585–2591 (2014).
25. Pulido, D., Albericio, F. & Royo, M. Controlling Multivalency and Multimodality: Up to Pentamodal Dendritic Platforms Based on Diethylenetriaminepentaacetic Acid Cores. *Org. Lett.* **16,** 1318–1321 (2014).
26. Jaspers, M. *et al.* Bundle Formation in Biomimetic Hydrogels. *Biomacromolecules* **17,** 2642–2649 (2016).
27. Presolski, S. I., Hong, V., Cho, S.-H. & Finn, M. G. Tailored Ligand Acceleration of the Cu-Catalyzed Azide−Alkyne Cycloaddition Reaction: Practical and Mechanistic Implications. *J. Am. Chem. Soc.* **132,** 14570–14576 (2010).
28. Hong, V., Presolski, S. I., Ma, C. & Finn, M. G. Analysis and Optimization of Copper-Catalyzed Azide–Alkyne Cycloaddition for Bioconjugation. *Angew. Chem. Int. Ed.* **48,** 9879–9883 (2009).
29. Lou, X. *et al.* Dynamic diversity of synthetic supramolecular polymers in water as revealed by hydrogen/deuterium exchange. *Nat. Commun.* **8,** ncomms15420 (2017).
30. Zhang, Y. *et al.* Pulsed hydrogen–deuterium exchange mass spectrometry probes conformational changes in amyloid beta (Aβ) peptide aggregation. *Proc. Natl. Acad. Sci.* **110,** 14604–14609 (2013).
31. Carulla, N. *et al.* Experimental characterization of disordered and ordered aggregates populated during the process of amyloid fibril formation. *Proc. Natl. Acad. Sci.* **106,** 7828–7833 (2009).
32. Saez Talens, V. *et al.* Aromatic Gain in a Supramolecular Polymer. *Angew. Chem. Int. Ed.* **54,** 10502–10506 (2015).
33. Carulla, N. *et al.* Molecular recycling within amyloid fibrils. *Nature* **436,** 554–558 (2005).
34. Rammensee, S., Janmey, P. A. & Bausch, A. R. Mechanical and structural properties of in vitro neurofilament hydrogels. *Eur. Biophys. J.* **36,** 661–668 (2007).
35. Gardel, M. L. *et al.* Scaling of F-Actin Network Rheology to Probe Single Filament Elasticity and Dynamics. *Phys. Rev. Lett.* **93,** 188102 (2004).
36. Broedersz, C. P. *et al.* Measurement of nonlinear rheology of cross-linked biopolymer gels. *Soft Matter* **6,** 4120–4127 (2010).
37. MacKintosh, F. C., Käs, J. & Janmey, P. A. Elasticity of Semiflexible Biopolymer Networks. *Phys. Rev. Lett.* **75,** 4425–4428 (1995).
38. Lieleg, O., Claessens, M. M. a. E., Heussinger, C., Frey, E. & Bausch, A. R. Mechanics of Bundled Semiflexible Polymer Networks. *Phys. Rev. Lett.* **99,** 088102 (2007).
39. Vader, D., Kabla, A., Weitz, D. & Mahadevan, L. Strain-Induced Alignment in Collagen Gels. *PLOS ONE* **4,** e5902 (2009).
40. Bauër, P. *et al.* A new method to measure mechanics and dynamic assembly of branched actin networks. *Sci. Rep.* **7,** 15688 (2017).
41. Onck, P. R., Koeman, T., van Dillen, T. & van der Giessen, E. Alternative Explanation of Stiffening in Cross-Linked Semiflexible Networks. *Phys. Rev. Lett.* **95,** 178102 (2005).
42. Koevoets, R. A. *et al.* Molecular Recognition in a Thermoplastic Elastomer. *J. Am. Chem. Soc.* **127,** 2999–3003 (2005).
43. Seitz, M. E. *et al.* Fracture and large strain behavior of self-assembled triblock copolymer gels. *Soft Matter* **5,** 447–456 (2009).
44. Erk, K. A., Henderson, K. J. & Shull, K. R. Strain Stiffening in Synthetic and Biopolymer Networks. *Biomacromolecules* **11,** 1358–1363 (2010).
45. Chuong, C. J. & Fung, Y. C. On Residual Stresses in Arteries. *J. Biomech. Eng.* **108,** 189–192 (1986).
46. Holzapfel, G. A., Gasser, T. C. & Ogden, R. W. Comparison of a Multi-Layer Structural Model for Arterial Walls With a Fung-Type Model, and Issues of Material Stability. *J. Biomech. Eng.* **126,** 264–275 (2004).

47. Fulmer, G. R. *et al.* NMR Chemical Shifts of Trace Impurities: Common Laboratory Solvents, Organics, and Gases in Deuterated Solvents Relevant to the Organometallic Chemist. *Organometallics* **29,** 2176–2179 (2010).

Chapter 4:

Reinforcing supramolecular strain-stiffening gels via internal and external fiber covalent fixation*

Abstract: *Fiber covalent reinforcement is essential in extracellular filamentous proteins such as collagen, fibrin or elastin and their networks as it increases stretching modulus and flexural rigidity generally at the expense of dynamics. Here we report on the cooperative effect of internal and external covalent fixation in gels of hierarchically self-assembled diacetylene bis-urea bolaamphiphiles (DA). Internal fixation of DA fibers via diacetylene topochemical polymerization (PDA) imparts sufficient mechanical stability to allow the fibers retain their integrity under prolonged exposure to ultrasonication. At the network level, covalent reinforcement provides the constituent fibers with enhanced axial strength and orientational persistence to sustain a broader range of nonlinear deformation. Here we show how the combined effect of internal and external fixation due to extensive intrafiber crosslink formation allows amplifying the macroscopic stiffening range of the hydrogels by a factor of 45 relative to an analogous hydrogel lacking covalent reinforcement (i.e. fully supramolecular). Thus, we access via this novel approach responsiveness, previously restricted to DA and PDA-based hydrogels, that are within the typical range of many biopolymer networks as well as strain-stiffening gels composed of covalent polyisocyanopeptide polymers.*

*Jürgen Schill is acknowledged for the cryo-EM analysis, Peter-Paul H. K. Fransen is acknowledged for the synthesis and characterization of the pentaazide linker, Gijs M. ter Huurne and Dr. Ilja K. Voets for their contribution to the SAXS characterization, Prof. Dr. Cornelis Storm is acknowledged for discussions on the interpretation of the results and Dr. Koen Pieterse (ICMS Animation Studio) is gratefully thanked for help with the graphics.

4.1. Introduction

Formation of covalent crosslinks in extracellular filamentous proteins is essential for many biochemical and biomechanical processes. For instance, ligation between fibrin fibers mediated by transglutaminase factor XIIIa stiffens the fibers and protects blood clots against degradation[1–3]. At the single filament level, this results in both enhancements of bending and stretching modulus by a factor of 8 and 4 respectively relative to unligated fibers[4]. Similarly, the formation of covalent bonds in collagen −primarily via lysine post-modifications between tropocollagen molecules[5,6]− plays a critical mechanical role, rendering the fibers stiffer, although more brittle as their ability to dissipate stress is reduced at higher crosslinking[7]. Taken as a whole, networks reconstituted from both collagen and fibrin fibers are capable of strain-stiffening, and the observed macroscopic nonlinear response to deformation is tightly coupled to the complex hierarchical structure and the relative amount of covalent crosslinks present within each biopolymer[8–12].

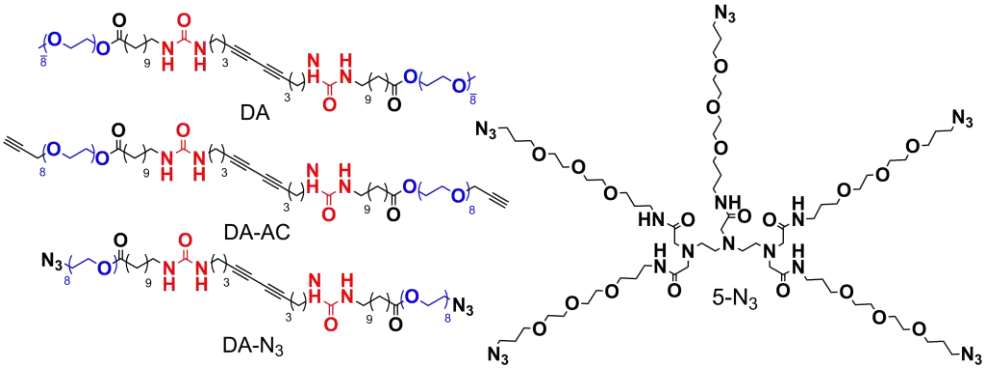

Fig. 4.1 | Molecular structure of the diacetylene bis-urea bolaamphiphile DA, its functionalized analogues DA-AC and DA-N_3 and the pentaazide 5-N_3 crosslinker.

Along these lines, it was shown in Chapter 3 that the formation of covalent intrafiber crosslinks in gels composed of fibers of self-assembled diacetylene bis-urea bolaamphiphiles (DA) (Fig. 4.1) yielded hydrogels with enhanced axial strength and orientational persistence able to withstand an increasingly extended regime of non-linear deformation depending on the degree of external fixation. This, in turn, translated into a concomitant increase of the stiffening range K'_{max}/G_0 (*i.e.* the overall relative increase in K' before failure) relative to hydrogels lacking external fiber reinforcement. In parallel, in Chapter 2 it was shown that gels whose fibers were

internally fixated via diacetylene cross-polymerization into polydiacetylene fibers (PDA) (Fig. 4.2) also stiffen pronouncedly under applied stress. There, the crosslinking strategy used was designed such that formation of intrafiber crosslinks was suppressed. Hence, we have thus far reported on two different approaches to mechanically reinforce self-assembled fibers via internal and external covalent fixation both of which were separately shown to lead to stress-responsive hydrogels. However, while networks reconstituted from intra- and extracellular filamentous proteins often respond to applied stress with an associated increase in modulus by more than a factor of 100 prior to failure[8,11,11,13–16], both DA and PDA gels are characterized by much weaker responsiveness below 10-fold.

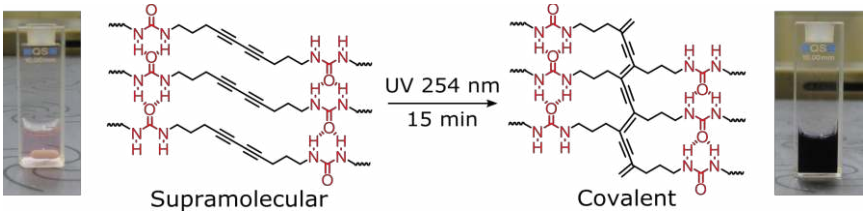

Fig. 4.2 | Photo-polymerization of self-assembled bis-urea diacetylenes with change in optical properties corresponding to the formation of a covalent π-conjugated ene-yne backbone.

Within the scope of this work, we seek to crosslink internally fixated PDA fibers using selective and non-selective approaches. We demonstrate that topochemical polymerization of self-assembled DA fibers mechanically reinforces the fiber backbone with the loss of dynamics. Thus, contrary to supramolecular DA fibers, PDA fibers retain their integrity under prolonged exposure to ultrasonication. At the network level, PDA covalent reinforcement produces hydrogels capable of stress-stiffening by more than 10-fold. Our most important finding is that the combined effect of internal and external fiber fixation extends the non-linear stiffening regime. Thus, the K'_{max}/G_0 can be selectively adjusted through the extent of external covalent reinforcement to match those of gels reconstituted from various types of biopolymers as well as synthetic polyisocyanopeptide (PIC) strain-stiffening hydrogels. In the latter system, both mechanical responsiveness and stability have been realised by making use of covalent polymers as their main structural components.

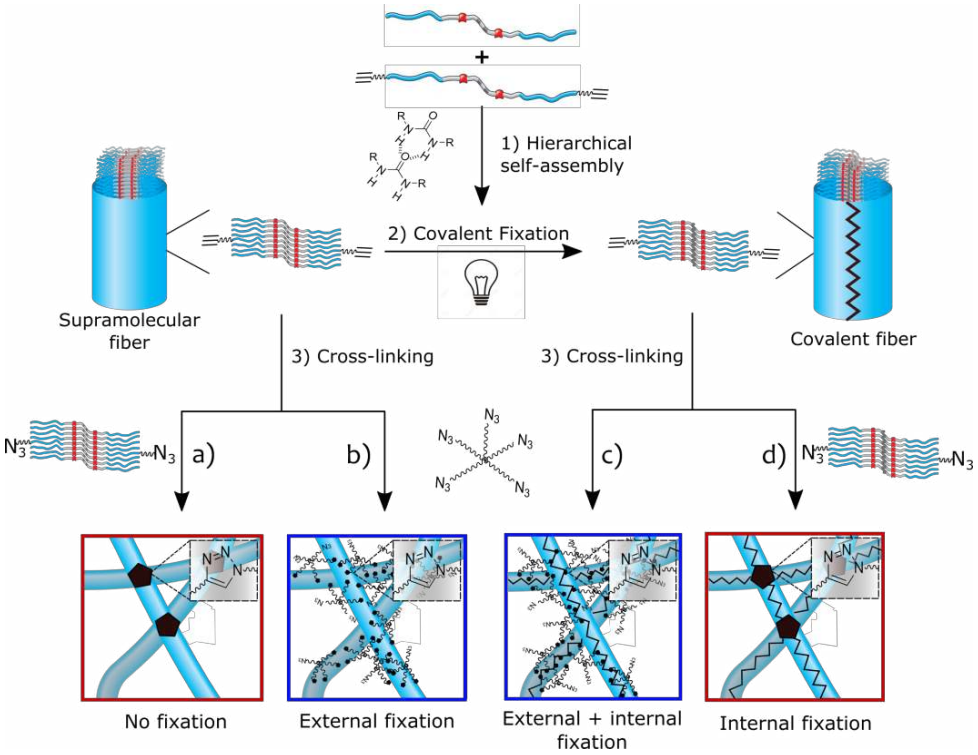

Scheme 4.3 | Hierarchical self-assembly in water of functionalized (DA-AC) and unfunctionalized (DA) diacetylene bis-urea bolaamphiphiles through intermolecular H-bonding and hydrophobic interactions into supramolecular fibers integrating 9-10 ribbons (left). Covalent fixation via diacetylene photo-polymerization to form identical fibers with a polydiacetylene (PDA) backbone (right). (a) Selective crosslinking (*i.e.* exclusively interfiber crosslinks) of supramolecular DA fibers with DA-N_3-labeled fibers. (b) Non-selective crosslinking (*i.e.* inter- and intrafiber crosslinks) of supramolecular DA fibers with 5-N_3. (c) Non-selective crosslinking of covalent PDA fibers. (d) Selective crosslinking of PDA fibers. Color coding is used to differentiate between selective (red) and non-selective (blue) crosslinking.

4.2. Results and discussion

PDA fibers under ultrasonication

To test the stability of the PDA backbone at the single fiber level, we subjected aqueous solutions of DA lacking backbone covalent fixation and PDA fibers to ultrasonication, and the morphology was studied with cryo-electron microscopy (cryo-EM). Thus, DA fibers were photo-polymerized at a concentration of 18 mg mL^{-1} following the procedure detailed in the experimental section and subsequently subjected to sonication by placing the solutions in a sonication bath for 2 h. Figs. 4.4.a

and b (taken from Chapter 3) show that, for self-assembled DA fibers lacking backbone fixation, sonication disrupts the morphology of the fibers breaking them into visibly shorter fragments. By contrast, PDA fibers retain their morphological integrity showing similar-sized fibers –preserving both length and diameter– before and after sonication for 2h (Figs. 4.4.c and d).

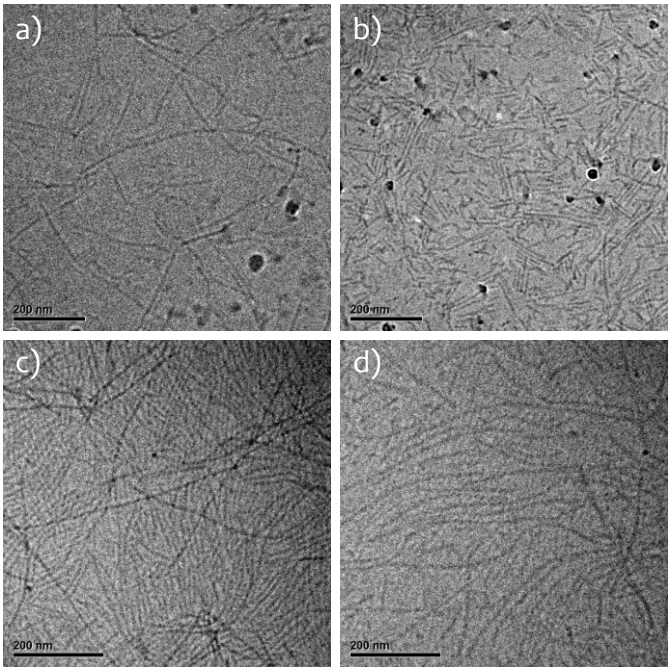

Fig. 4.4 | Cryo-EM micrographs of DA and PDA fibers in water (1 mM): (a) DA unperturbed system. (b) DA after 1 h of sonication. (c) PDA unperturbed system. (d) PDA After 1h of sonication. Scale bars: 200 nm.

To illustrate further the effect of backbone covalent fixation, we sonicated aqueous solutions of DA and PDA fibers functionalized through the incorporation of reactive DA-AC (Fig. 4.1) prior to crosslinking with 5-N_3. Immediately after addition of the catalyst, solutions were transferred to the rheometer where the gelation process was monitored under continuous oscillatory strain until a stable value of the elastic modulus G' was reached. Gels formed by chemical crosslinking of a mixture of unreactive DA and reactive DA/DA-AC fibers directly after ultrasonication were approximately ten times less stiff than an identical solution crosslinked without sonication thereby inferring shortening of the fibers (Fig. 4.5.a). Conversely,

crosslinking of an analogous mixture of unreactive PDA fibers and reactive PDA/DA-AC after 1 h of sonication had no measurable impact on the final modulus of the gels obtained in the absence and after 1 h sonication (Fig. 4.5.b). These results support those derived from cryo-EM and indicate that the process of backbone covalent reinforcement via diacetylene cross-polymerization imparts sufficient mechanical stability to the fibers enabling them to withstand prolonged exposure to ultrasonication under the experimental conditions here reported.

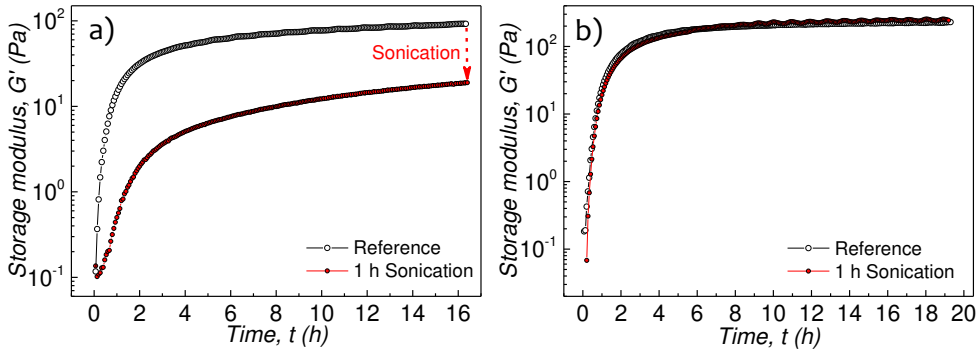

Fig. 4.5 | Time course of storage modulus G' measured by applying oscillatory shear γ=1% and ω = 6.28 rad s^{-1} during Cu-catalyzed click reaction with 5-N_3 of: (a) 18 mg mL^{-1} DA/DA-AC (20 mol% DA-AC) mixed with 18 mg mL^{-1} DA subjected to 1 h ultrasonication, (b) 25 mg mL^{-1} PDA/DA-AC (20 mol% DA-AC) mixed with 18 mg mL^{-1} PDA subjected to 1 h ultrasonication.

SAXS characterization of PDA hydrogels

Structural analysis of the so-formed hydrogels was performed by Small-Angle X-Ray scattering (SAXS). The SAXS profiles of a mixture of PDA/DA-AC (20 mol% DA-AC) fibers and 5-N_3 with a stoichiometric molar ratio of azide/acetylene groups were recorded in the absence (sol) and 24 h after addition of the catalyst (gel). The results were analyzed in relation to an identical sample consisting of unpolymerized (DA) fibers (taken from Chapter 3). Fig. 4.6 shows that both DA and PDA hydrogels exhibit identical structural features as the system undergoes gelation, where in the low *q*-regime the scattering profiles of the gels feature a slightly more pronounced increase in scattering intensity relative to the uncrosslinked system (sol). While these differences cannot be explicitly attributed to a change in the fiber's length or rigidity solely based on SAXS (Fig. 4.6), the overlap in the high *q*-region suggests that the cross-sectional diameter of the fibers remains unchanged before and after crosslinking

without additional bundling. Specifically, the cross-sectional radius calculated from fitting of the scattering profiles in Chapter 3 gave a value of 3.3 ± 0.2 nm in excellent agreement with the value obtained from cryo-EM. Moreover, the overlap over the whole *q*-range between DA and PDA before and after chemical crosslinking confirms previous observations in Chapter 2 indicating that the process of diacetylene topochemical polymerization does not bring about morphological changes to the fibers.

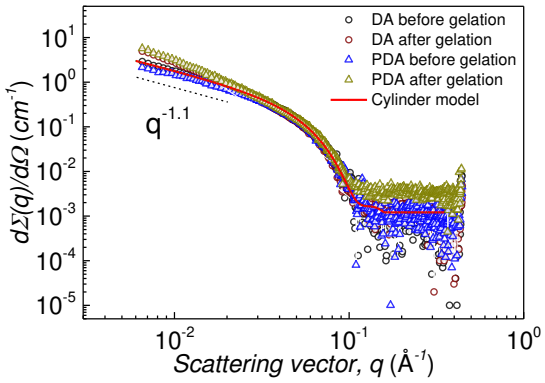

Fig. 4.6 | SAXS profiles recorded before and 24 h after crosslinking of 15 mg mL^{-1} DA and PDA (20 mol% DA-AC) solutions with 5-N_3.

Concentration dependence

The mechanical behaviour of PDA gels formed via non-selective chemical crosslinking of PDA/DA-AC fibers with 5-N_3 (Scheme 4.3.c) was studied as a function of PDA concentration at a fixed degree of DA-AC incorporation (*i.e.* 10 mol% DA-AC) ensuring a stoichiometric molar ratio of azide and acetylene groups. Gels formed via this method were mechanically tested using the protocol described in previous chapters[17], in which the differential modulus K (the elastic part of which relates the change in stress with strain, $K' = \delta\sigma/\delta\gamma$) was recorded and plotted as a function of the applied steady pre-stress σ.

Figs. 4.7.a and S4.1 show that the low-stress plateau modulus G_0 of the gels scales strongly with PDA within this concentration regime, whereby a 2-fold increase rises the value of G_0 by 100-fold, *i.e.* from 2.2 to 218 Pa. All gels have a linear mechanical response at low stress. However, with sufficiently large applied stress, beyond the critical stress σ_c, the moduli of the networks increase for a concentration-dependent

range of applied σ until rupture beyond the stress at failure σ_{max}. Scaling of K' to its value in the low-stress linear regime G_0 and σ to σ_c collapses all data remarkably well onto a single master curve (Fig. 4.7.b) featuring the characteristic linear relationship between K' and σ ($K' \propto \sigma^1$) also reported in Chapter 3 for unpolymerized DA fibers crosslinked under the same conditions. However, while the relative overall increase in moduli associated to DA hydrogels was about 2-fold (Chapter 3), gels formed by crosslinking of PDA fibers with 5-N_3 exhibit much broader stiffening ranges K'_{max}/G_0, surpassing the order of magnitude within the concentration range of 13 to 17 mg mL^{-1}. On increasing PDA concentration beyond 17 mg mL^{-1}, the magnitude of K'_{max}/G_0 was found to decrease continuously reaching a value of 5.6 at 25 mg mL^{-1} (Fig. 4.7.b, inset). The drop in K'_{max}/G_0 is consistent with that observed in Chapter 2 where at higher concentrations it was shown that the increased confinement of PDA fibers results in both decrease in responsiveness and stiffening range. A similar trend has been measured in synthetic PIC gels where at a concentration of 0.5 mg mL^{-1} K'_{max}/G_0 reaches a maximum value of 80, whereas at 2.5 mg mL^{-1} K'_{max}/G_0 drops to values as low as 7[18]. We can, therefore, conclude that at a fixed [PDA]/[DA-AC] molar ratio, the relative extent of external fixation due to non-selective 5-N_3 crosslinking remains constant yielding a homogeneous distribution of K'_{max}/G_0 values in sufficiently diluted PDA networks.

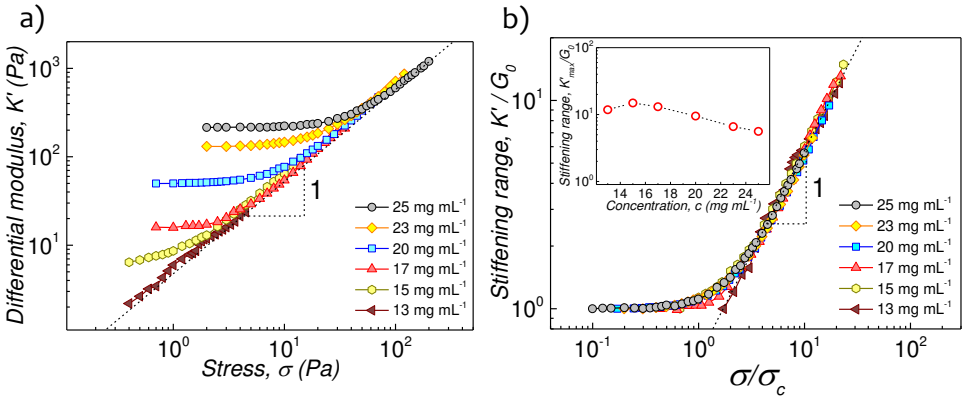

Fig. 4.7 | (a) Differential modulus K' vs stress σ for crosslinked PDA mixtures containing 10 mol% DA-AC of different concentrations. (b) Plot of K' vs stress σ with K' normalized to G_0 and σ normalized to σ_c, showing collapse onto single master curve with $K' \propto \sigma^1$ dependency at high σ. Inset: Stiffening range K'_{max}/G_0 vs PDA concentration.

Effect of crosslink density

To study the effect of fiber external fixation on PDA hydrogel mechanics, fibers containing varying [PDA]/[DA-AC] molar ratios were prepared and chemically crosslinked with 5-N_3 using a stoichiometric ratio of alkyne and azide groups (Scheme 4.3.c). All gels were prepared using PDA concentrations in the range of 13 to 17 mg mL^{-1} where we expect the highest K'_{max}/G_0 values as inferred from the results in Fig. 4.7.b. (inset). At the lowest DA-AC incorporation (*i.e.* 5 mol% DA-AC) however, we failed to form a hydrogel at concentrations below 20 mg mL^{-1}. Gels formed via this procedure were mechanically tested by applying a full range of steady pre-stress σ and the elastic part of the differential modulus K' was plotted as a function of σ. Fig. 4.8.a displays the expected low-stress linear regime immediately followed by a pronounced increase in modulus within the non-linear stiffening regime at stresses higher than σ_c for all networks. Within the stress-stiffening regime, all curves converge asymptotically without the need for data normalization. Normalization of the curves allows for calculation of the stiffening range K'_{max}/G_0 (Fig. 4.8.b inset). This ratio reaches remarkably high values, previously inaccessible for PDA hydrogels in which K'_{max}/G_0 is substantially amplified above 15 mol% DA-AC incorporation. In striking agreement with DA hydrogels in Chapter 3, K'_{max}/G_0 is maximized at 20 mol% DA-AC where it reaches a value of 89 followed by a decrease at 25 mol% DA-AC related to the miscibility limit of DA-AC in the unfunctionalized DA host (Fig. 4.8.b). Plotting K'_{max}/G_0 against the molar percentage of DA-AC within the fibers (Fig. 4.8.b inset) yields an upward trend reminiscent of that observed for unpolymerized DA hydrogels in Chapter 3. There, the magnitude of K'_{max}/G_0 was found to be intimately coupled to the extent of external fiber reinforcement as a result of non-selective 5-N_3 crosslinking. Also in analogy to DA hydrogels, the steepest increase in K'_{max}/G_0 is observed just above 10-15 mol% DA-AC corresponding to a degree of incorporation at which 2 acetylene groups are expected every urea-urea repeat distance of 0.46 nm along the fiber axis[19]. Thus, above 10-15 mol% DA-AC we expect full external fixation in combination with cross-fixation of the ribbons aggregated perpendicular to the fiber axis upon chemical crosslinking with 5-N_3. The K'_{max}/G_0 obtained for PDA gels at 20 mol% is in the same range as that measured for various types of biopolymer gels reconstituted from fibrin[11], collagen type I[8], actin[13,14,20], and neurofilament fibers[15] as well as synthetic strain-stiffening PIC hydrogels[18,21]. In the latter example, both

mechanical responsiveness and stability are realised through physical aggregation of covalent polymers.

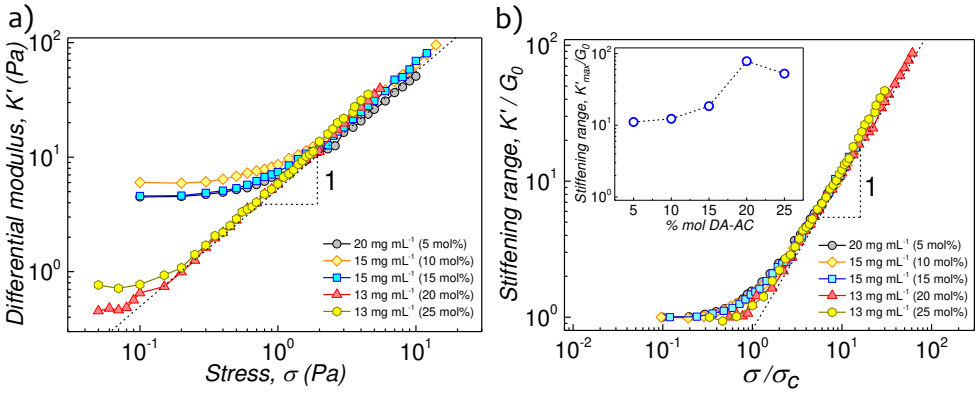

Fig. 4.8 | (a) Differential modulus K' vs stress σ for different DA/DA-AC ratios. (b) Plot of K' vs stress σ with K' normalized to G_0 and σ normalized to σ_c, showing collapse onto single master curve with $K' \propto \sigma^1$ dependency at high σ. Inset: Stiffening range K'_{max}/G_0 vs. molar percent of DA-AC.

Suppressing external fiber fixation through selective crosslinking

Similar to the experiments shown in Chapter 3, in order to isolate the mechanical contribution arising exclusively from the PDA matrix, we utilized the same crosslinking strategy reported in Chapter 2 to suppress the formation of intrafiber crosslinks and by extension also the effect of fiber surface fixation. Herein, every crosslink that is formed by reaction of an acetylene and an azide group contributes to the network's modulus (Scheme 4.3.b). Thus, DA was blended with its cross-linkable analogues DA-AC and DA-N_3 separately and dissolved in water. The so-obtained fibers were covalently fixated via diacetylene photo-polymerization followed by mixing of equal volumes ensuring a stoichiometric ratio between azide and acetylene groups (Fig. 4.9.a). At this stage, insertion of a DA-N_3 bolaamphiphile into a DA-AC-labelled fiber to form an intrafiber crosslink can be fully neglected due to loss of dynamics upon covalent fixation as was previously inferred in Figs. 4.4 and 4.5 for PDA fibers under sonication. The mechanical properties of gels formed by chemical crosslinking of PDA/DA-AC and PDA/DA-N_3 fibers were studied in relation to the degree of DA-AC and DA-N_3 incorporation. Thus gels within the concentration range of 15 to 22 mg mL^{-1} (similarly to experiments shown in Fig. 4.8, we failed to gelate a mixture of fibers containing 5 mol% functionalized DA-R at a concentration

below 22 mg mL^{-1}) were prepared. Gels formed via this procedure responded to applied stress the featuring the expected linear and nonlinear regimes. In the nonlinear regime, above the critical stress, all curves converge asymptotically at high σ. Upon rescaling the data, the curves collapse onto a single master curve featuring a $K' \propto \sigma^1$ dependency inherent to DA and PDA hydrogels as well as type-I collagen networks[8]. The magnitude of K'_{max}/G_0 was calculated from the normalized curves and plotted against the molar percent of cross-linkable DA-R in the fibers. Fig. 4.9.c (inset) demonstrates that in the absence of external fiber fixation the stiffening range of the hydrogels is independent of the density of crosslinks and thereby yields the contribution associated to the PDA matrix which features a relative increase in modulus of approximately 10-fold prior to rupture. The K'_{max}/G_0 measured for PDA selectively crosslinked is in stark contrast to DA hydrogels formed under identical conditions where the relative increase in modulus was found to be around 2-fold (Chapter 3).

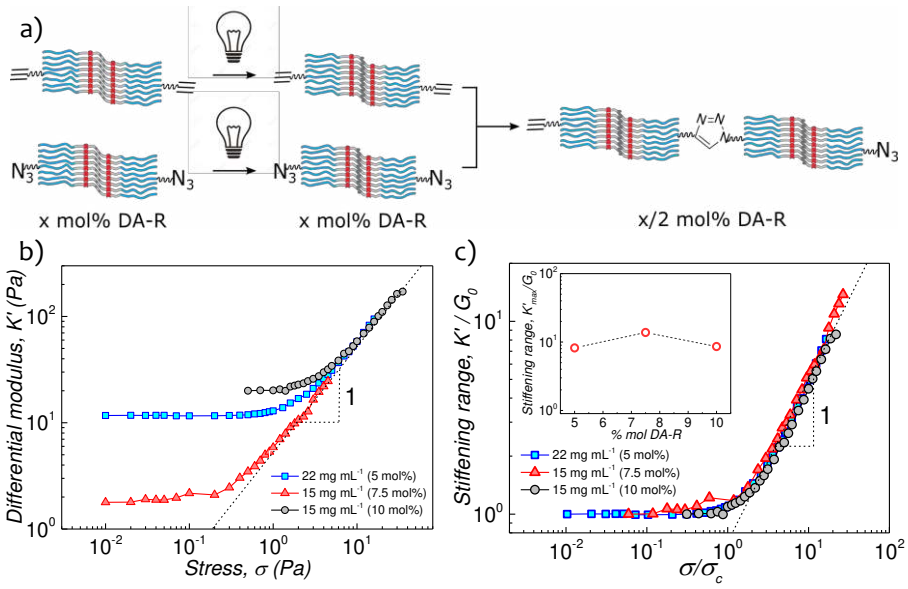

Fig. 4.9 | (a) Suppression of intrafiber crosslinks via mixing of separated solutions containing DA-AC/DA and DA-N_3/DA fibers followed by covalent fixation via diacetylene photo-polymerization and chemical crosslinking into strain-stiffening gels. (b) Differential modulus K' vs stress σ obtained from PDA gels formed through selective crosslinking strategies. (c) Plot of K' vs stress σ with K' normalized to G_0 and σ normalized to σ_c, showing collapse onto single master curve with $K' \propto \sigma^1$ dependency at high σ. Inset: Stiffening range K'/G_0 plotted against molar percent of crosslinkable DA-R, with R = -AC or -N_3.

Comparison between DA and PDA networks

To capture the overall differences in mechano-responsiveness caused by the different crosslinking approaches adopted thus far for self-assembled (DA) and polymerized (PDA) fibers (Scheme 4.3.a-d), we plotted the stiffening ranges as a function of the density of crosslinks. Fig. 4.10 clearly illustrates the appearance of two distinct regimes delimited at around K'_{max}/G_0 = 8.5 corresponding to the transition between fully externally to only internally fixated fibers. For gels formed lacking external covalent reinforcement via selective crosslinking (Scheme 4.3.a and d), the relative increase in stiffness is independent of the density of crosslinks present within the 3 D meshwork. By contrast, gels crosslinked via non-selective approaches reflect the dependence of K'_{max}/G_0 on the extent surface fiber reinforcement due to 5-N_3 intrafiber crosslink formation (Scheme 4.3.b and c). Furthermore, the K'_{max}/G_0 from gels of DA and PDA fibers selectively crosslinked converge remarkably well with their non-selectively crosslinked counterparts at the point where the effect of external fixations becomes negligible at lower crosslink densities.

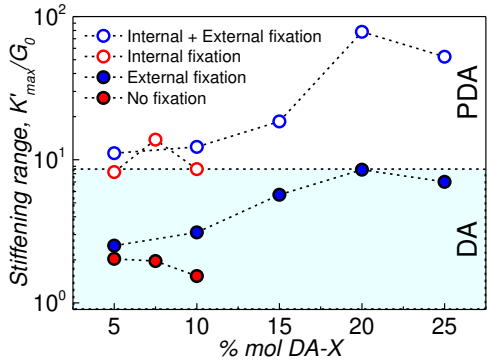

Fig. 4.10 | Stiffening range K'/G_0 plotted against molar percent of DA-R, with R = -AC or -N_3. The blue rectangle illustrates the K'_{max}/G_0 that separates the nonlinear mechanics of hydrogels based on supramolecular (DA) (solid) and internally fixed (PDA) (empty) fibers.

4.3. Conclusions

From the results presented in this Chapter it is clear that the mechanics of connected meshworks of semi-flexible supramolecular polymers are greatly influenced by the presence and relative amount of covalent crosslinks within and between fibers. Here, we show that covalent backbone fixation is sufficient to protect the fibers from forces exerted in a conventional ultrasonication apparatus, known to disrupt the morphology of assemblies from both synthetic and biological building blocks[22,23]. From an applied perspective, these results expand the application range of polydiacetylenes which has been classically limited to their outstanding chromatic and semi-conducting properties[24–27].

Furthermore, the combination of internal and external reinforcement prompted by the formation of intrafiber crosslinks between PDA/DA-AC fibers and 5-N_3 has proven to be a useful technique to maximize the nonlinear deformation regime of PDA hydrogels in a fully controlled manner. Following this approach the stiffening response of PDA hydrogels was maximized to reach values only accessible thus far to biopolymer gels and synthetic PIC hydrogels formed through physical aggregation of covalent polymers. Ultimately, we have illustrated the versatility and scope for manipulation of DA bolaamphiphiles covalently cross-linked using selective and non-selective strategies.

4.4. Experimental section

Materials

All solvents used were of reagent grade quality or better and purchased from Biosolve, Sigma-Aldrich or Actu-All Chemicals. DCM was dried using molecular sieves (3 Å) prior use. The synthesis of 5-N_3 has been detailed in Chapter 3, DA was prepared according to literature procedures[28]. The synthesis of DA-AC has been described in Chapter 2.

General methods

Small angle X-Ray scattering (SAXS) profiles were recorded on SAXLAB GANESHA 300 XL SAXS equipped with a GeniX 3D Cu Ultra Low Divergence micro focus sealed tube source producing X-rays with a wavelength $\lambda = 1.54$ Å at a flux of 1×10^8 ph/s and a Pilatus 300 K silicon pixel detector with 487 × 619 pixels of

172 × 172 μm^2 in size placed a three sample-to-detector distances of 113, 713, and 1513 mm respectively to cover a q-range of $0.07 \leq q \leq 3.0$ nm^{-1} with $q = 4\pi/\lambda(\sin \theta/2)$. Silver behenate was used for calibration of the beam center as well as the q-range. Samples were measured within 2 mm quartz capillaries (Hilgenberg GmbH, Germany). The two-dimensional SAXS patterns were brought to an absolute intensity scale using the calibrated detector response function, known sample-to-detector distance, measured incident and transmitted beam intensities, and azimuthally averaged to obtain one dimensional SAXS profiles. The scattering curves of the fibers were obtained by subtraction of the scattering contribution of the solvent and quartz cell.

The mechanical properties of the hydrogels were tested by oscillatory rheology. Dynamic viscoelastic measurements were performed on a stress-controlled Anton Paar and a Physicia MCR 501 Discovery HR-3 and TA Instruments rheometers equipped with a 25-mm stainless steel sand-blasted plate-plate geometry to prevent slippage of the sample in a temperature-controlled environment. Measurements were performed at a fixed temperature of 20 ^oC sealed by placing mineral oil around the sample to minimize evaporation at a fixed plate-to-plate gap of 500 μm. After addition of the catalyst, gelation was monitored under continuous oscillations with a strain amplitude of 1 % and an angular frequency of 6.28 rad s^{-1}. To probe the elasticity of the gels, we applied a steady prestress, σ on which a oscillatory stress, $\delta\sigma(t) = \delta\sigma e^{iwt}$ is superimposed with an amplitude at most 10% of σ and at an angular frequency of ω = 6.28 rad s^{-1}.

Gel preparation method

Non-selective crosslinking of DA/DA-AC fibers with 5-N_3 was performed by weighing DA and DA-AC in the solid state to the desired molar ratio followed by the addition of ca. 300 μL chloroform which was subsequently allowed to evaporate overnight. The resultant solid was dissolved in mili-Q water to a concentration of 50 mg mL^{-1} assisted by applying combined cycles of ultrasonication (ca. 30 min) and vortex until full dissolution of the solid material. The solutions were then placed in a UV-protected environment for a minimum of 2 d. Samples were then prepared by adding mili-Q and an aqueous solution of 5-N_3 (20 mg mL^{-1}) to the desired concentration ensuring a stoichiometric azide/alkyne molar ratio. For PDA samples, solutions at the desired concentration were transferred to quartz cuvettes (1×1 cm)

equipped with stirring bars (see Fig. 4.2) and irradiated with UV-light (254 nm) for 15 min under continuous stirring using a Luzchem photoreactor (model LCZ 4V) equipped with 7.2 W UV-C lamp. Chemical crosslinking was initiated upon addition of premixed aqueous solutions of $CuSO_4$/THPTA and Na-Ascorbate to a final concentration of 0.1, 0.5 and 10 mM respectively.

For selective crosslinking of DA/DA-AC and DA/DA-N_3 fibers an analogous procedure was carried out in which DA was separately blended in chloroform with DA-AC or DA-N_3 to the desired molar ratio. After allowing the solvent to evaporate overnight, the remaining solids were dissolved in mili-Q water to a concentration of 50 mg mL^{-1} and the fibers were allowed to grow for a minimum of 2 d. The concentration was then adjusted upon addition of mili-Q water. At this stage, PDA samples were transferred to quartz cuvettes and irradiated with UV-light using the experimental conditions previously reported. Equal volumes of DA/DA-AC and DA/DA-N_3 or PDA/DA-AC and PDA/DA-N_3 were mixed and chemical crosslinking was initiated by adding the catalyst.

Cryo-EM sample preparation

DA aqueous solutions (18 mg mL^{-1}) were placed in a sonication bath for 1 h and allowed to re-assemble for 2 d in a UV-protected environment unless otherwise noted. Samples were diluted by a factor of 1000 with mili-Q water prior imaging.

Vitrified films were prepared in an automated vitrification robot (Vitrobot™ Mark III, FEI) at 20 ^{o}C and at a relative humidity of 100%. In the preparation chamber, 3 μL sample was applied on a Quantifoil grid (carbon support film on a copper grid, typeR 2/2, Electron Microscopy Sciences), which was glow discharged prior use (Cressington 208 carbon coater operation at 5 mA for 40s). Subsequently, the samples were blotted to remove the excess of solution and vitrified in liquid ethane. The vitrified films were transferred to a cryoholder (Gatan 626) and studied in a FEI Tecnai 20 (type Sphera) microscope operating at 200 kV, equipped with a LaB_6 filament. The images were recorded using a 1k × 1k Gatan CCD camera. Gatan DigitalMicrograph was used for image analysis.

Scaling relationships

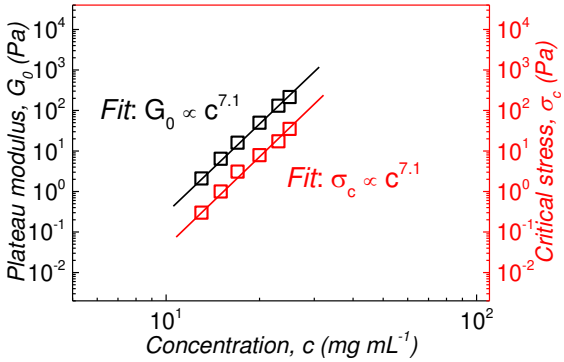

Fig. S4.1 | Plateau modulus G_0 (black) and critical stress σ_c (red) plotted against concentration with dash lines indicative of the corresponding power-law fits.

4.5. References

1. Kurniawan, N. A., Grimbergen, J., Koopman, J. & Koenderink, G. H. Factor XIII stiffens fibrin clots by causing fiber compaction. *J. Thromb. Haemost.* **12,** 1687–1696 (2014).
2. Ariëns, R. A. S., Lai, T.-S., Weisel, J. W., Greenberg, C. S. & Grant, P. J. Role of factor XIII in fibrin clot formation and effects of genetic polymorphisms. *Blood* **100,** 743–754 (2002).
3. Shen, L. & Lorand, L. Contribution of fibrin stabilization to clot strength. Supplementation of factor XIII-deficient plasma with the purified zymogen. *J. Clin. Invest.* **71,** 1336–1341 (1983).
4. Collet, J.-P., Shuman, H., Ledger, R. E., Lee, S. & Weisel, J. W. The elasticity of an individual fibrin fiber in a clot. *Proc. Natl. Acad. Sci. U. S. A.* **102,** 9133–9137 (2005).
5. Robins, S. P. & Bailey, A. J. The chemistry of the collagen cross-links. Characterization of the products of reduction of skin, tendon and bone with sodium cyanoborohydride. *Biochem. J.* **163,** 339–346 (1977).
6. Yamauchi, M. & Sricholpech, M. Lysine post-translational modifications of collagen. *Essays Biochem.* **52,** 113–133 (2012).
7. Buehler, M. J. Nanomechanics of collagen fibrils under varying cross-link densities: Atomistic and continuum studies. *J. Mech. Behav. Biomed. Mater.* **1,** 59–67 (2008).
8. Licup, A. J. *et al.* Stress controls the mechanics of collagen networks. *Proc. Natl. Acad. Sci.* **112,** 9573–9578 (2015).
9. Motte, S. & Kaufman, L. J. Strain stiffening in collagen I networks. *Biopolymers* **99,** 35–46 (2013).
10. Brown, A. E. X., Litvinov, R. I., Discher, D. E., Purohit, P. K. & Weisel, J. W. Multiscale Mechanics of Fibrin Polymer: Gel Stretching with Protein Unfolding and Loss of Water. *Science* **325,** 741–744 (2009).
11. Piechocka, I. K. *et al.* Multi-scale strain-stiffening of semiflexible bundle networks. *Soft Matter* (2016). doi:10.1039/C5SM01992C
12. Piechocka, I. K., Bacabac, R. G., Potters, M., MacKintosh, F. C. & Koenderink, G. H. Structural Hierarchy Governs Fibrin Gel Mechanics. *Biophys. J.* **98,** 2281–2289 (2010).
13. Gardel, M. L. *et al.* Scaling of F-Actin Network Rheology to Probe Single Filament Elasticity and Dynamics. *Phys. Rev. Lett.* **93,** 188102 (2004).
14. Gardel, M. L. *et al.* Elastic Behavior of Cross-Linked and Bundled Actin Networks. *Science* **304,** 1301–1305 (2004).

15. Lin, Y.-C. *et al.* Origins of Elasticity in Intermediate Filament Networks. *Phys. Rev. Lett.* **104,** 058101 (2010).
16. Yao, N. Y. *et al.* Elasticity in Ionically Cross-Linked Neurofilament Networks. *Biophys. J.* **98,** 2147–2153 (2010).
17. Broedersz, C. P. *et al.* Measurement of nonlinear rheology of cross-linked biopolymer gels. *Soft Matter* **6,** 4120–4127 (2010).
18. Jaspers, M. *et al.* Ultra-responsive soft matter from strain-stiffening hydrogels. *Nat. Commun.* **5,** 5808 (2014).
19. Koevoets, R. A. *et al.* Molecular Recognition in a Thermoplastic Elastomer. *J. Am. Chem. Soc.* **127,** 2999–3003 (2005).
20. Koenderink, G. H. *et al.* An active biopolymer network controlled by molecular motors. *Proc. Natl. Acad. Sci.* **106,** 15192–15197 (2009).
21. Kouwer, P. H. J. *et al.* Responsive biomimetic networks from polyisocyanopeptide hydrogels. *Nature* **493,** 651–655 (2013).
22. Saez Talens, V. *et al.* Aromatic Gain in a Supramolecular Polymer. *Angew. Chem. Int. Ed.* **54,** 10502–10506 (2015).
23. Carulla, N. *et al.* Molecular recycling within amyloid fibrils. *Nature* **436,** 554–558 (2005).
24. Chance, R. R. Chromism in Polydiacetylene Solutions and Crystals. *Macromolecules* **13,** 396–398 (1980).
25. Deb, P., Yuan, Z., Ramsey, L. & Hanks, T. W. Synthesis and Optical Properties of Chiral Polydiacetylenes. *Macromolecules* **40,** 3533–3537 (2007).
26. Okada, S., Peng, S., Spevak, W. & Charych, D. Color and Chromism of Polydiacetylene Vesicles. *Acc. Chem. Res.* **31,** 229–239 (1998).
27. Park, D.-H., Hong, J., Park, I. S., Lee, C. W. & Kim, J.-M. A Colorimetric Hydrocarbon Sensor Employing a Swelling-Induced Mechanochromic Polydiacetylene. *Adv. Funct. Mater.* **24,** 5186–5193 (2014).
28. Pal, A. *et al.* Topochemical polymerization in self-assembled rodlike micelles of bisurea bolaamphiphiles. *Soft Matter* **10,** 952–956 (2014)

Chapter 5:

Mimicking active biopolymer networks with a synthetic hydrogel*

Abstract: *Stiffening due to internal stress generation is of paramount importance in living systems and underlies many biomechanical processes. For example, cells stiffen their surrounding matrix by pulling on collagen and fibrin fibers. At the subcellular level, molecular motors prompt fluidisation and actively stiffen the cytoskeleton by sliding polar actin filaments in opposite directions. Synthetic materials able to change their stiffness in response to internally generated and externally applied forces remain unexplored. Here, we demonstrate that chemical crosslinking of thermoresponsive poly(N-isopropylacrylamide) (PNIPAM) in a fibrous matrix of synthetic semi-flexible polymers allows for internal stress generation upon induction of coil-to-globule transition resulting in a macroscopic stiffening response that spans by up to three orders of magnitude. The forces generated through PNIPAM collapse are sufficient to drive a fluid material into a stiff gel within a few minutes. Moreover, rigidified networks dramatically stiffen in response to applied stress featuring power law rheology with exponents that match those of reconstituted actomyosin networks pre-stressed by molecular motors. This concept holds potential for the rational design of synthetic materials that are fluid at room temperature and rapidly rigidify at body temperature to form hydrogels mechanically and structurally akin to cells and tissues.*

*Dr. Robert Göstl and Huda Shaik are acknowledged for the synthesis and characterization of the PNIPAM linker, Gijs M. ter Huurne and Dr. Ilja K. Voets for their contribution to the SAXS characterization, Prof. Dr. Cornelis Storm is acknowledged for discussions on the interpretation of the results and modelling of the data and Dr. Koen Pieterse (ICMS Animation Studio) is gratefully thanked for help with the graphics.

5.1. Introduction

Filamentous biomaterials, such as the actin cytoskeleton, collagen-based extracellular matrix, and fibrin blood clots are three-dimensional, interlinked meshworks of protein biopolymers. They are the scaffold of life, shaping and supporting our cells and tissues. In order to do so in a robust and adaptive manner, their architecture (the spatial arrangement of, and connections between fibers) is highly dynamic – both in terms of constituent polymers, that grow, shrink and reorient[1–7] and in terms of connections which relocate, dissociate and (re)bind[8–10]. In parallel, the mechanical response of a given architecture may be actively amplified; previous work in cells, tissues and reconstituted protein meshworks has demonstrated the capacity of external and internal stresses and strains to change the stiffness of a material by orders of magnitude[8,11–16]. One such active control modality consists of the exertion of small and highly localized forces on a polymer network. At subcellular scales, these forces may be imparted by molecular motors[17–24], in the extracellular matrix they arise from contractile cells (platelets, smooth muscle cells (SMCs))[25–30]. This microscopic pinching is at the root of a number of highly functional biomechanical behaviours: motors may prompt flow and fluidization of the cellular cytoskeleton to permit cell motility[18,23,31,32], SMC mediated forces exert significant pre-stress on the aortic wall, which strengthens it by prompting remodeling and deposition of additional collagen[30,33]. Platelet-mediated forces prompt the collapse and contractility of blood clots. Clearly, such responsive functionality allows biopolymer materials to robustly perform and respond at different lengthscales, and to a variety of external cues. Inspired by these biological regulatory mechanisms, recent work of Rowan and co-workers[34], successfully exploited the potential of lower-critical solution temperature (LCST) polymers to augment the mechanical response of composite materials upon induction of coil-globule collapse. In their work, stiff fibers were grafted with thermo-responsive LSCT polymers and embedded within a soft rubbery matrix. Gels made from these materials reversibly change modulus with heating and cooling. Stiffening arises from the formation of a percolated network of stiff fibers brought into physical contact via the collapse of the thermo-responsive element and softening to recover the original modulus is brought about re-hydration of the collapsed globules below their LSCT point.

In this work, we combine the potential of LCST polymers to induce local contractile forces with the strain-stiffening behaviour intrinsic to meshworks of semi-flexible polymers[35]. We demonstrate that the induction of LCST coil-globule collapse of poly(*N*-isopropylacrylamide) (PNIPAM) chains that crosslink semi-flexible fibers of poly(diacetylene) bis-urea bolaamphiphiles (PDA) (Scheme 5.2.b), dramatically changes the linear mechanical response, rigidifying a previously fluid system to produce a robust and elastic material. Moreover, we show that in the nonlinear deformation regime, universal strain-stiffening occurs, with a power-law stiffening exponent that matches that of collagen networks. This process happens at a constant overall volume. With this work we engineer the first strain-stiffening soft material that shows a temperature-controlled, local strain-induced rigidification transition, directly mimicking cytoskeletal biopolymer-motor composites in both linear and nonlinear response.

In Chapter 4 it was illustrated that, fiber reinforcement through diacetylene cross-polymerization (Scheme 5.2.a) dramatically enhances the non-linear stiffening regime of the hydrogels, enabling them to prevent rupture over broader ranges of applied stress. We showed that the stiffening range of these hydrogels is maximized at the miscibility limit of crosslinkable monomers (DA-AC or DA-N_3) in the unfunctionalized DA host.

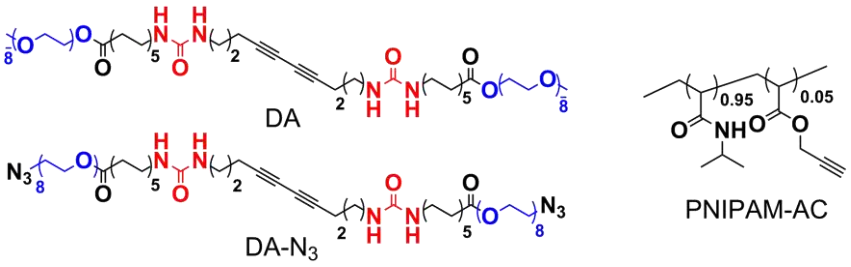

Fig. 5.1 | Molecular structure of the fiber-forming diacetylene bis-urea bolaamphiphile DA, its azide-functionalized analogue DA-N3 and the linear, thermo-responsive PNIPAM-AC linker.

In the current Chapter, we use PDA fibers functionalized by incorporation of 20 mol% DA-N_3 during assembly, followed by fiber reinforcement through diacetylene photo-polymerization. These azide functionalized fibers were chemically crosslinked with a PNIPAM copolymer containing 5% propargyl acrylate residues (PNIPAM-AC, Fig. 5.1) with a ligand-accelerated Cu-catalyzed cycloaddition reaction (CuAAC)[36,37]

(Scheme 5.2.a). The reaction yielded fibrous hydrogels covalently crosslinked with a thermo-responsive linear polymer.

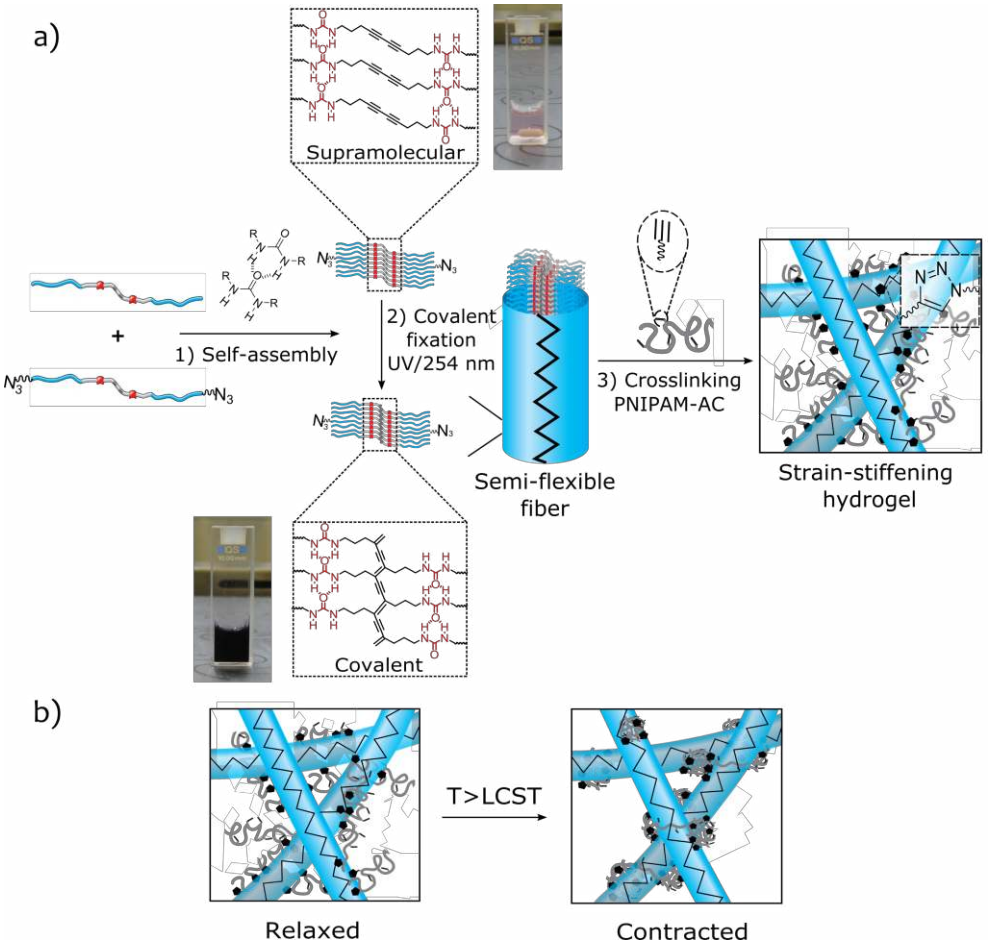

Scheme 5.2 | (a) Hierarchical self-assembly through intermolecular H-bonding and hydrophobic interactions of functionalized (DA-N_3) and unfunctionalized (DA) diacetylene bisurea bolaamphiphiles followed by topochemical polymerization of the self-assembled diacetylenes. Covalent fixation results in the formation a PDA π-conjugated ene-yne framework that leads to strong absorptions in the visible spectral region. Each fiber integrates 9-10 ribbons arranged perpendicular to the fiber axis. Chemical crosslinking with linear PNIPAM-AC into strain-stiffening networks with triazole crosslinks. (b) Internal stress generation within the fibrous PDA scaffold through PNIPAM-AC coil-to-globule transition above its LCST.

5.2. Results and discussion

Synthesis and characterization of PNIPAM-AC

PNIPAM-AC was prepared via reversible addition-fragmentation chain-transfer (RAFT) copolymerization of NIPAM and trimethylsilyl(TMS)-protected propargyl acrylate. TMS-protection was carried out in order to prevent unwanted branching and eventual crosslinking of the individual chains by polymerization of the somewhat polymerizable terminal alkyne moieties[38]. In the final step, the TMS groups were removed with tetra-*n*-butylammonium fluoride (TBAF) to give a linear polymer with an average molecular weight of M_n = 6.96 kDa and a dispersity index of (Đ) = 1.08 (see experimental section for details). Thus, each polymer chain consists of 62 repeat units on average, of which 4 are propargyl acrylate residues. The LCST behaviour of PNIPAM-AC in water was studied by measuring the drop in transmittance at 600 nm in a UV-vis spectrophotometer over a temperature range from 20 to 55 °C. Solutions became turbid at ca. 27 °C at a concentration of 5 mg mL^{-1} and shifted towards lower temperatures at increased polymer concentration (Fig. 5.3). The LCST was taken as the temperature at which transmission had dropped by 50%, and was lower than the literature value of 32 °C[39,40], likely due to the incorporation of a hydrophobic co-monomer as has been previously reported for other PNIPAM copolymers[41–43]. In fact, increasing the amount of propargyl acrylate to 10 mol% in the monomer feed rendered the polymers insoluble in water.

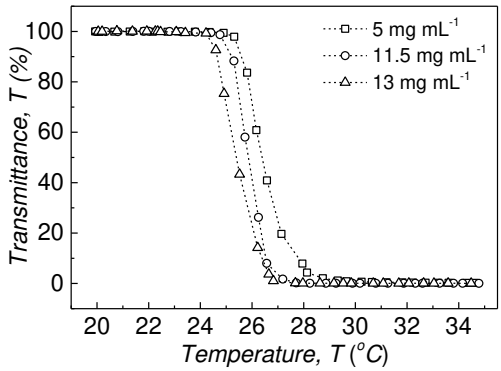

Fig 5.3. | LCST behaviour of PNIPAM-AC in water measured at different concentrations.

Gelation and thermal analysis of the hydrogels

Chemical crosslinking was initiated by adding the catalyst mixture to an aqueous solution of polymerized PDA (containing 20 mol% DA-N_3) fibers and PNIPAM-AC (see experimental section). Solutions were immediately transferred to the rheometer where the gelation process was monitored by measuring the change in moduli at a constant temperature of 20 ^{o}C under continuous oscillatory strain until a constant value of the elastic modulus was reached. Concurrently, networks below the critical connectivity threshold (no measurable storage modulus G' at 20 ^{o}C) were allowed to react for ca. 15 h in the rheometer prior to analysis.

Thermal analysis was performed by subjecting the hydrogels to a linear temperature ramp from 20 to 55 ^{o}C while continuously recording the change in moduli under small-amplitude oscillatory strains. At room temperature, increasing of PDA concentration at a fixed molar ratio of [PNINAM-AC]/[PDA] = 0.089 produced progressively stiffer materials with moduli G' ranging from 2 to 200 Pa in the concentration range of 13 and 23 mg mL^{-1} (Fig. 5.4.a). Below 10 mg mL^{-1} PDA however, the G' of the networks could not be probed at room temperature. Within this concentration regime, all networks remained in the liquid state below the LCST of PNIPAM-AC and rapidly evolved into elastic hydrogels by placing the vials in a water bath at 50 ^{o}C. After removal of the vials from the heating source, all gels remained irreversibly in a gel state. Interestingly, the gel transition happened at a constant overall volume with no visible gel shrinkage, nor was water expelled from the hydrogel (Fig. 5.4.c). Rheology during the T-ramp showed an increase of G´ by more than two orders of magnitude (Fig. 5.4.a). Stiffening sets in at temperatures slightly above the measured LSCT of PNIPAM-AC in water (Fig. 5.3) and gradually shifted towards lower temperatures at increased polymer concentrations (Fig. 5.4.a). The significant increase in G' prompted by PNIPAM-AC coil-to-globule transition here observed for PDA/PNIPAM-AC networks can be related to the isotropic nature of the induced deformation, whereby PNIPAM-AC collapse pulls on PDA fibers regardless of their initial orientation. By contrast, stiffening due to anisotropic shear stress preferentially recruits fibers aligned in the direction of the imposed deformation[35,44,45]. The large increase in stiffness of approximately 100-fold in the PNIPAM containing system is reminiscent of filamin A (FLNa)-crosslinked F-actin networks isotropically stressed

via contractile forces imparted by embedded myosin II motor proteins or fibrin in blood clots stiffened by contractile platelet-mediated forces[20,23,46–48].

Recent *in vitro* experiments on actomyosin networks have shown that the magnitude of the stiffening response is strongly coupled to the relative amount of force-generating and crossliking proteins. Accordingly, high [myosin]/[actin] or high [FLNa]/[actin] molar ratios translate into higher degrees of mechanical responsiveness[20,23,49,50]. To test the influence of density of crosslinks and force-generating elements on PDA/PNIPAM-AC mechanics, 15 mg mL^{-1} PDA aqueous solutions were crosslinked with varying concentrations of PNIPAM-AC. (note that, much like in myosin in actin networks, PNIPAM-AC acts simultaneously as force-generator and cross-linker). Fig. 5.4.b shows that the magnitude of the stiffening response is indeed coupled to the [PNINAM-AC]/[PDA] molar ratio leading to an striking 1000-fold increase in the linear modulus G´ at the highest PNIPAM-AC concentration studied. Conversely, at the lowest PNIPAM-AC concentration, the network remained initially below the connectivity threshold and rapidly evolved into an elastic gel only when prompted by PNIPAM-AC collapse. Thus, the temperature-induced rigidification can depending on the concentration, be either a switch from low to high modulus or a proper sol-gel transition.

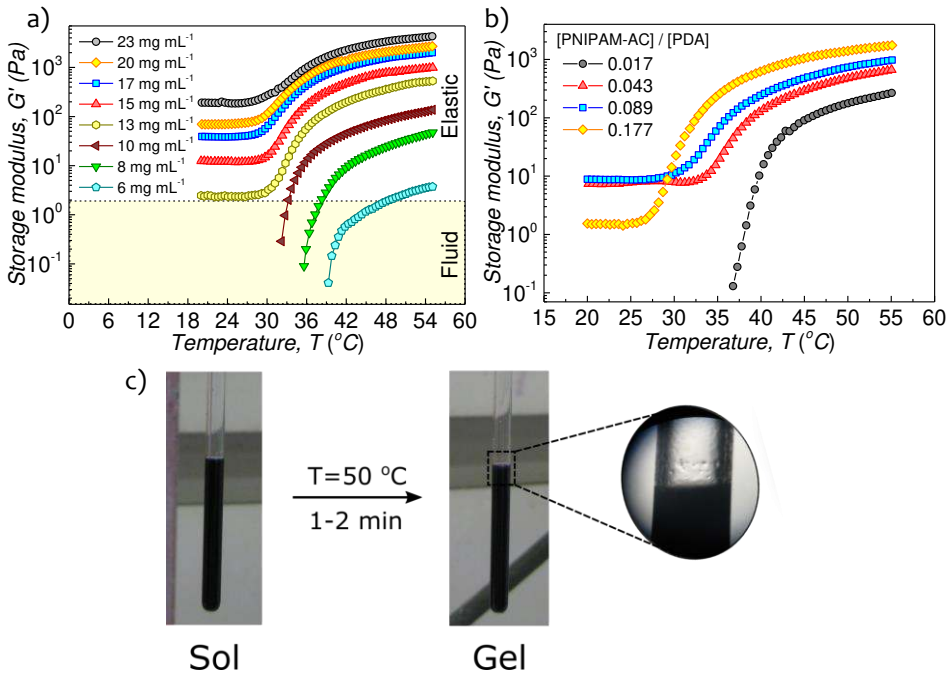

Fig. 5.4 | Linear storage modulus G' vs temperature recorded by applying γ = 1% and ω = 6.28 rad s^{-1} at a heating rate of 1.25 °C min^{-1}. (a) Concentration series of PDA (20 mol% DA-N_3) crosslinked using a fixed molar ratio [PNINAM-AC]/[PDA] = 0.086. The yellow rectangle represents the concentration threshold required for connectivity at 20 °C. (b) 15 mg mL^{-1} PDA (20 mol% DA-N_3) crosslinked using different molar ratios [PNINAM-AC]/[PDA]. (c) Network below the connectivity threshold plunged into a water bath at 50 °C for 1-2 min resulting in the formation of an elastic gel able to support its own weight upon tilting the tube at a constant overall volume. Up-close, at the air-gel interphase, no water was expelled upon induction of PNIPAM-AC LCST transition.

Proposed mechanism of the thermally induced stiffening transition

To identify the underlying mechanisms governing the LCST behavior of PDA/PNIPAM-AC networks, the moduli of the gels were monitored as they were heated to 55 °C and subsequently cooled back to 20 °C before and after chemical crosslinking of PNIMAM-AC and PDA/DA-N_3 fibers (Figs. 5.5.c and d). For chemically crosslinked networks (Fig 5.5.a and c), heating above the LCST of PNIPAM-AC prompts a 100-fold increase in modulus G´ that infers strong pulling of PNIPAM-AC on PDA fibers as the linker undergoes coil-to-globule transition. After cooling back to 20 °C, the hydrogel remained in a stiffened state, consistent with previous observations (in Fig. 5.4.c) showing a permanent fluid-gel transition after removing the gel from the heating source. In other words, networks remain pinned to a stiffened state after PNIPAM-AC collapse. Surprisingly, a solution of PDA fibers and PNIPAM-AC coils without covalent connections between the two components also exhibited a sol-gel transition at around 35 °C. However, this network relaxes part of the built-up stress upon cooling back to 20 °C, as inferred from a decrease in modulus, although it remains above the connectivity threshold at room temperature (Fig. 5.5.d). These results are in clear contrast to the work of Cudjoe *et al* [34] showing a fully reversible stiffness transition in thermo-responsive composites of stiff cellulose nanocrystals (CNCs) grafted with an LCST polymer and embedded within a flexible poly(vinyl acetate) (PVAc) matrix. There, the increase in modulus was ascribed to the formation of a percolating network of stiff CNC fibers brought into physical contact via collapse of the LCST polymers. Recovery of the initial modulus occurs through dissociation of the CNC network as the globules, directly exposed to water, begin to swell below their LCST point, increasing the steric repulsions between CNCs. By contrast, the irreversibility of the stiffening transition found in PDA/PNIPAM-AC networks might be rooted in the amphiphilic nature of PDA fibers combined with a ubiquitous presence of urea groups parallel to the fiber axis. Thus, according to this explanation, globules formed above the LCST of PNIPAM-AC would be efficiently shielded from interaction with water, embedded within the hydrophobic inner core of the fibers. Several reports have identified urea to be an efficient stabilizing agent of the PNIPAM globule state due to its ability to bridge several carbonyl groups by means of intermolecular hydrogen bonds, both in solution[51–54] and within an hydrogel matrix[55]. Thus, stabilization of PNIPAM-AC inside the hydrophobic envelope of PDA fibers combined with hampered diffusion of water into their inner core would

impede rehydration of PNIPAM-AC within the experimental timescales while, at the same time they create new physical connections (Fig. 5.5.b). This mechanism explains the formation of an elastic gel in the absence of chemical crosslinks connecting PDA and PNIPAM-AC (Fig. 5.5.b).

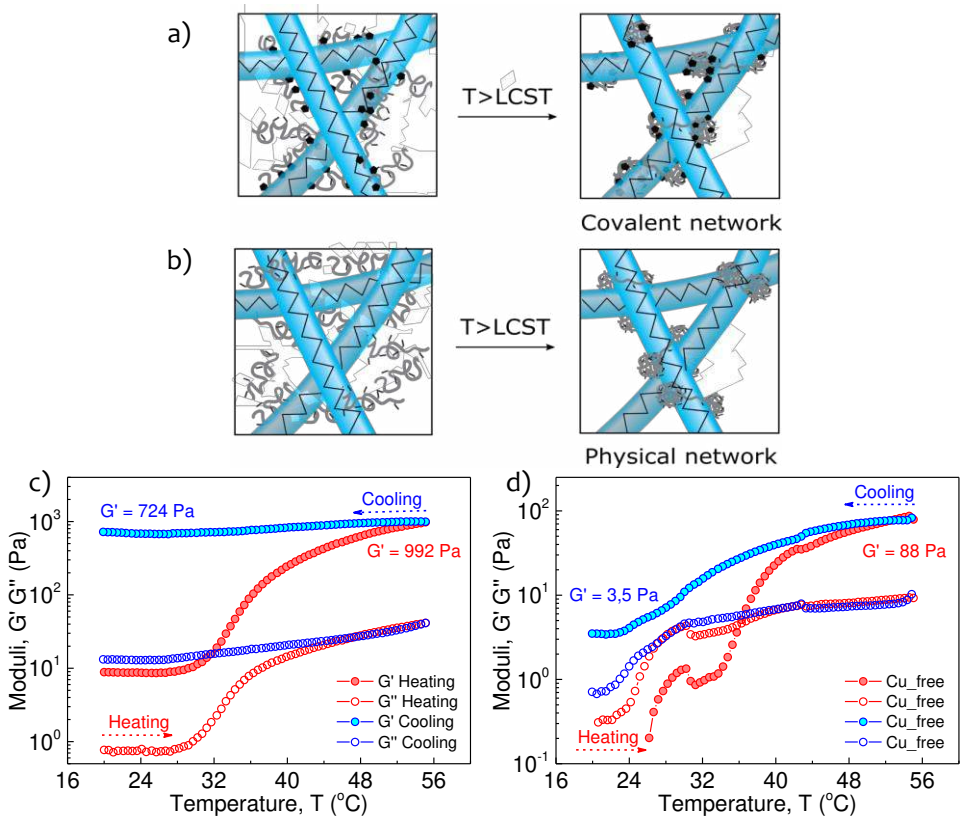

Fig. 5.5 | (a) Mechanism proposed for stiffening transition at a constant overall volume observed in a covalently crosslinked PDA/PNIPAM-AC network, and (b) Sol-gel transition via formation of a physical network in the absence of chemical crosslinks between PDA and PNIPAM-AC. Storage modulus G' vs temperature recorded by applying γ = 1% and ω = 6.28 rad s^{-1} at a heating/cooling rate of 1.25 °C min^{-1} (c) 15 mg mL^{-1} PDA (20 mol% DA-N_3) crosslinked with [PNINAM-AC]/[PDA] = 0.086, (d) 15 mg mL^{-1} PDA mixed with [PNINAM-AC]/[PDA] = 0.086 in the absence of added catalyst.

SAXS Characterization

To get more insight into the structure of the PDA/PNIPAM-AC system, small-angle X-ray scattering (SAXS) experiments were performed both below and above the LCST of PNIPAM-AC for chemically and physically crosslinked systems. Most of the

obtained profiles were featureless curves, typical for elongated systems. The continuous slope at low q-values confirms that the fibers are longer than what can be measured using the available setup (>±15 nm). While the observed differences in slope cannot be explicitly attributed to a change in the fiber's length or rigidity solely based on SAXS (Fig. 5.6.a), the overlap in the high q-region shows that the diameter of the fibers remains 3 nm upon heating from 20 to 55 °C. This cross-sectional radius matches well with the value obtained in cryo-EM (Chapter 2). Similar results are obtained for the covalently crosslinked PDA/PNIPAM-AC. While the change in slope between covalent and physical networks (Figs. 5.6.a and b) can be attributed to different origins, the higher scattering intensity observed at 55 °C in the low q-regime suggests a higher local electron density difference on the ±15 nm lengthscale. This could be attributed to the system becoming more compact as a result of a contraction induced by the collapse of the covalently bonded PNIPAM-AC crosslinks. Furthermore, for the collapsed system an additional feature is observed in the scattering curve at around q = 0.08 Å^{-1} (Fig. 5.6.a). This oscillation implies the presence of a regular structure of about 4-5 nm. This structural organization is most likely related to the collapsed PNIPAM coils or the inter-fiber distance resulting from the contraction.

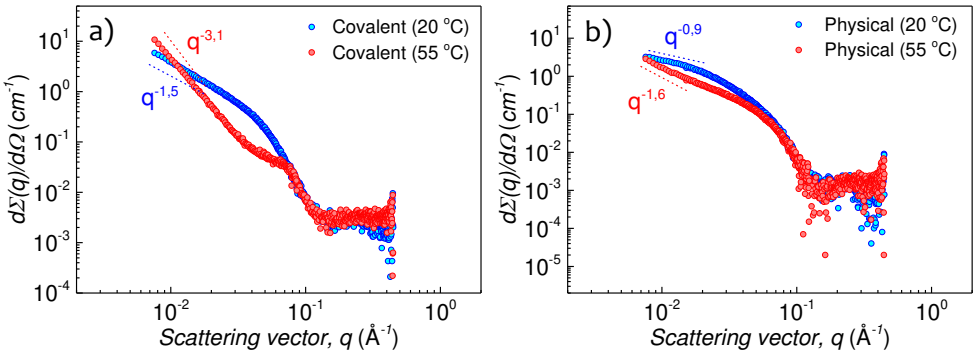

Fig. 5.6 | Small-angle X-ray scattering profiles of PDA (15 mg mL^{-1}) measured below and above the LCST of PNIPAM-AC. (a) PDA crosslinked with [PNINAM-AC]/[PDA] = 0.086 measured 24 h after addition of the catalyst. (b) PDA mixed with [PNINAM-AC]/[PDA] = 0.086 in the absence of added sodium ascorbate.

Nonlinear mechanics of pre-stressed PDA/PNIPAM hydrogels

To more accurately study the mechanical response to applied stress of PDA/PNIPAM-AC networks brought into a non-linear stiffened state via PNIPAM-AC collapse, we applied the rheological protocol[56] described in previous Chapters to pre-rigidified PDA/PNIPAM-AC gels by measuring their stiffness (recorded as the differential modulus $K' = \delta\sigma/\delta\gamma$) as a function of the imposed pre-stress σ. Upon application of an additional steady pre-stress to the gels of Fig. 5.4.a at 20 ^{o}C, all networks exhibit an apparently linear response over a concentration-dependent range of applied σ (Fig. 5.7.a). However, at a characteristic critical stress σ_c the moduli of the gels begin to increase. The critical stress shifts towards higher values when PDA concentrations increase. Strikingly, a 4-fold increase in PDA concentration at [PNIPAM-AC]/[PDA] ratio of 0.086 combined with an externally applied stress rises the modulus from 2 Pa to 10 kPa, nearly 4 orders of magnitude. Concomitantly, the maximum pre-stress σ_{max} before gel rupture rises by 3 full decades (Fig 5.7.a). For the highest PDA concentration, σ_{max} has a value of 1.3 kPa, vastly surpassing the maximum stress of synthetic polyisocyanopeptides (PICs)-based biomimetic gels, *i.e.* $\sigma_{max} \sim$ 40-100 Pa[57,58]. This has important implications for mimicking biomechanics because at this specific molar ratio ([PNIPAM-AC]/[PDA] = 0.086), just above the range (0.005 to 0.05) for the myosin to actin ratios in adherent cells[59–61], we can match the stiffness of PDA hydrogels to that of contractile cells, which spans the range from 0.5 to 10 kPa (Fig. 5.7.a)[62–65].

The curves in Fig. 5.7.a can be collapsed onto a single master curve by normalizing K' to its value in the low-stress linear regime G_0 and by normalizing σ to σ_c (Fig. 5.7.b). The master curve exhibits a power-law dependence $K' \propto \sigma^1$ above σ_c. This value of the so-called stiffening exponent m features universally in biopolymer materials at all lengthscales. In subcellular scales, m = 1 has been reported for reconstituted, active networks of FLNa-crosslinked actin stiffened by myosin II[23]. At whole-cell scales, m = 1 is robustly seen in entire fibroblast[66]. Macroscopically, m = 1 is likewise reported for extracellular hydrogels of reconstituted type I collagen[15]. In general, a stiffening exponent of 1 arises when the stress rises exponentially with strain, such that $K' = \delta\sigma/\delta\gamma \propto \sigma^1$. Such mechanical response, in a range of systems from synthetic to entire vascular tissue, is captured phenomenologically by the Fung-

Shull model[67], which (in Fig. 5.7.b) adequately represent the collapsed data, without any fitting parameters.

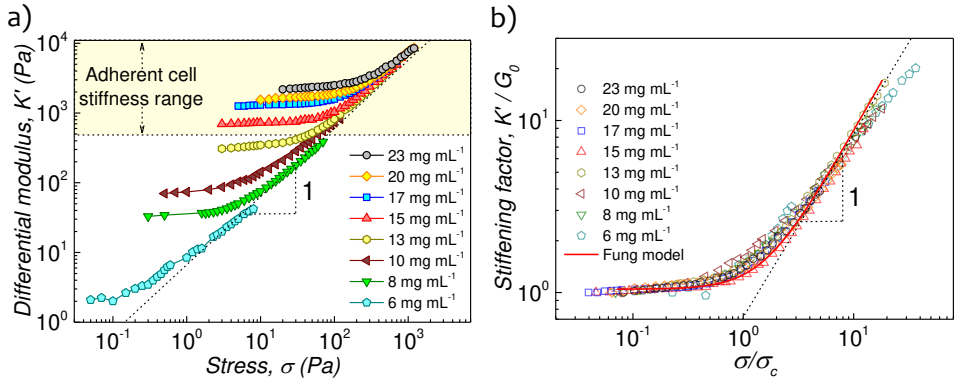

Fig. 5.7 | (a) Differential modulus K' plotted against stress σ measured at 20 °C for different concentrations of PDA crosskinked using a fixed molar ratio [PNINAM-AC]/[PDA] = 0.086 obtained from pre-stressed gels of Fig. 5.4.a. (b) Plot of K' vs stress σ with K' normalized to G_0 and σ normalized to σ_c, showing collapse onto single master curve with $K' \propto \sigma^1$ at high σ.

Combined temperature- and mechano-responsiveness

So far, we have shown that PDA fibers crosslinked with thermo-responsive PNIPAM-AC integrate thermo- and mechano-responsiveness. The combined effect of temperature and applied stress translates into a macroscopic network stiffening spanning a broad range of elastic moduli. To illustrate this principle further on the same hydrogel, the modulus of a PDA/PNIPAM gel was recorded at different temperatures —both below and above the LCST of PNIPAM-AC— by carefully applying a range of steady pre-stresses below the stress at which the gel ruptures, σ_{max}. Fig. 5.8.a shows that the combination of externally applied stimuli in the form of temperature and mechanical stress triggers a strong macroscopic response that drives the network from an initial soft state with a modulus of 1.5 Pa at 20 °C to a final modulus of 2000 Pa at 55 °C just before failure. This exceptional change is mediated by local contractile forces —caused by PNIPAM-AC coil-to-globule transition— and the nonlinear response to deformation of the constituent PDA fibers. Fig. 5.6 also illustrates that stress-stiffening sets in exclusively due to the stiff PDA matrix as a result of which the mechanical responsiveness is present, both below and above the LSCT of PNIPAM-AC. Similar physics behind the stiffening is also supported by the collapse of the data at all three temperatures onto a single master curve (Fig. 5.8.b).

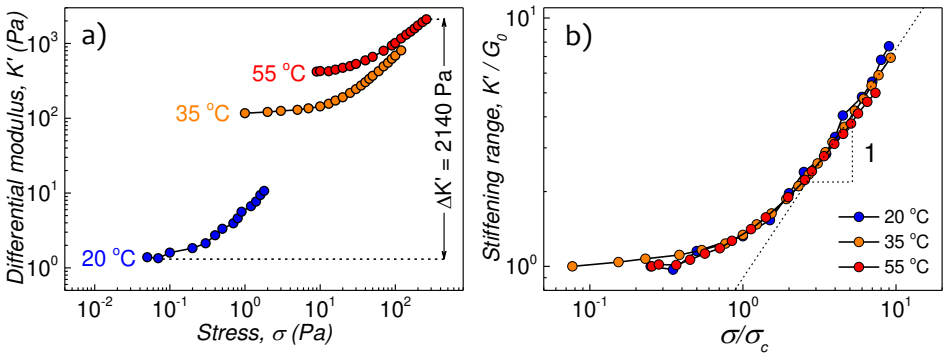

Fig. 5.8 | (a) Differential modulus K' plotted against stress σ for a PDA hydrogel (12 mg mL^{-1}) crosslinked using a [PNIPAM-AC]/[PDA] = 0.086 molar ratio, measured at different temperatures. The gel was brought to its σ_{max} only in the last run at 55 °C. (b) Plot of K' vs stress σ with K' normalized to G_0 and σ normalized to σ_c, showing collapse onto single master curve with K' ∝ σ^1 dependency at high σ.

5.3. Conclusions

We have shown that chemical crosslinking of semi-flexible PDA fibers with an LCST polymer endows the resultant hydrogels with thermo- and stress-responsiveness. The coil-to-globule transition of PNIPAM-AC produces internal stress within the PDA semi-flexible fibrous matrix that drives the system into a stressed regime with an associated network stiffening by up to 1000 times its room temperature linear modulus. The LCST of the linker rigidifies a previously fluid PDA network to rapidly form elastic, strain-stiffening hydrogels. This holds promise in the biomedical field where it opens the door to their use as injectable scaffolds that quickly form gels at body temperature mechanically indistinguishable from the surrounding cells and tissues. We have also shown that the so-formed hydrogels mimic biological systems both in linear and non-linear regimes. In the linear regime, the shear modulus of the gels can be readily tuned with temperature and concentration to access the typical stiffness of adherent contractile cells. In the nonlinear stiffening regime, the gels feature a linear relationship of the differential modulus with stress that mimics the stiffening of collagen gels and, most notably, of reconstituted, active actomyosin networks and fibroblast subjected to mechanical pre-stress. Ultimately, we have illustrated the power and versatility of internally generated forces to enhance the mechanical response of soft materials constructed from entirely man-made building blocks, allowing us to emulate complex biomechanical functions.

5.4. Experimental section

Materials

All solvents used were of reagent grade quality or better and purchased from Biosolve, Sigma-Aldrich or Actu-All Chemicals. THF and DCM were dried using molecular sieves (3 Å). 3-(trimethylsilyl) propargyl alcohol, triethylamine and acrylochloride were used as received from Sigma Aldrich. Degassed tetrahydrofuran (THF) was used in the initial stages of the reaction. For the RAFT polymerisation 4-cyano4[(dodecylsulfanylthiocarbonyl)sulfanyl]pentanol was used as received. N-isopropylacrylamide was recrystallised from hexane at 65°C, AIBN was recrystallised from methanol at 45°C and dioxane (stab. BHT) was freshly distilled for the synthesis. For the deprotection, tertbutyl ammonium fluoride in tetrahydrofuran (1 M) and glacial acetic acid were used as received. Degassed tetrahydrofuran was used in the initial stages of the deprotection and stabilized THF was used to wash the silica column during the removal of the TBAF impurities from the reaction mixture. DA was prepared according to literature procedures[68]. The synthesis of DA-N_3 has been detailed in Chapter 2.

General methods

NMR spectra were recorded 400 MHz Bruker UltraShield Magnet (100 MHz for ^{13}C-NMR). Chemical shifts (δ) are reported in parts per million (ppm) using residual solvent signal or tetramethylsilane (TMS) as internal standards.[69] Splitting patterns are labeled as singlet (s), doublet (d), double doublet (dd), triplet (t), quartet (q), pentet (p) and multiplet (m). Infrared spectra were measured on a Perkin Elmer 1600FT-IR equipped with a Perkin Elmer Universal ATR Sampler Accessory. Matrix-Assisted laser desorption ionization time-of-flight (MALDI-TOF) measurements were carried out on a Perseptive DE PRO Voyager mass spectrometer using α-cyano-4-hydroxycinnamic acid as the calibration matrix. (LC-MS).

Small-Angle X-Ray scattering (SAXS) profiles were recorded on SAXLAB GANESHA 300 XL SAXS equipped with a GeniX 3D Cu Ultra Low Divergence micro focus sealed tube source producing X-rays with a wavelength $\lambda = 1.54$ Å at a flux of 1×10^8 ph/s and a Pilatus 300 K silicon pixel detector with 487 × 619 pixels of 172 × 172 μm² in size placed a three sample-to-detector distances of 113, 713, and 1513 mm respectively to cover a q-range of $0.07 \leq q \leq 3.0$ nm^{-1} with $q = 4\pi/\lambda(\sin$

θ/2). Silver behenate was used for calibration of the beam center as well as the *q*-range. Samples were measured within 2 mm quartz capillaries (Hilgenberg GmbH, Germany). The two-dimensional SAXS patterns were brought to an absolute intensity scale using the calibrated detector response function, known sample-to-detector distance, measured incident and transmitted beam intensities, and azimuthally averaged to obtain one-dimensional SAXS profiles. The scattering curves of the fibers were obtained by subtraction of the scattering contribution of the solvent and quartz cell.

Gel permeation chromatography (GPC) was carried out on a Shimadzu Prominence-i LC-2030C 3D system equipped with a RID-20A refractive index detector.

Ultraviolet-visible (UV-vis) transmittance spectra were recorded on a Jasco V-650 UV-vis spectrometer equipped with a Jasco ETCT-762 temperature controller. All samples were measured using quartz cuvettes (1 cm).

The mechanical properties of the hydrogels were tested by oscillatory rheology. Dynamic viscoelastic measurements were conducted on a stress-controlled Anton Paar and a Physicia MCR 501 Discovery HR-3, TA Instruments rheometers equipped with a 25-mm stainless steel sand-blasted plate-plate geometry to prevent slippage of the sample in a temperature-controlled environment. Measurements were performed by placing mineral oil around the sample to minimize evaporation at a fixed plate-to-plate gap of 500 μm. After addition of the catalyst, gelation was monitored by continuous oscillations with a strain amplitude of 1 % and an angular frequency of 6.28 rad s^{-1}. To probe the elasticity of the gels, we applied a steady pre-stress, σ on which an oscillatory stress, $\delta\sigma(t) = \delta\sigma e^{iwt}$ is superimposed with an amplitude at most 10% of σ and an angular frequency of ω = 6.28 rad s^{-1}.

Synthetic procedures

Synthesis of 3-(trimethylsilyl) prop-2-argyl acrylate

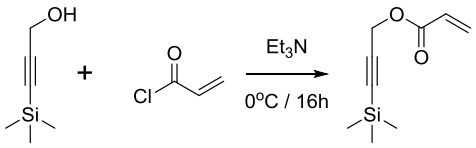

1
94%

3-(trimethylsilyl) propargyl alcohol (1.00 g, 7.8 mmol) and triethylamine (1.2 mL, 8.6 mmol) were placed in a Schlenk flask under flow of Argon. Approximately 5 mL of degassed THF was added to this, and the whole solution was cooled in an ice bath for approximately 10 min. Then, acrylochloride (0.81 g, 8.6 mmol) was added dropwise to the solution, whereupon $Et_3N{\cdot}HCl$ salt precipitated. Further THF was added to allow free stirring and mixing of the reactants for complete conversion. The resulting solution was left stirring at room temperature overnight and in the dark. The reaction was then diluted with Et_2O and extracted with dil. aq. Na_2CO_3 solution. Subsequently, the organic layer was separated, dried over $MgSO_4$ and concentrated *in vacuo* to yield a clear yellow/brown solution of 3-(trimethylsilyl) prop-2-argyl acrylate (**1**) (1.33 g, 7.28 mmol, 94%).

^{1}H-NMR (400 MHz, $CDCl_3$, 295 K): δ ppm 6.47 (dd, 1 H), 6.16 (dd, 1 H), 5.88 (dd, 1 H), 4.77 (s, 2 H), 0.19 (s, 9 H).

^{13}C-NMR (100 MHz, $CDCl_3$): δ ppm 165.7, 132.0, 128.1, 99.2, 92.6, 53.2, 0.1.

RAFT co-polymerization of NIPAM and Synthesis of 3-(trimethylsilyl) prop-2-argyl acrylate

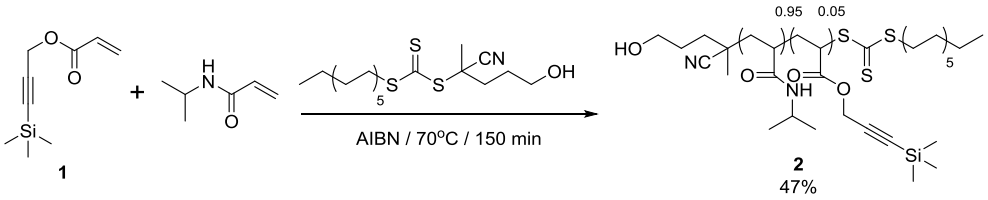

N–isopropylacrylamide (1.45 g, 12.83 mmol), 4-cyano-4-[dodecylsulfanylthiocarbonyl) sulfanyl] pentanol (52.57 mg, 0.13 mmol), AIBN (4.62 mg, 0.026 mmol) and 3-(trimethylsilyl) prop-2-argyl acrylate (**1**) (0.12 g, 0.64 mmol) were dissolved in 2 mL of freshly distilled dioxane. The resulting homogeneous solution was degassed by 3 consecutive freeze pump thaw cycles. The solution was then heated to 70°C and stirred for 3 h. Polymerization was stopped by cooling to room temperature and exposing the reaction mixture to air. Further, dioxane was added to the resulting viscous mixture and then precipitated into ice cold diethyl ether once. The precipitate was collected and dried *in vacuo* to afford the final product as a yellowish powder (0.74 g, 45%).

^{1}H-NMR (400 MHz, $CDCl_3$, 295 K): δ ppm 6.48 (m, 117 H), 4.63 (m, 12 H), 4.01 (br. s. 120 H), 3.33 (m, 2 H), 0.17 (s, 57 H).

TMS removal

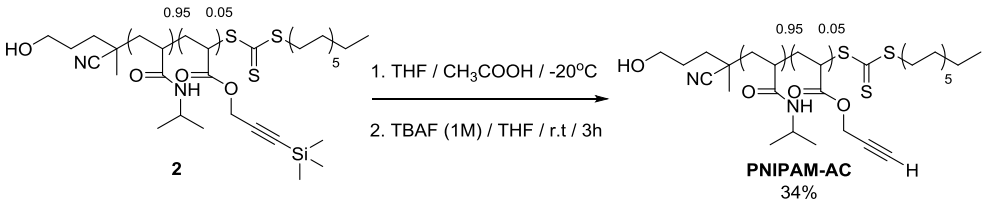

2 (0.74 g) was dissolved in 5 mL of degassed THF and 1.5 equivalents of glacial acetic acid relative to the number of TMS groups. The whole was degassed by purging with Argon for 10 min. The solution was cooled to -20°C and 1.5 equivalents of TBAF (1.0 M) in THF was added slowly and dropwise. The solution was left to stir at -20°C for a further 30 min then warmed to room temperature and left for a further 2 h to ensure complete deprotection. The resulting solution was diluted with THF and

passed through a short silica column to remove TBAF impurities. The filtrate was dried *in vacuo* and then put under high vacuum for 1 h to remove the volatiles. The resultant solid was precipitated from dichloromethane into ice cold diethyl ether twice. The yellowish powder product obtained was dried *in vacuo* to yield **PNIMPAM-AC** (0.25 g, 34%).

^{1}H-NMR (400 MHz, $CDCl_3$, 295 K): δ ppm 6.45 (m, 54 H), 4.67 (m, 9 H), 3.99 (br. s. 56 H), 3.65 (m, 2 H), 3.32 (m, 2 H), 2.20-0.86 (m, 642 H).

Mn (GPC) = 6.96 kD , **Mw/Mn** (GPC): 1.08.

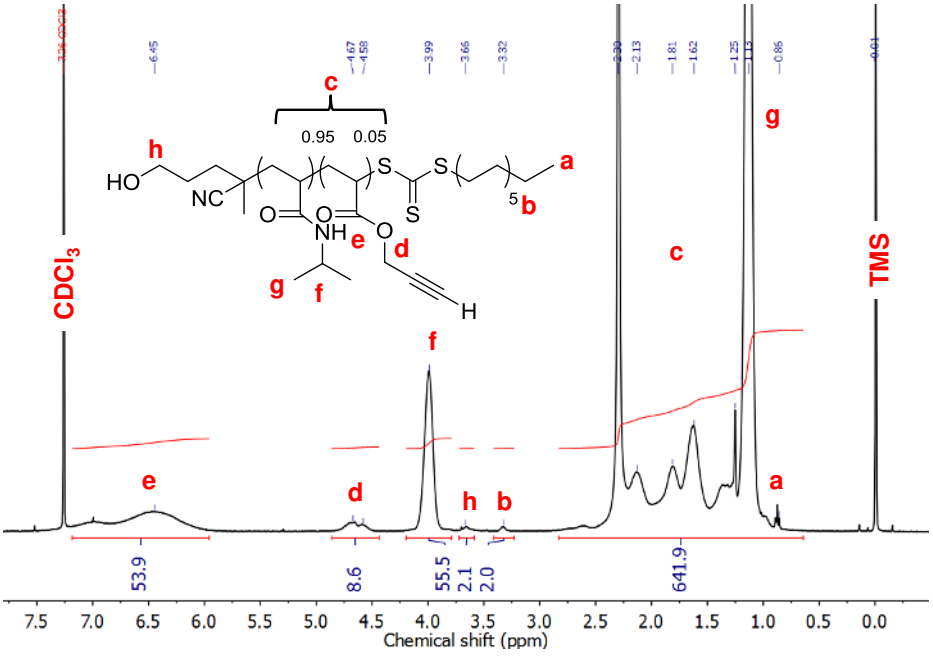

Fig. S5.1 | ^{1}H-NMR ($CDCl_3$, 25 °C) spectrum of PNIPAM-AC.

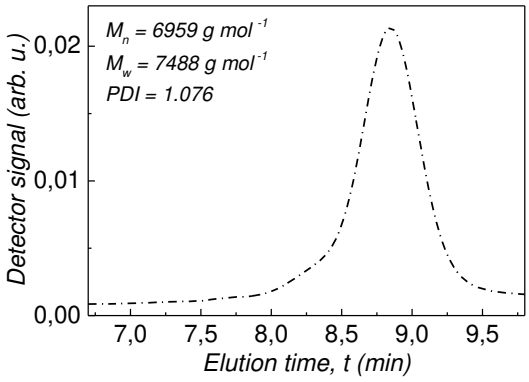

Fig. S5.2 | GPC trace of PNIPAM-AC.

Gel preparation method

Samples were prepared by weighing DA and DA-N_3 in the solid state followed by the addition of ca. 300 μL chloroform. The organic solvent was allowed to evaporate overnight and the remaining solid subsequently re-dissolved in mili-Q water to a concentration of 50 mg mL^{-1} assisted by applying combined cycles of sonication (30 min) and vortex (1 min) until the full dissolution of the solid material. The micelles were then allowed grow at this concentration for a minimum of 2d in a UV-protected environment. The samples were diluted with mili-Q water and an aqueous stock solution (20 mg mL^{-1}) of PNIPAM-AC (stored at 5 ^{o}C) to the desired concentration. Covalent fixation was performed by transferring the mixtures to quartz cuvettes (1×1 cm) and irradiating at 254 nm for 15 min under continuous stirring using a Luzchem photoreactor (model LCZ 4V) equipped with 7.2 W UV-C lamp. Gelation of the solutions was performed upon addition of premixed aqueous solutions of $CuSO_4$/Tris(3-hydroxypropyltriazolylmethyl)amine (THPTA) and sodium ascorbate (Na-Ascorbate) to a final concentration of 0.1, 0.5 and 10 mM respectively.

Scaling relationships

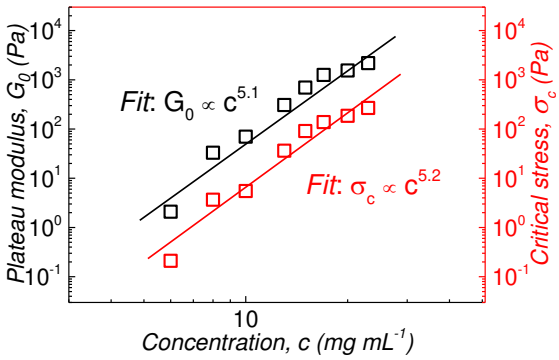

Fig. S5.3 | Plateau modulus G_0 (black) and critical stress σ_c (red) plotted against concentration with dash fitted lines.

5.5. References

1. Pollard, T. D. & Borisy, G. G. Cellular Motility Driven by Assembly and Disassembly of Actin Filaments. *Cell* **112,** 453–465 (2003).
2. Helfand, B. T. *et al.* Vimentin organization modulates the formation of lamellipodia. *Mol. Biol. Cell* **22,** 1274–1289 (2011).
3. Kirschner, M. & Mitchison, T. Beyond self-assembly: From microtubules to morphogenesis. *Cell* **45,** 329–342 (1986).
4. Swaney, K. F., Huang, C.-H. & Devreotes, P. N. Eukaryotic Chemotaxis: A Network of Signaling Pathways Controls Motility, Directional Sensing, and Polarity. *Annu. Rev. Biophys.* **39,** 265–289 (2010).
5. Windoffer, R., Beil, M., Magin, T. M. & Leube, R. E. Cytoskeleton in motion: the dynamics of keratin intermediate filaments in epithelia. *J. Cell Biol.* **194,** 669–678 (2011).
6. The Three-Dimensional Dynamics of Actin Waves, a Model of Cytoskeletal Self-Organization. *Biophys. J.* **96,** 2888–2900 (2009).
7. Goldman, R. D., Khuon, S., Chou, Y. H., Opal, P. & Steinert, P. M. The function of intermediate filaments in cell shape and cytoskeletal integrity. *J. Cell Biol.* **134,** 971–983 (1996).
8. Gardel, M. L. *et al.* Scaling of F-Actin Network Rheology to Probe Single Filament Elasticity and Dynamics. *Phys. Rev. Lett.* **93,** 188102 (2004).
9. Gardel, M. L. *et al.* Prestressed F-actin networks cross-linked by hinged filamins replicate mechanical properties of cells. *Proc. Natl. Acad. Sci. U. S. A.* **103,** 1762–1767 (2006).
10. Ruddies, R., Goldmann, W. H., Isenberg, G. & Sackmann, E. The viscoelasticity of entangled actin networks: the influence of defects and modulation by talin and vinculin. *Eur. Biophys. J.* **22,** 309–321 (1993).
11. Gardel, M. L. *et al.* Elastic Behavior of Cross-Linked and Bundled Actin Networks. *Science* **304,** 1301–1305 (2004).
12. Lin, Y.-C. *et al.* Origins of Elasticity in Intermediate Filament Networks. *Phys. Rev. Lett.* **104,** 058101 (2010).
13. Yao, N. Y. *et al.* Elasticity in Ionically Cross-Linked Neurofilament Networks. *Biophys. J.* **98,** 2147–2153 (2010).
14. Piechocka, I. K. *et al.* Multi-scale strain-stiffening of semiflexible bundle networks. *Soft Matter* (2016). doi:10.1039/C5SM01992C

15. Licup, A. J. *et al.* Stress controls the mechanics of collagen networks. *Proc. Natl. Acad. Sci.* **112,** 9573–9578 (2015).
16. Brown, A. E. X., Litvinov, R. I., Discher, D. E., Purohit, P. K. & Weisel, J. W. Multiscale Mechanics of Fibrin Polymer: Gel Stretching with Protein Unfolding and Loss of Water. *Science* **325,** 741–744 (2009).
17. Fletcher, D. A. & Mullins, R. D. Cell mechanics and the cytoskeleton. *Nature* **463,** 485–492 (2010).
18. Toyota, T., Head, D. A., Schmidt, C. F. & Mizuno, D. Non-Gaussian athermal fluctuations in active gels. *Soft Matter* **7,** 3234–3239 (2011).
19. Brangwynne, C. P., Koenderink, G. H., MacKintosh, F. C. & Weitz, D. A. Nonequilibrium Microtubule Fluctuations in a Model Cytoskeleton. *Phys. Rev. Lett.* **100,** 118104 (2008).
20. Mizuno, D., Tardin, C., Schmidt, C. F. & MacKintosh, F. C. Nonequilibrium Mechanics of Active Cytoskeletal Networks. *Science* **315,** 370–373 (2007).
21. Bertrand, O. J. N., Fygenson, D. K. & Saleh, O. A. Active, motor-driven mechanics in a DNA gel. *Proc. Natl. Acad. Sci.* **109,** 17342–17347 (2012).
22. Ennomani, H. *et al.* Architecture and Connectivity Govern Actin Network Contractility. *Curr. Biol.* **26,** 616–626 (2016).
23. Koenderink, G. H. *et al.* An active biopolymer network controlled by molecular motors. *Proc. Natl. Acad. Sci.* **106,** 15192–15197 (2009).
24. Ndlec, F. J., Surrey, T., Maggs, A. C. & Leibler, S. Self-organization of microtubules and motors. *Nature* **389,** 38532 (1997).
25. Saez, A., Ghibaudo, M., Buguin, A., Silberzan, P. & Ladoux, B. Rigidity-driven growth and migration of epithelial cells on microstructured anisotropic substrates. *Proc. Natl. Acad. Sci.* **104,** 8281–8286 (2007).
26. Jansen, K. A., Bacabac, R. G., Piechocka, I. K. & Koenderink, G. H. Cells Actively Stiffen Fibrin Networks by Generating Contractile Stress. *Biophys. J.* **105,** 2240–2251 (2013).
27. Brown, A. C. *et al.* Ultrasoft microgels displaying emergent platelet-like behaviours. *Nat. Mater.* **13,** 1108–1114 (2014).
28. Lam, W. A. *et al.* Mechanics and contraction dynamics of single platelets and implications for clot stiffening. *Nat. Mater.* **10,** nmat2903 (2010).
29. Jawerth, L., Muenster, S. & Weitz, D. A. The Mechanical Mechanism of Platelet Induced Clot Stiffening. *Biophys. J.* **104,** 150a (2013).
30. Lacolley, P., Regnault, V., Segers, P. & Laurent, S. Vascular Smooth Muscle Cells and Arterial Stiffening: Relevance in Development, Aging, and Disease. *Physiol. Rev.* **97,** 1555–1617 (2017).
31. Alvarado, J., Sheinman, M., Sharma, A., MacKintosh, F. C. & Koenderink, G. H. Molecular motors robustly drive active gels to a critically connected state. *Nat. Phys.* **9,** 591–597 (2013).
32. Weirich, K. L. *et al.* Liquid behavior of cross-linked actin bundles. *Proc. Natl. Acad. Sci.* **114,** 2131–2136 (2017).
33. Rachev, A. & Hayashi, K. Theoretical Study of the Effects of Vascular Smooth Muscle Contraction on Strain and Stress Distributions in Arteries. *Ann. Biomed. Eng.* **27,** 459–468 (1999).
34. Cudjoe, E. *et al.* Biomimetic Reversible Heat-Stiffening Polymer Nanocomposites. *ACS Cent. Sci.* **3,** 886–894 (2017).
35. Storm, C., Pastore, J. J., MacKintosh, F. C., Lubensky, T. C. & Janmey, P. A. Nonlinear elasticity in biological gels. *Nature* **435,** 191–194 (2005).
36. Presolski, S. I., Hong, V., Cho, S.-H. & Finn, M. G. Tailored Ligand Acceleration of the Cu-Catalyzed Azide−Alkyne Cycloaddition Reaction: Practical and Mechanistic Implications. *J. Am. Chem. Soc.* **132,** 14570–14576 (2010).
37. Hong, V., Presolski, S. I., Ma, C. & Finn, M. G. Analysis and Optimization of Copper-Catalyzed Azide–Alkyne Cycloaddition for Bioconjugation. *Angew. Chem. Int. Ed.* **48,** 9879–9883 (2009).

38. Geng, J., Lindqvist, J., Mantovani, G. & Haddleton, D. M. Simultaneous Copper(I)-Catalyzed Azide–Alkyne Cycloaddition (CuAAC) and Living Radical Polymerization. *Angew. Chem. Int. Ed.* **47,** 4180–4183 (2008).
39. Heskins, M. & Guillet, J. E. Solution Properties of Poly(N-isopropylacrylamide). *J. Macromol. Sci.* (2006). doi:10.1080/10601326808051910
40. Schild, H. G. & Tirrell, D. A. Microcalorimetric detection of lower critical solution temperatures in aqueous polymer solutions. *J. Phys. Chem.* **94,** 4352–4356 (1990).
41. Jain, K., Vedarajan, R., Watanabe, M., Ishikiriyama, M. & Matsumi, N. Tunable LCST behavior of poly(N -isopropylacrylamide/ionic liquid) copolymers. *Polym. Chem.* **6,** 6819–6825 (2015).
42. Brazel, C. S. & Peppas, N. A. Synthesis and Characterization of Thermo- and Chemomechanically Responsive Poly(N-isopropylacrylamide-co-methacrylic acid) Hydrogels. *Macromolecules* **28,** 8016–8020 (1995).
43. Zhou, S. & Chu, B. Synthesis and Volume Phase Transition of Poly(methacrylic acid-co-N-isopropylacrylamide) Microgel Particles in Water. *J. Phys. Chem. B* **102,** 1364–1371 (1998).
44. Head, D. A., Levine, A. J. & MacKintosh, F. C. Deformation of Cross-Linked Semiflexible Polymer Networks. *Phys. Rev. Lett.* **91,** 108102 (2003).
45. Onck, P. R., Koeman, T., van Dillen, T. & van der Giessen, E. Alternative Explanation of Stiffening in Cross-Linked Semiflexible Networks. *Phys. Rev. Lett.* **95,** 178102 (2005).
46. Chen, P. & Shenoy, V. B. Strain stiffening induced by molecular motors in active crosslinked biopolymer networks. *Soft Matter* **7,** 355–358 (2011).
47. Lam, W. A. *et al.* Mechanics and contraction dynamics of single platelets and implications for clot stiffening. *Nat. Mater.* **10,** 61 (2011).
48. Broedersz, C. P. & MacKintosh, F. C. Molecular motors stiffen non-affine semiflexible polymer networks. *Soft Matter* **7,** 3186–3191 (2011).
49. MacKintosh, F. C. & Levine, A. J. Nonequilibrium Mechanics and Dynamics of Motor-Activated Gels. *Phys. Rev. Lett.* **100,** 018104 (2008).
50. Liverpool, T. B., Marchetti, M. C., Joanny, J.-F. & Prost, J. Mechanical response of active gels. *EPL* **85,** 18007 (2009).
51. Zhang, Y. & Cremer, P. S. Chemistry of Hofmeister Anions and Osmolytes. *Annu. Rev. Phys. Chem.* **61,** 63–83 (2010).
52. Wang, J., Liu, B., Ru, G., Bai, J. & Feng, J. Effect of Urea on Phase Transition of Poly(N-isopropylacrylamide) and Poly(N,N-diethylacrylamide) Hydrogels: A Clue for Urea-Induced Denaturation. *Macromolecules* **49,** 234–243 (2016).
53. Fuchise, K. *et al.* Control of thermoresponsive property of urea end-functionalized poly(N-isopropylacrylamide) based on the hydrogen bond-assisted self-assembly in water. *J. Polym. Sci. Part Polym. Chem.* **47,** 6259–6268 (2009).
54. Pica, A. & Graziano, G. On urea's ability to stabilize the globule state of poly(N-isopropylacrylamide). *Phys. Chem. Chem. Phys.* **18,** 14426–14433 (2016).
55. Sagle, L. B. *et al.* Investigating the Hydrogen-Bonding Model of Urea Denaturation. *J. Am. Chem. Soc.* **131,** 9304–9310 (2009).
56. Broedersz, C. P. *et al.* Measurement of nonlinear rheology of cross-linked biopolymer gels. *Soft Matter* **6,** 4120–4127 (2010).
57. Jaspers, M. *et al.* Ultra-responsive soft matter from strain-stiffening hydrogels. *Nat. Commun.* **5,** 5808 (2014).
58. Kouwer, P. H. J. *et al.* Responsive biomimetic networks from polyisocyanopeptide hydrogels. *Nature* **493,** 651–655 (2013).
59. Verkhovsky, A. B. & Borisy, G. G. Non-sarcomeric mode of myosin II organization in the fibroblast lamellum. *J. Cell Biol.* **123,** 637–652 (1993).

60. Hartwig, J. H. & Shevlin, P. The architecture of actin filaments and the ultrastructural location of actin-binding protein in the periphery of lung macrophages. *J. Cell Biol.* **103,** 1007–1020 (1986).
61. Bendix, P. M. *et al.* A Quantitative Analysis of Contractility in Active Cytoskeletal Protein Networks. *Biophys. J.* **94,** 3126–3136 (2008).
62. Wang, N. *et al.* Mechanical behavior in living cells consistent with the tensegrity model. *Proc. Natl. Acad. Sci.* **98,** 7765–7770 (2001).
63. Wang, N. *et al.* Cell prestress. I. Stiffness and prestress are closely associated in adherent contractile cells. *Am. J. Physiol. - Cell Physiol.* **282,** C606–C616 (2002).
64. Fabry, B. *et al.* Scaling the Microrheology of Living Cells. *Phys. Rev. Lett.* **87,** 148102 (2001).
65. Solon, J., Levental, I., Sengupta, K., Georges, P. C. & Janmey, P. A. Fibroblast Adaptation and Stiffness Matching to Soft Elastic Substrates. *Biophys. J.* **93,** 4453–4461 (2007).
66. Fernández, P., Pullarkat, P. A. & Ott, A. A Master Relation Defines the Nonlinear Viscoelasticity of Single Fibroblasts. *Biophys. J.* **90,** 3796–3805 (2006).
67. Zhou, J. & Fung, Y. C. The degree of nonlinearity and anisotropy of blood vessel elasticity. *Proc. Natl. Acad. Sci.* **94,** 14255–14260 (1997).
68. Pal, A. *et al.* Topochemical polymerization in self-assembled rodlike micelles of bisurea bolaamphiphiles. *Soft Matter* **10,** 952–956 (2014).
69. Fulmer, G. R. *et al.* NMR Chemical Shifts of Trace Impurities: Common Laboratory Solvents, Organics, and Gases in Deuterated Solvents Relevant to the Organometallic Chemist. *Organometallics* **29,** 2176–2179 (2010).

Chapter 6:

Epilogue

The contents presented in this thesis describe novel approaches towards biomimetic strain-stiffening hydrogels relying on polymerizable, hierarchically self-assembled diacetylene bis-urea bolaamphiphiles as their main structural components. Herein, we briefly discuss the limitations of the current setup and put forward suggestions to gain deeper insight into the network's architectural parameters. Furthermore, based on the results derived from this work, we propose future directions to engineer fully synthetic hydrogels, mechanically indistinguishable from cells and tissues that harness the rich structural diversity and dynamics inherent to supramolecular polymers.

Current system limitations

From the results discussed throughout this manuscript, it is clear that DA bolaamphiphiles are a versatile motif to engineer biopolymer network mimics. The supramolecular nature of DA monomers offers a unique opportunity to introduce reactivity along the fiber contour in a fully controlled manner by co-assembling cross-linkable analogues such as DA-AC and DA-N_3. However, while having supramolecular monomers may offer distinctive advantages, control over the fiber length −one of the key parameters in strain-stiffening materials− remains challenging. Indeed, Chapters 2, 3 and 4 showed relatively broad distributions in fiber lengths when visualized with cryo-EM. To minimize this effect, from Chapter 3 onwards, the sample preparation method was optimized such that, samples at a given functionalized (DA-AC or DA-N_3) to unfunctionalized (DA) molar ratio were prepared from the same concentrated stock solution thus providing consistent results in concentration-dependent studies. Nonetheless, a systematic research on the parameters that control the length and length distribution of DA-fibers (*e.g.* temperature, addition of co-solvents, incorporation of salts, optimization of molecular design, etc…) would be rather desirable in order to gain superior control over the macroscopic properties of DA and PDA hydrogels. Also in relation to fiber lengths, it is noteworthy that, while the typical contour lengths of common filamentous proteins are by up to several microns, DA and PDA fibers are restricted to much shorter lengthscales of a few hundred nanometers, thereby limiting their morphological resemblance to biopolymers, and increasing the minimal concentration needed to form three-dimensional networks.

Fiber covalent fixation through diacetylene topochemical polymerization has proven to be a useful technique to reinforce self-assembled DA fibers, dramatically changing the mechanical properties of PDA hydrogels especially in their nonlinear deformation regime as illustrated in Chapter 4. PDA fibers combine the hierarchical structure inherent to this type of supramolecular polymers with the mechanical strength of covalent polymers. However, the formation of a π-conjugated ene-yne framework produces materials that strongly absorb in the visible spectral region. This feature, intrinsic to all polyconjugated polymers, reduces the palette of available optical techniques such as dynamic and static light scattering (DLS/SLS) or diffusing wave-spectroscopy (DWS) that could be used to extract valuable information about the network structure. Specifically, little is known about the mesh size of PDA hydrogels as the length scales needed are beyond the resolution accessible by conventional small-angle X-ray scattering (SAXS), where $q_{min}^{-1} \approx 30$ nm. Additionally, magnetic particle imaging[1,2] and nanorheology[3–5] have emerged as promising techniques, in which tracer iron oxide nanoparticles are embedded within the material and the magnetic field generated by these particles is used to measure the modulus or create a topographic image of the material using a magnetic scanner. Thus, the combined use of these techniques might allow extracting structural and mechanical information from PDA hydrogels without the need for an optical setup.

Additionally, one major drawback related to the non-transparent nature of PDA gels is that it will likely hamper their application in the biomedical field where, regardless of biocompatibility, optically transparent materials are required in cell-based studies[6]. A potential alternative to retaining the mechanical properties of PDA gels while having a transparent material would consist of reducing the double bonds of the PDA framework to produce a non-conjugated covalent backbone. For that purpose, we propose the *in situ* generation of diimides: A homogeneous reduction method widely used to convert unsaturated compounds −including π-conjugated systems such as porphyrins− into alkane products that is compatible with water[7,8]. Thus, we argue that this approach could potentially lead to optically transparent gels whose fibers remain covalently anchored by an alkane backbone.

Future perspectives

Future directions of DA and PDA hydrogels

Chapters 3 to 5 showcased the versatility of introducing reactive analogues (DA-AC and DA-N_3) into a fiber-forming host (DA). This feature was herein exploited to 'click' DA and PDA fibers to a pentavalent linker (Chapters 3 and 4) as well as to a force-generating LCST polymer (Chapter 5). Hence, we believe that this crosslinking strategy offers an exceptional platform to link DA and PDA fibers as well as other supramolecular constructs to a large variety of systems. Here, we propose future directions to provide DA and PDA fibers with specific functionality and biomimicry.

While replicating the mechanical and structural features of biopolymers and their networks is of paramount importance, several other factors need to be accounted for when using synthetic materials for biomedical purposes. Seminal work by Rowan *et al.*[9] showed that grafting of cell-adhesive peptides to synthetic strain-stiffening polysiocyanopeptide (PIC) hydrogels allowed for controlled stem cell differentiation into either into adipocytes or osteoblasts by tuning the mechanics of the stress-responsive matrix. In line with these results, similar approaches could be adopted for DA hydrogels, whereby clicking of cells-adhesive motifs to fibers containing DA-AC or DA-N_3 could impart these materials the correct bioactivity and biocompatibility making them suitable matrices for cell culture applications.

Moreover, in Chapter 5 it was shown that crosslinking of poly(N-isopropylacrylamide) (PNIPAM) into a fibrous matrix of PDA fibers induced both thermo- and mechano-responsiveness. Interestingly, at low fiber concentrations, the materials remained liquid at room temperature and rapidly formed strain-stiffening gels upon heating beyond the LCST of the PNIPAM linker. Such rapid sol-gel transition offers attractive prospects from an applied perspective as it potentially allows for injection of the desired cargo (*e.g.* mesenchymal cells) suspended in a cold solution below the LCST of PNIPAM, and quickly settle into a strain-stiffening matrix at body temperature, all while at a constant overall volume. Also along those lines, we conjecture that crosslinked PDA/PNIPAM networks are ideal candidates for encapsulation into sufficiently stable, cell-sized coacervate microdroplets while in the liquid state[10]. Thereby, gel formation beyond the LCST of the linker may lead to compartmentalized cytoskeleton mimics that could bring the realization of artificial cells one step closer.

Supramolecular fibers as building block for strain-stiffening materials

As alluded to earlier in Chapter 1, the design of synthetic strain-stiffening materials holds promising potential, particularly in the biomedical field, where there is a growing need to develop highly customizable materials that are structurally and mechanically akin to cells and tissues. In this context, we believe that the results derived from Chapter 3 are of particular relevance because they prove that strain-stiffening materials can be obtained through covalent crosslinking of sufficiently robust supramolecular polymers. Thus, we argue that the field of biomimetic gels could considerably benefit from the incorporation of hierarchical supramolecular polymers, where the rich variety of structures (*e.g.* helices, tubes, ribbons, fibers, etc.), lengthscales, persistence lengths and dynamics could aid to develop an extensive catalogue of novel, nanostructured, reversible hydrogels with targeted, on-demand mechanical properties[11–13]. These new materials are expected to mimic more closely the dynamic environment of cells, allowing to integrate mechano-responsiveness and self-healing behavior within the same material, whereby the balance between dynamics and mechanical performance may be leveraged through the strength of the supramolecular interaction.

Chapters 3 and 4 also yielded a valuable concept, as it introduced a novel method to reinforce self-assembled fibers with covalent bonds via non-selective crosslinking with 5-N_3. This approach offers a series of distinctive advantages, namely: (1) The extent of covalent fixation can be programmed through the molar ratio functionalized to unfunctionalized monomer, (2) It does not require a complex synthesis, (3) The fixated product does not absorb in the visible region of the spectrum, (4) Unlike PDAs, the monomers don't require to be pre-organized at a specific distance and orientation for the polymerization to occur. Thus, external fiber covalent fixation via non-selective 5-N_3 crosslinking will likely provide the means to reinforce an extensive library of supramolecular fibers in which tight packing of monomers along the fiber axis is no longer an essential requirement. Along these lines, we envision to incorporate monomers capable of forming micrometre-long fibers in water including, for instance, benzenetricarboxyamide (BTAs) amphiphiles[14] or ester-based triblock copolymers[15] which we argue are as least as well suited as DA or PDA fibers to mimic the morphological attributes of filamentous proteins (see Figs. 6.1.a and b respectively).

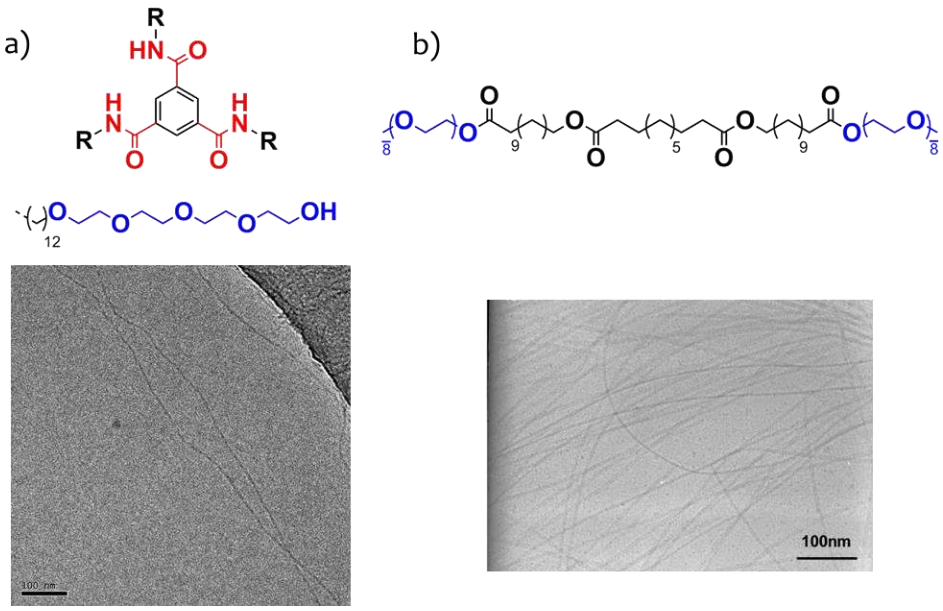

Fig. 6.1 | Cryo-EM micrographs showing the formation of micrometre-long supramolecular fibers in water from: (a) BTA derivative reprinted with permission from ref. [14]. Published by the Royal Society of Chemistry; (b) Ester-based bolaamphiphile adapted with permission from ref. [15]. Copyright © 2005, Royal Society of Chemistry. Scale bars: 100 nm.

References

1. Weizenecker, J., Gleich, B., Rahmer, J., Dahnke, H. & Borgert, J. Three-dimensional real-time in vivo magnetic particle imaging. *Phys. Med. Biol.* **54,** L1 (2009).
2. Pankhurst, Q. A., Connolly, J., Jones, S. K. & Dobson, J. Applications of magnetic nanoparticles in biomedicine. *J. Phys. Appl. Phys.* **36,** R167 (2003).
3. Roeder, L., Bender, P., Tschöpe, A., Birringer, R. & Schmidt, A. M. Shear modulus determination in model hydrogels by means of elongated magnetic nanoprobes. *J. Polym. Sci. Part B Polym. Phys.* **50,** 1772–1781 (2012).
4. Panorchan, P. *et al.* Probing Cellular Mechanical Responses to Stimuli Using Ballistic Intracellular Nanorheology. in *Methods in Cell Biology* **83,** 113–140 (Academic Press, 2007).
5. Ziemann, F., Rädler, J. & Sackmann, E. Local measurements of viscoelastic moduli of entangled actin networks using an oscillating magnetic bead micro-rheometer. *Biophys. J.* **66,** 2210–2216 (1994).
6. Ooi, H. W., Hafeez, S., Blitterswijk, C. A. van, Moroni, L. & Baker, M. B. Hydrogels that listen to cells: a review of cell-responsive strategies in biomaterial design for tissue regeneration. *Mater. Horiz.* **4,** 1020–1040 (2017).
7. Whitlock, H. W., Hanauer, R., Oester, M. Y. & Bower, B. K. Diimide reduction of porphyrins. *J. Am. Chem. Soc.* **91,** 7485–7489 (1969).
8. Marsh, B. J., Heath, E. L. & Carbery, D. R. Organocatalytic diimide reduction of enamides in water. *Chem. Commun.* **47,** 280–282 (2010).
9. Das, R. K., Gocheva, V., Hammink, R., Zouani, O. F. & Rowan, A. E. Stress-stiffening-mediated stem-cell commitment switch in soft responsive hydrogels. *Nat. Mater.* **15,** 318–325 (2016).

10. Mason, A. F., Buddingh', B. C., Williams, D. S. & van Hest, J. C. M. Hierarchical Self-Assembly of a Copolymer-Stabilized Coacervate Protocell. *J. Am. Chem. Soc.* **139,** 17309–17312 (2017).
11. Brunsveld, L., Folmer, B. J. B., Meijer, E. W. & Sijbesma, R. P. Supramolecular Polymers. *Chem. Rev.* **101,** 4071–4098 (2001).
12. Krieg, E., Bastings, M. M. C., Besenius, P. & Rybtchinski, B. Supramolecular Polymers in Aqueous Media. *Chem. Rev.* **116,** 2414–2477 (2016).
13. Aida, T., Meijer, E. W. & Stupp, S. I. Functional Supramolecular Polymers. *Science* **335,** 813–817 (2012).
14. Leenders, C. M. A. *et al.* Supramolecular polymerization in water harnessing both hydrophobic effects and hydrogen bond formation. *Chem. Commun.* **49,** 1963 (2013).
15. Chebotareva, N., Bomans, P. H. H., Frederik, P. M., Sommerdijk, N. & Sijbesma, R. P. Morphological control and molecular recognition by bis-urea hydrogen bonding in micelles of amphiphilic tri-block copolymers. *Chem. Commun.* 4967–4969 (2005). doi:10.1039/b507171b

Summary

Biomimetic Strain-Stiffening Hydrogels

The intra- and extracellular environment is rife with networks of filamentous proteins that are collectively capable of stiffening in response to stress or strain in a fully reversible manner without the need for structural adaptation. Strain-stiffening plays a pivotal role in biology protecting cells and tissues from rupture under stresses exerted by external or internal sources, and allowing for mechanical signalling at various length scales. In recent decades, the marriage of biology and physics has enabled scientists to elucidate the central mechanisms governing strain-stiffening, and their findings have hinted towards the main design principles required to reconstitute the structure and mechanics of biopolymer networks using synthetic materials, namely: (1) The polymers should be stiff or semi-flexible to access their nonlinear extensional regime prompted by small deformations, (2) Bundling of individual polymer chains is essential to enhance stretching and bending resistance, while providing the filaments with sufficiently high persistence lengths. The design of artificial cellular matrices represents exciting new avenues in a variety of fields ranging from tissue engineering, regenerative medicine to cell culture, where there is a growing need to develop highly customizable materials with lifelike structural and mechanical properties.

In this context, amphiphilic, self-assembling molecules equipped with directional, self-recognition motifs are excellent building blocks to produce supramolecular fibers that recapitulate some of the most fundamental features of structural proteins: (1) they typically form long and rigid filaments, in which tight packing of monomers within the hydrophobic core results in an elongated conformation of the backbone, (2) the monomers are reversibly bound and the exchange dynamics can be adjusted through the strength of the supramolecular interaction, (3) many of the so-formed fibers exist as bundled structures where individual polymers assemble in water via segregation of their hydrophobic cores.

This thesis aims to develop biomimetic strain-stiffening hydrogels by chemically crosslinking fibers of hierarchically self-assembled diacetylene bisurea bolaamphiphiles

(DA). The fibers can be mechanically reinforced with covalent bonds via photo-polymerization of the assembled diacetylenes to produce a π-conjugated polydiacetylenic (PDA) backbone. In **Chapter 2**, the morphology and structure of PDA fibers are studied in their native environment with cryo-electron microcopy (cryo-EM) and small-angle X-Ray scattering (SAXS). The results reveal comparable contour and persistence lengths (*i.e.* semi-flexible) while inferring no changes in morphology after covalent fixation of the fibers. SAXS analysis shows moreover that each fiber integrates 9-10 ribbons in water thereby meeting all requisites mentioned above for DA and PDA to be applied as protein mimics. Introduction of cross-linkable analogues within the fiber-forming DA host allows for chemical crosslinking of the fibers by a Cu-catalyzed click reaction. The so-formed hydrogels feature strain-stiffening with universal power-law rheology sharing metrics with hydrogels reconstituted from neurofilament and collagen type-I fibers.

In **Chapter 3**, the mechanical properties of self-assembled DA fibers that are not fixated via diacetylene polymerization are studied after crosslinking via selective (*i.e.* suppression of inactive, intra-fiber crosslinks) and non-selective strategies. First, the dynamics of DA fibers are studied in aqueous solution showing slow exchange rates that infer strong intermolecular interactions. The fibers are fragmented under ultrasonication and self-heal to recover their equilibrium length owing to their fully reversible nature. Hydrogels formed after chemical crosslinking exhibit pronounced strain-stiffening with stiffening ranges that can be selectively adjusted through the extent of external intra-fiber crosslinking. However, the most critical finding is that, in the absence of external covalent reinforcement, the gels do stiffen in response to applied stress with a rise in modulus by up to 3-fold relative to the value in the low-stress linear regime prior failure. These results demonstrate that fully supramolecular strain-stiffening hydrogels can be formed as long as the fibers are robust enough to withstand a prolonged regime of nonlinear deformation.

Chapter 4 explores the potential of covalent reinforcement to amplify the nonlinear stiffening regime of hydrogels constructed from self-assembled DA fibers. Internal crosslinking via diacetylene photo-polymerization imparts sufficient mechanical stability to PDA fibers to enable them retaining their integrity under prolonged exposure to ultrasonication. Such reinforcement is also manifested at the network level, whereby PDA hydrogels display much broader stiffening ranges than their non-fixated, supramolecular DA analogues. The combined effect of internal and

external fiber covalent reinforcement (*i.e.* via non-selective crosslinking) produces hydrogels that stiffen under applied stress by nearly 2 orders of magnitude prior rupture. Such stiffening ranges are reminiscent of many *in vitro* biopolymer hydrogels as well as covalent polyisocyanopeptide (PIC) gels.

Finally, in **Chapter 5** a thermo-responsive polymer is covalently crosslinked into a matrix of semi-flexible PDA fibers. Induction of coil-to-globule transition tenses the filaments regardless of their orientation resulting in a macroscopic stiffening that rises the modulus of the network by up to 3 orders of magnitude relative to its value at room temperature. Interestingly, diluted networks exhibit fluid behavior at room temperature and rapidly form strong hydrogels upon collapsing the linker above its LCST point. The resultant rigidified networks are also mechanically responsive under applied shear stress exhibiting power-law rheology with stiffening exponents similar to those of reconstituted actin/filamin networks stiffened by embedded myosin II molecular motors as well as entire fibroblast subjected to mechanical pre-stress. The combined effect of internally generated contractile forces and externally applied shear stress is sufficient to increase the modulus of the same hydrogel by a factor of 1500.

Curriculum Vitae

Marcos Fernández-Castaño Romera was born on May 12th 1986 in Madrid (Spain). In 2011, he graduated in Chemistry (B.Sc/M.Sc) at the Universidad Complutense of Madrid doing his graduation project at the Technical Universtity of Berlin (Germany) with a Socrates Erasmus European Fellowship at the department of Bio-inorganic Chemistry. Under the supervision of prof.dr. Andreas Grohmann, he explored charge transfer in iron(II) complexes with N-donor ligands. Afterward, he obtained his M.Sc degree in Polymer Science at the Free University (FU), Technical University, Humboldt University (HU) of Berlin and the University of Potsdam (UP). In 2013, he undertook his graduation project at Max-Planck Institute for Colloids and Interfaces in Potsdam in the department of Colloid Chemistry under the supervision of prof.dr. Markus Antonietti. His graduation project focussed on the synthesis of imidazolium compounds from naturally occurring precursors. In 2014, he started his Ph.D research as an Early Stage Researcher (ESR) in the laboratory of Macromolecular Organic Chemistry at the Eindhoven University of Technology (TU/e) and SupraPolix B.V. Under the supervision of prof.dr. Rint P. Sijbesma and dr. Tonny Bosman, Marcos focused on the development of biomimetic strain-stiffening hydrogels from hierarchically self-assembled fibers. The main results of his research are described in this thesis.

List of Publications

[1] P. van der Asdonk, H. C. Hendrikse, M. Fernandez-Castano Romera, D. Voerman, B. E. I. Ramakers, D. W. P. M. Löwik, R. P. Sijbesma, P. H. J. Kouwer. Patterning of Soft Matter across Multiple Length Scales. *Adv. Funct. Mater.*, **2016**, *26*, 2609–2616.

[2] M. Fernandez-Castano Romera, R. P. M. Lafleur, C. Guibert, I. K. Voets, C. Storm, R. P. Sijbesma. Strain Stiffening Hydrogels through Self-Assembly and Covalent Fixation of Semi-Flexible Fibers. *Angew. Chem. Int. Ed.*, **2017**, *56*, 8771.

[3] M. Fernandez-Castano Romera, R. Göstl, H. Shaik, G. M. ter Huurne, I. K. Voets, C. Storm, R. P. Sijbesma. Mimicking Active Biopolymer Networks with a Synthetic Hydrogel. *Submitted*, **2018**.

[4] M. Fernandez-Castano Romera, J. Schill, P. P. H. K. Fransen, G. M. ter Huurne, I. K. Voets, C. Storm, R. P. Sijbesma. Strain-Stiffening Supramolecular Polymer Networks. *Submitted*, **2018**.

Acknowledgments

I would very much like to use the remaining paragraphs of this thesis to sincerely thank a number of persons that have directly or indirectly contributed to the gestation of this thesis. Thanks to many of you, the past 4 years in the capital of the world (aka Eindhoven) have become a never-ending source of personal and professional growth. Whatever the future brings, I am pretty sure that I will look back and remember my days @ MST with acute nostalgia. So! Without further delay, let´s get started!

First and foremost, I would like to express my sincerest gratitude to my supervisor Rint Sijbesma −*i.e.* the supreme leader of the Sijbes(wo-)men− for giving the chance to work on such an amazing project. Your ability come up with ingenious solutions to complex problems has taken me out the ditch in countless occasions where, due to my own numerous limitations, I was scientifically stuck in the mud. I also admire your passion for science and teaching: If it wasn´t for your devoted supervision, my whole Ph.D would have probably been like rowing one-armed.

I am also hugely indebted to my administrative supervisor and, to some extent, life guru Tonny Bosman. I still have vivid memories of my job interview here @ MST, for which I had included on my resume that I was a proficient German speaker. My claims were immediately shattered as soon as you started addressing me in the language of Goethe with remarkable fluency. Your laid-back/charismatic yet efficient managerial style has made my days in Eindhoven way more pleasurable, and will surely serve as a guide to navigate the unpredictable world of work.

I'd also like to dedicate a few lines to thank my co-promotor Kees Storm with whom I have crossed the invisible force field separating the realms of chemistry and physics. Your input to this project has been truly invaluable and, despite my 'low-cost' understanding of basic polymer physics, you have managed to provide me with a clear picture of the ins and outs governing strain-stiffening. I would also like to add that your enthusiasm for this project has been always infectious, and I wish you a meteoric career as full professor unravelling, among other things, the mysteries surrounding Rubik's cube.

To the committee members: Alan Rowan, Laurent Boutellier, Bert Meijer, Jan van Hest and René Janssen. I am very grateful to you all for agreeing to participate on my defense and taking the time and effort needed to read through and comment on my thesis. Alan, I appreciate you undertaking the massive effort of semi-circling the planet to attend my defense. René thank you so much for chairing the event.

Over the past years I had the chance to collaborate with a number of persons. Many of these projects were doomed to fail from the very beginning but others crystalized into some of the results captured on this thesis or published elsewhere. First of all, I would like to thank Paul Kouwer and Pim van der Asdonk for persuading me into patterning fibers of bisurea bolaamphiphiles. I have to admit that my net input to the project was limited yet spending quality time both in Eindhoven and Nijmegen, and getting acquainted with a bunch of new characterization techniques was tremendously rewarding. I´d also like to acknowledge Robert Göstl and Huda Shaik for synthesizing the PNIPAM (aka poly-Shaik-PAM) that was the cornerstone of Chapter 5, and represents only the tip of the iceberg of your contribution to this project. Thanks to Jurgen Schill and René Lafleur (aka ice´s worst nightmare) for providing me with top-quality cryo-EM images which have been essential to the coming together of this thesis. I am also indebted to Peter-Paul Fransen and, by extension, to his former colleges at the University of Barcelona for providing me with the pentavalent linker used in Chapters 3 and 4 which has (totally unexpectedly) evolved into a completely new method to reinforce supramolecular polymers. Special thanks go out to Ilja Voets, Gijs ter Huurne and Clément Guibert for their crucial help with measuring and working up the SAXS (on the beach) data that is ubiquitous throughout this manuscript.

To all MST staff members, thanks for making my life infinitely easier over the past 4 years. Thanks to Ralf, Joost and Lou for keeping the analytical lab functioning like a Swiss clock all year round, and to Hans Damen, Bas de Waal and Jolanda Spiering for keeping us all well-sorted and safe inside the lab (aka God´s kitchen). Your contribution has been determinant for the completion of my PhD. I´d also like to acknowledge former and current secretaries Joke, Marjo and Martina who first made my arrival in Eindhoven smooth as a landing feather, and continuously resolved all sort of administrative/bureaucratic issues with extraordinary efficiency. Especial thanks also go out to Koen from the ICMS animation studio for the crucial help with

the graphics. To Christien Sanders: thank you very much for teletransporting me every morning to the beautiful island of Majorca.

I also had the pleasure of supervising a few students over the course of my PhD from whom I have perhaps learned more than what I might have passed on. Many thanks to Bernette, Menno, Huda and Hent with whom I´ve shared very nice moments. I wish you all a terrific career, and always try to keep in mind this rule of thumb: Never do what I wouldn´t do.

During slightly more than 4 years I have cohabited STO 3.49 with a series of individuals that have turned that office into a second home (besides the bike shed) away from home. Thanks to my Angebrother Sebastian for forming such a bullet-proof alliance and for the numerous parties @ your crib with Paulance and other celebrities. Thanks to ´Xiao from Dow´ for introducing the word ´halasment´ in the English dictionary. As we say in Spain: They broke the mold when they made you. Jessica, the way you dealt with Sebastian, Xiao and me in such a confined space reminds of the following quote: ´Only two things are infinite, the universe and Jessica´s patience, and I´m not sure about the universe´. Pauline, our sweet tradition of dining as an office died with your departure. Saaaad. Annelies you are the living proof that Dutch people can also dance like Puerto Ricans. I wish you an astronomic Ph.D!

As already mentioned Eindhoven has become THE place to be and the following persons are guilty for making my stay here an experience worth remembering: Jody (mi guacamole brother): The past years have shown me you're loyal friend and a better person, and I am convinced that the show will go on for many years amigo mio. Robert: I've never managed to sell you my bs: the only thing stronger than your brains are your gains. Peter-Paul: You´re one the most proactive persons I´ve ever met (and perhaps also the biggest fan I know of "el negro de whatssap"). Anne Helene & DJ: Only when you left I realized how massive the void you left behind was. Eveline: You're probably the only female friend I have that appreciates the content of my phone (and I love it). Sander & Esther: Thanks for borreling like two champs, and for the fantastic dinner/parties at your place, which will remain vividly imprinted in my memories for eons. Berrynator: Thanks for the fascinating moments shared at the beginning of my Ph.D, and for accepting with great sportsmanship all the nicknames I bestowed upon you. Berroqui (aka Jose a tope): Winning you at basketball has made

me even prouder than finishing this thesis. Dove posso trobaaaare?? Gijs: Thanks to you I haven't fully colonized the bike shed. I also owe you a hairless back. Jeroen: your seemingly endless conversation capabilities are only surpassed by your talent playing the ukulele. Wouter (aka Butter) & Nerea: You're probably the couple with the best combined resume I ever had the pleasure to meet. Expect my own resume in a no too distant future as well as my auto-invitation to the next Oktoberfest. Emma Giakoumate: You are by far one of the most "fair dinkum sheilas" I ever had the pleasure to meet. Marcin: May the gods of Roermond bless you with a bright future within the beating heart of Limburg. Romà: Because there´s only one thing sexier than kissing a beautiful woman´s hand: Kissing your own hand. Neus: I wish you a fascinating new stage in your life here in Eindhoven replacing calçots for frikandel speciaal. I would like sincerely acknowledge current and former MSTers & SFDers: Eva, Maarten, Sam Jurgen, Olga, Ghislaine, Hitesh, Monali, Ting, Nick, Bao, Eline, Pim, Samaneh, Marko, Nic, Nate, Miguel, Annelore, Jie, Yanwu, Koen, Janus, Marcel, Tristan, Røy, Pascal, Davo, Bas(s), Remco, Patricia, Elisabeth, Brigitte, Erik, Dylan, Antonio, Subham, Loai, Mike, Tom(s), Sangria, Thuur, Matt, Alex, Imke, Ilia, Bastiaan, Anniek, Bea, Dario, Tristan. To you and those I regrettably left out: I would need a full thesis to thank you enough for the colossal moments experienced together.

A mis padres Eduardo y Mari Cruz a los cuales dedico esta tesis en señal del más sincero agradecimiento: La dedicatoria no es casual ya que sin vuestro apoyo y amor incondicionales, este libro que sujetáis en vuestras manos jamás habría llegado a existir. Sin vuestro estímulo jamás habría abandonado Madrid. Sois y seréis para mí el espejo en el que espero verme reflejado algún día (ya empiezan a aflorar las arrugas). Tan sólo espero poder llegar a transmitir el legado que me habéis transmitido. A vosotros: gracias de todo corazón por ser unos padres tan cojonudos.

To my lovely Luiza van Ruremunda: For you I have reserved the very last lines of my scientific novel. Thank you very much for your endless patience. Thank you for you loyalty. Thanks for being there in the good times and (especially) in the bad times. For the countless sacrifices you´ve made. For your seemingly endless perseverance. You have consistently shown me that you´re a strong, intelligent, inspiring and, above all, gigantic-hearted person, and I would be an imbecile if I didn´t follow to the end of the world. Ik hou van jou guapa!!

Marcos